

# UC Irvine

## UC Irvine Electronic Theses and Dissertations

### Title

In vitro hippocampal network axonal transmission during patterned theta burst stimulation and a platform for recording in 3D

### Permalink

<https://escholarship.org/uc/item/3c69x9rb>

### Author

CHEN, RUIYI

### Publication Date

2022

Peer reviewed|Thesis/dissertation

UNIVERSITY OF CALIFORNIA,  
IRVINE

In vitro hippocampal network axonal transmission during patterned theta burst  
stimulation and a platform for recording in 3D

DISSERTATION

submitted in partial satisfaction of the requirements  
for the degree of

DOCTOR OF PHILOSOPHY

in Chemical and Biochemical Engineering

by

Ruiyi Chen

Dissertation Committee:  
Professor William Tang, Chair  
Professor Gregory Brewer  
Professor Han Li

2022



## **DEDICATION**

To

my parents who are the permanent source of love, courage, persistence

# TABLE OF CONTENTS

	Page
LIST OF FIGURES	v
LIST OF TABLES	vi
ACKNOWLEDGEMENTS	vii
CURRICULUM VITAE	viii
ABSTRACT OF THE DISSERTATION	ix
CHAPTER 1: INTRODUCTION	1
Brain machine interfaces	1
Electrophysiology	3
MEMS based neural platform and micro-tunnel technique	4
Hippocampal network	6
Theta burst stimulation (TBS)	10
The gap, 3D neuronal culture	13
CHAPTER 2: STUDY OF AXONAL TRANSMISSION DURING PATTERNED STIMULATION ON AN ENGINEERED HIPPOCAMPAL NETWORK	17
Background	17
Methodology	20
Device fabrication and assembly	20
Cell culture	22
Fluorescent imaging	24
Electrophysiology and stimulating protocol	25
Data processing	28
Jaccard distance and similarity	29
Statistics	29
Results and Discussion	30
Network formation on MEAs and optimization	30
Analysis of axonal activities in response to patterned stimulation	34
CHAPTER 3: DESIGN, FABRICATION & CHARACTERIZATION OF A 3D ELECTROPHYSIOLOGICAL SYSTEM	55
Background	55
Material choice	58
Methodology	62
Fabrication	62
Functional characterization	68
Surface preparation	68
3D primary neuron culture	68

Results and Discussion	70
3D platform design and ITO electrodes fabrication	71
Characterization of top electrodes	72
Platform set-up and actuation	74
Planar culture and recording	77
3D culture construction	81
CHAPTER 4: CONCLUSION AND FUTURE PERSPECTIVES	89
BIBLIOGRAPHY	93

## LIST OF FIGURES

	Page	
Figure 1.1	Hippocampus and transsynaptic circuit	7
Figure 1.2	Brief illustration of retrieving information of cognitive function through reciprocal process	11
Figure 1.3	Illustration of the patterned TBS	13
Figure 2.1	SU8 mold masks and the MEA-PDMS culture recording device	22
Figure 2.2	Hippocampal dissection illustration	24
Figure 2.3	Reverse engineered hippocampal network and patterned TBS	27
Figure 2.4	Phase contrast and fluorescent images of reverse engineered hippocampal network	31
Figure 2.5	Cell densities in the mature hippocampal network	33
Figure 2.6	The active electrode numbers increased after BrainPhys Media Change	33
Figure 2.7	Image of tunnel electrodes and recordings on axons connecting adjacent regions	35
Figure 2.8	Selected examples of analogue data in 4 tunnels and the Jaccard Distance (JD) calculation	37
Figure 2.9	Uniqueness of 3 site pattern stimulation	40
Figure 2.10	Dissimilar responses from 3-site stimulation presented at the 0.2 s repeats	41
Figure 2.11	Comparison of axon activity from 10 s repeats between subregions reveals major differences in CA3-CA1, EC-DG	45
Figure 2.12	Between tunnel similarity calculation and subregional differences to assess synchrony	48
Figure 2.13	CA3-CA1 responds substantially different to other stim site combinations	50
Figure 2.14	Individual axons carry similar patterns in response to partial two-site stimulus nine minutes after training with three-site stimulation as a test of pattern completion	53
Figure 3.1	Schematic of designed 3D hippocampal culture and signaling platform	58

Figure 3.2	Patterned metal thin film on PDMS and 150 nm ITO pattern on PDMS	61
Figure 3.3	A typical photolithography process	62
Figure 3.4	PCB designs for connecting top electrodes	65
Figure 3.5	Fabrication process flow for top ITO electrode	66
Figure 3.6	Photos and transmittance measurements of finished ITO electrode	72
Figure 3.7	Impedance measurements of the electrodes	74
Figure 3.8	Photos of device setup and schematic of cross-sectional view to explain how the platform works	76
Figure 3.9	2D planar neuron culture demonstrates good biocompatibility	79
Figure 3.10	ITO electrode recordings and single channel data processed by MATLAB based algorithm Wave_clus	80
Figure 3.11	3D cell culture on Matrigel and the hydrogel degradation.	83
Figure 3.12	3D encapsulated culture with VitroGel	85
Figure 3.13	3D culture on glass beads	87

## LIST OF TABLES

	Page
Table 3.1	Mechanical properties for material candidates of making the electrodes 55

## ACKNOWLEDGEMENTS

I would like to express the deepest appreciation to my committee chair, Professor William Tang, who has continuously given his help and encouragement for me to pursue my degree. He has not only provided precious suggestions on my research, but also supported me in developing agency for exploration. Being a great mentor to me, he shares valuable experience towards academic and career success. Without Dr. Tang's guidance, this dissertation would not have been possible

I would like to thank my committee members, Professor Gregory Brewer and Professor Han Li. Dr. Brewer has profound knowledge in neuroscience. He always gives patient instructions, which guide me through hippocampal neural coding project. His passion on conducting research always motivates me. Dr. Li's expertise is synthetic biology. She provided insightful comments with me at many key points of my Ph.D. training. The way Dr. Li guided me composition kept impressing me towards finishing my writing tasks.

I also want to thank my colleagues Yuntian Xue and Joanne Ly, who are my comrades during the past years and friends forever. They helped to build the lab environment open for research discussion and idea exchange. Their knowledge in their field shed inspirations which helps me to polish my skills. In addition, I would like thank Yash Vakilna, Samuel Brandon Lassers, Josh McWhirt, and Ben Harlan for their offering of kind helps in many aspects of my research.

This research is funded in part by NIH, Grant No: R01 NS052233, the UC Irvine Foundation and unrestricted funding by Prof. William Tang.

Thank Elsevier for the reprint permission of Figure 1.1A, and Springer Nature for the reprint permission of Figure 3.2A.

Last but most important, a sincere thank you to my parents. They educated me to pursue knowledge relentlessly and never give up easily. It's their incomparable love supported me taking the trails under the galaxy.

# CURRICULUM VITAE

**Ruiyi Chen**

## EDUCATION

- 2022                    **Ph.D., Chemical Engineering**  
University of California, Irvine
- 2016                    **M.S, Chemical Engineering**  
University of California, Irvine
- 2014                    **B.S., Chemical Engineering**  
Dalian University of Technology, China

## RESEARCH EXPERIENCE

- 2016 –2022            **Graduate Student Researcher**  
MicroBioMechanics Lab, University of California, Irvine
- 2013 –2014            **Undergraduate Researcher**  
Dalian University of Technology, China

## TEACHING EXPERIENCE

- 2018 –2020            **Teaching Assistant** - Chemical Engineering 140A/140B Unit  
Operation  
Dr. Daniel Knight

## PUBLICATIONS

Ruiyi Chen, William Tang, Gregory Brewer “Plasticity of single axon transmission during multi-site patterned theta burst stimulation in a reverse engineered in-vitro hippocampal network” under preparation.

Ruiyi Chen, Gregory Brewer, William Tang “Novel microfabricated 3D neuronal culture chamber for electrophysiological studies” under preparation.

## **ABSTRACT OF THE DISSERTATION**

In vitro hippocampal network axonal transmission during patterned theta burst stimulation  
and a platform for recording in 3D

By:

Ruiyi Chen

Doctor of Philosophy in Chemical and Biochemical Engineering

University of California, Irvine, 2022

Professor William Tang, Chair

Neuronal network dynamics by in vitro electrophysiology serves as an objective and convenient method to explore neurophysiological mechanisms and communication. Theta burst stimulation (TBS) recapitulates natural brain rhythms which is efficacious for synaptic potentiation in hippocampal circuits. TBS is typically applied to a bundle of axons to measure the immediate response in a single downstream subregion like the CA1. Yet little is known about axonal transmission between subregions as the response to TBS propagates to other subregions from upstream stimulation in the entorhinal cortex. We reverse engineered the hippocampal network on micro-electrode arrays (MEAs) contained in a four-chambered silicon rubber device with interconnecting microfluidic. Tunnels. The micro tunnels allow monitoring single axon transmission which is hard to realize in vivo or in slices. The patterned TBS was delivered to the entorhinal cortex (EC), the gateway to cortical entry into the hippocampus. Temporal Jaccard distance was used to quantify the spike pattern

similarity. We recorded the network responses to stimulation patterns that produced unique response patterns on axons at three timescales. The response to short-term stimulus repeats at 0.2 s has high variability. The 10 s repeats show some retention of similar responses, especially in the axons from CA3 to CA1, suggestive of pattern completion. While in EC to DG, the repeats evoked unique responses with similarity significantly lower than random, implying pattern separation. Between-tunnel similarity in CA3-CA1 was higher for single site stimulation than from multisite stimulation. Using the temporal pattern metric, axons carried similar responses when an incomplete stimulating pattern was presented. Our design and interrogation approach offers understanding of dynamic pattern variations at the subregional level in response to TBS.

To extend this 2D network model, a 3D model was designed to bridge the gap between multi-subregion electrophysiology in vitro and in vivo recordings with high complexity from the dense packing of neurons at single regions in vivo. Here, we report fabrication of a transparent 60-electrode array that forms a second layer of recording sites above a commercial MEA. This 3D culture chamber enables recording from a 400  $\mu\text{m}$  thick reconstruction of four hippocampal subregions. The electrodes are easily fabricated and assembled. Optical and electrical characterizations of the electrodes have been performed. Good biocompatibility enabled successful electrophysiological recording. Two hydrogel substrates and solid glass beads for the integrated 3D culture scaffold were evaluated. Only the micro glass beads supported the 3D neuronal network formation on the platform over 21 days. Building this 3D signaling system demonstrates feasibility to access the information coded in the 3D hippocampal network in vitro for comparison to the 2D network spike and burst dynamics in response to stimulation.

# CHAPTER 1: INTRODUCTION

## Brain machine interfaces

Brain machine interface (BMI) has become an intriguing field where allows live access to nervous system from outside world. In the field, neuroscientist, behaviorist, bioengineer, and the researchers from multi-disciplinary areas extensively explored the physiological properties of neurons, neural circuits, cognitive function, neural prosthesis etc. Recent news in this field from Neuralink's brain chip (LINK) worked with a monkey to play video game. In the experiment, a silicon-based electrode array was implanted in the monkey's brain and received signals from multiple neuronal units when monkey is performing a specific task (Musk 2019). The recorded neuronal activity at a specific brain area is decoded with computer software to model the relationship between the physical movement and neural signal patterns. It demonstrated the capability of BMI to functionally connect 'mind' with machine and its huge potential for treating neurological disorder.

Due to the low patient acceptance, strict FDA approval, risk of the operation, the BMI technique has been barely applied to humans for research or treatment. However, it's already come into the era of extensive human and machine interactions. Besides bridging up machine and neuron electrically, a key part for constructing the interface is to explore, understand and apply the brain cognitive function. It is not surprising that over the last few decades, researchers have put great effort on building the knowledge: how it is structured, how it works, how it develops, how it malfunctions, and how it can be changed. As core parts of human body, brain tissue and nervous system help to administrate both physical and

psychological activities of human. In the main branch of neuroscience, a better understanding of specific brain site function and brain neural network contributes to better human health and wellness. At the same time, research have shown that a few diseases such as Parkinson's disease, Alzheimer's, seizure, stroke, and major depression are caused by neural degradations and disorders. Therefore, there long existed a great need on neural electrophysiological research.

Researchers used various methodologies on studying sensory area, neural coding (Nirenberg and Latham 1998) network connectivity and so on. Among all the ways, neural probes or electrodes become a key tool to record action potentials from neurons and stimulate specific site of brain. Traced back to 18th century, early research initiated the investigation on using electrical signals to cure neural diseases. In year 1939, Hodgkin and Huxley first demonstrated the recording of action potentials from inside a nerve fiber (HODGKIN and HUXLEY 1939). Later, they quantitatively described the membrane current and mechanism of action potential (HODGKIN and HUXLEY 1952). Over the past decades, researchers initiated using implantable prosthesis, which is known as neural probe, to record action potential, stimulate neurons and ultimately understanding the brain function.

With the development of decellularizing brain tissue to build the neuronal models in vitro, researchers gain easy access of exploring the brain functions and diseases. This could reduce the complexity on operational procedures to a great degree. In vitro brain function study involves conducting electrophysiology on the neural circuits. An important aspect is interrogation of the neural circuitry when delivering the stimuli on-site, the methods include electrical, chemical and optogenetic stimulations. These stimulations either evoke stronger

activities or suppress the neural firing of nearby neurons. In electrical stimulation, typically the electrical current is delivered to targeted neurons to investigate some causal effects.

## **Electrophysiology**

Electrophysiology, often called the “gold standard” to investigate neuronal signal, it includes a wide range of electrical activity measurements from single ion channel to whole organs. To study the neuronal activities at the mesoscale (larger scale than single neuron and smaller than large area brain activity such as measured by fMRI), extracellular recording using microelectrodes have been widely adopted. The network activities generate local field potential which can be detected by closely localized electrodes, and the electrical signal can be further analyzed using sorting technique based on the wave characteristics such as frequencies and amplitudes etc.

Microelectrode array (MEA) is a powerful tool to gain electrophysiological activities from neuronal tissues at multiple sites. The commercial MEAs usually provide 60-120 electrodes that spacing few hundred micrometers. Higher resolution MEAs with more than a thousand electrodes have been fabricated for specific research goals (Müller et al. 2015; Ballini et al. 2014). The incorporation of MEA allows long-term recording of neuron culture, which provided integral information rather than just the acute slice recording (Draniyas et al. 2013). The network coupled on the micro-electrodes provide access to investigate functional connections for specific cell assemblies (Poli et al. 2018; Poli and Massobrio 2018), and their response to electrical (Poli, Pastore, and Massobrio 2015) and chemical stimuli (Ciba et al. 2020). In addition, efficient building of in-vitro model takes advantages of this non-invasive protocol. Researchers reported network learning after repeated low frequency stimulation

in a cortical model (Shahaf and Marom 2001), Frega and co-workers built 3D model enable neurites outgrowth (Frega et al. 2014), and Amyloid  $\beta$  toxicity was studied through quantifying NMDA activation on the in-vitro AD model (Amin et al. 2017).

### **MEMS based neural platform and micro-tunnel technique**

In the biomedical area, engineers design reliable products to fulfil requirements from basic science research and purposeful applications that solve real clinical problems. One obstacle that hinder the development of the mechanism study on episodic memory, spatial navigation and information processing is the lack of read-out tools or methods that precisely target deep brain tissues or regions. Especially, these regions such as hippocampus, medial temporal lobe, thalamus theoretically carry the potential abilities to important brain functions. That being said, one promising alternative is to reverse engineer the biological structural compartment and gain access to the neuronal information processing with high spatial and temporal resolution in vitro (Vakilna et al. 2021).

The dissociated neuron cultured on in vitro neural platform allow researchers to study network formation (Lam et al. 2019) short-term memory (Draniyas et al. 2013) and functional connections (Poli and Massobrio 2018) etc. However, most of the research focused on forming a homogenous cortical or hippocampal culture, which lost the specific function differentiations associated with different brain regions. In recent years, people manipulated the dissociated neuronal assemblies to control the connectivity. The technique involving control cell attachment (Macis et al. 2007; Boehler et al. 2012), and micro-tunnels (Pan et al. 2015; Brewer et al. 2013; Kanagasabapathi et al. 2011). The micro-tunnels are typically smaller than the size of cell body that only allows axons to grow through. The embedded

micro-tunnels in disassociated neuronal cultures allow to rebuild the structural connectivity in vitro. In previous researches, most of the work has been done based on 2 compartment cocultures (Pan et al. 2015; Brewer et al. 2013; Daniele Poli<sup>1,2,\*</sup>, Bruce C. Wheeler<sup>3,4</sup>, Thomas B. DeMarse<sup>5</sup>, and Gregory J. Brewer<sup>1,6</sup> 2017; Brofiga et al. 2020). They demonstrated excellent accessibility of micro-tunnel technique and gain insights into network dynamics and functionalities.

One critical aspect of in vitro electrophysiological study is to mimic specific conditions, physical environment and retrieve their activities. There is a fundamental difference of cellular behavior in the way of neuronal culture from 2D (monolayer) to 3D (multiple layers) such as in the forms of cells attachment, morphology and polarity, the response to stimuli and electrophysiological functions (Frega et al. 2014; Peretz et al. 2007; Henstridge, Christopher M., Spires-Jones 2018). Isolated cells placed onto a planar surface are prone to become progressively flatter (Baker and Chen 2012), where their functional behaviors will be changed. To be more specific, the network complexity, connection polarity, characteristics of spontaneous activities are subjected under change and so on. There are also valid concerns about in vitro recordings, including the likely possibility that neuronal activities of tissue isolated from the brain may not represent what would happen in the natural 3D. Imagine the information routing in 3 dimension increases the complexity of processing than on 2D. To investigate the neuronal network properties more approaching in vivo status, a system allows to simultaneously monitor the neural signal transmission on z direction should be incorporated. To fulfill this research aims, we need a 3D culture chamber with top and bottom electrodes. Specifically, the top electrodes will have facing-down contacting pads to measure the electrical activities from top layer of neuronal culture. The electrodes should

be transparent to facilitate the microscopic observation of cultured tissue. Moreover, perforations on the electrode substrate would allow oxygen and nutrient exchange for the neurons underneath. The corresponding signal transmitting compartments will also be designed and fabricated.

In this dissertation, we report a 3D neural culture platform that allows neurons to grow in a 3D environment for up to 3 weeks. It is designed with both a bottom and a top array of electrodes that can stimulate or detect neuronal activities with any of the electrodes. The top electrode array consists of 60 electrode sites and transparent conductors made of indium tin oxide (ITO) supported on a polyethylene terephthalate (PET) film, which is also transparent to facilitate visual imaging and monitoring of the neuronal tissues. With both electrode arrays in use simultaneously, the neuronal communications in all 3 dimensions (x, y, and z). Further, the platform is designed with 4 compartments within the culture chamber, with micron-sized tunnels connecting the compartments to facilitate controlled axonal connections among different subregions of the hippocampus. This represents a significant advance over our previous 2-compartment chamber design, which demonstrated the self-wired connection between subregions (Brewer et al. 2013).

### **Hippocampal network**

Hippocampus is responsible for the episodic memory formation and spatial navigation. The behavioral experiments in rodent have been widely conducted to study the key factors for the formation of episodic memory. Meanwhile, hippocampus is believed to be a general-purpose creator of cognitive brain algorithms, but the exact function of each subregion is incompletely understood. Four sub-regions comprise the hippocampal formation, which are

entorhinal cortex, dentate gyrus, CA1 and CA3. Their unique laminar cytoarchitecture was also intensively investigated through molecular biology, electrophysiology of ex vivo slices, and anatomy. The well-arranged cellular construction has intriguing neuronal network connectivity and dynamics. The electrical events vary with different sub-regions and the sub-regions have a polar interconnection. A famous trisynaptic circuit was found by Cajal (Andersen 1975) (Fig. 1.1 B), where EC will have the initial signal input into hippocampus and DG serves as a downstream receptor, then the signal will pass into CA3, followed by CA1, and finally transfer back to EC. The hippocampus and its location in brain is shown in Figure 1.1 A (Amaral and Witter 1989). Hippocampus receives its input from sensory, spatial, and motor representations into the EC from which unknown features are channeled into the hippocampus.

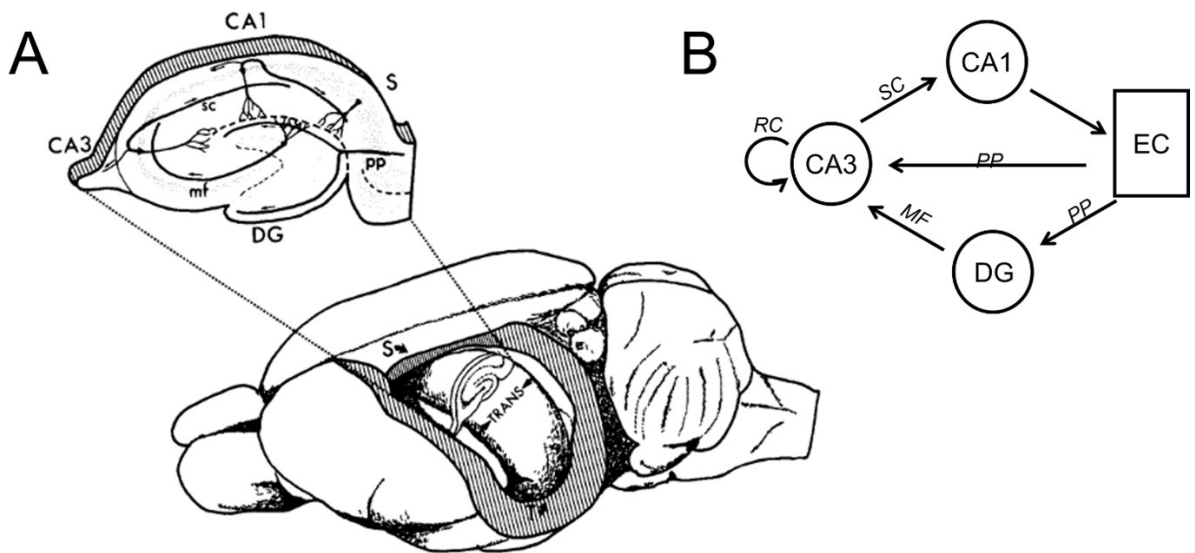


Figure 1.1 Hippocampus and trisynaptic circuit **A.** Position of hippocampus in the rat brain and cross section of transverse axis (Amaral and Witter 1989). Reprinted with permission from Elsevier © 1989. **B.** Schematic of trisynaptic circuit involving 4 subregions of hippocampus. PP: perforant path; MF: mossy fibers; SC: Schaffer collateral; RC: recurrent collateral.

Memory formation involves neurogenesis and plasticity changes (Aebbersold et al. 2016; Palop and Mucke 2010). Production of granule cells in the hippocampal region continues throughout life (Gage 2019). Hippocampal neurons undergo dynamic modifications in the form of dendritic spine extension and retraction, as well as synapse formation and elimination (Sporns 2013). All these types of structural plasticity are subject to modification by a variety of factors and conditions, suggesting that they may be substrates for experience-dependent change. The learning process and environmental experience can cause the change in structural plasticity. Many animal behavioral studies show the relevance between structural plasticity and hippocampal functions (Morris 1984; Pastalkova et al. 2008; Roesler and McGaugh 2016).

Multiple generic functions are extensively studied in hippocampus. They include but not limited to episodic memory formation, spatial navigation, patterns separation, pattern completion and novelty detection. Episodic memory contains specific spatial information and events, and it is essentially linked together in the hippocampus (Lisman et al. 2017; Rolls 2010; Rugg, Otten, and Henson 2002). Computational models suggest that DG separates overlapping populations of active EC neurons into less overlapping populations of active GCs, which forms a fan-out structure to realize pattern separation (Rolls 2013; Chavlis, Petrantonakis, and Poirazi 2017; Poli et al. 2018). Pattern completion refers to the ability of retrieving or recognizing previous learned patterns when a partial cue is presented. CA3 is considered as the auto-associative network performing pattern completion (Rolls 2010; 2013; Poli et al. 2018). The CA3-CA3 recurrent collaterals are thought to be the substrate finishing this function (Guzman et al. 2016). Meanwhile, a key function contributes to efficacious memory formation is novelty detection. Novelty detection is ability of the brain

react to a stimulus that lacks a pre-existing representation. Posterior hippocampus showed greater activity in response to novel items than familiar items (Kafkas and Montaldi 2018) but the details of processing are unspecified. Neuroscience provides a rich repertoire on inspiring computation algorithms (Hassabis et al. 2017). The complexity emerges as single function may engage multiple brain regions. Therefore, the functional significances of subregions are far away from fully explored or established.

However, there exist gaps to unveil the hippocampal algorithm at both scale and system level from animal behavioral model. Studies presented from the computational point of view that the hippocampus as a sequence generator that encodes event-space links and planning of actions (Pastalkova et al. 2008). The generic purpose of hippocampus which means the general computational algorithms irrespective of its input source, render complexity to the function of hippocampus from animal behavioral recordings. What's more, because of the different experiment setting involve space, time, sound frequency, odor etc., the investigators might examine how different ensembles give responses to those different cues.

Neuroscience provides a rich source of inspiration for new types of algorithms and architectures, independent of and complementary to the mathematical and logic-based methods and ideas that have largely dominated traditional approaches to AI (Hassabis et al. 2017). More closely understanding hippocampal network and scrutinizing the potential memory coding algorithms will benefit from developing neuroscience inspired AI technologies. Here, we focused on computational and structural connectivity, gaining these transferrable insights into mechanisms of hippocampal functions through our engineered live network, MEA with micro-tunnel technology, and signal processing.

## **Theta burst stimulation (TBS)**

Theta burst stimulation (TBS) are short bursts of stimulation pulses at high frequency (~100 Hz), with the burst itself applied at theta frequency (4-10 Hz). It serves as the brain stimulation that closely mimic the natural rhythm of neuronal activities in the brain and has stronger and long-lasting effect on changing neuronal plasticity, also known as enhancing the synaptic strength, which leads to long-term potentiation (LTP).

In hippocampus, the theta oscillation is a pivotal rhythmic component. It coordinates interregional communication (Wang et al. 2015; Patel et al. 2012). Theta oscillation also couples with gamma to code sequence ensembles (Lisman and Buzsáki 2008). Because TBS recapitulates natural brain rhythms, it is speculated to be efficacious for modulating the activity of brain circuits responsible for cognitive processing or memory (Rounis and Huang 2020; Solomon et al. 2021). In the in vitro model of acute hippocampal slice, TBS has constantly shown elicit plasticity change (Zhu et al. 2015) in neuronal network. The intracellular calcium oscillation induced by TBS activates transcriptional factors (Sheridan et al. 2014). Though growing studies explored the memory mechanism with TBS neurobiologically in which the stimulus and response could be traced directly, little is known about the network functionally responses to TBS or subregional processes of this artificial cue and transmission between subregions.

A key aspect is to understand how the brain processes information, the stimulus from outside and induced neural responses on finishing certain tasks or cognitive function are involved in a reciprocal process, as illustrated in Figure 1.2. Interpretation of cognitive function always falls into an ill-posed question from looking at the neural autonomy or the

neural activities themselves. Intensive effort has been put into constructing neural architecture mimicking real brain part or remodel the isolated neuronal tissues to gain the multiplex level of understanding of the neuronal network. (Kim et al. 2017a; Poli et al. 2017; Jang et al. 2015). Limited work elucidated the generic computation properties or the plasticity change when the network is exposed to stimulus. Therefore, In-vitro experiments with high-resolution network recordings and designed pattern of stimulus input as done here could facilitate the deciphering process.

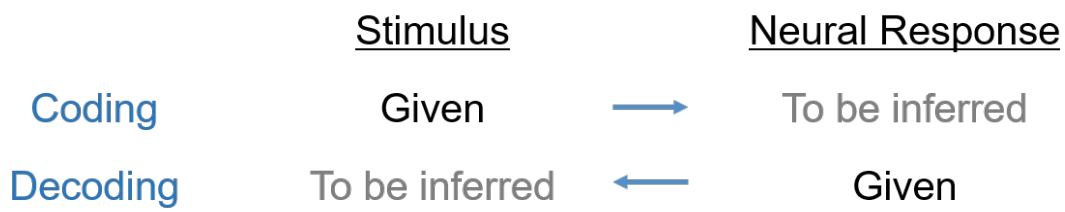


Figure 1.2 Brief illustration of retrieving information of cognitive function through reciprocal process

Encoding is the transduction of stimulus into neural activity patterns. Decoding is to understand what information is conveyed by certain neural activities.

In electrical stimulations, voltage pulses have shown to induce highly reproducible responses in neurons in direct vicinity of stimulating electrodes. (Habibey et al. 2017a; Wagenaar, Pine, and Potter 2004). However, the ion environment between neurons and the electrodes keeps changing which render a constant variation of seal impedance in the equivalent circuit. In this case, the voltage pulse stimulus is not able to produce stable level of stimulation on the target. On the contrast, the choice of injecting constant current pulse will have relatively steady source of electrons for the targeted neurons. On the other hand,

Habibey et al. found a 20-30-fold activity increase during the first 35 ms peri-stimulus window (Habibey et al. 2017b). The pulse train interval is about 150 ms and guarantee us the basic idea to design our experiment, set proper time window to investigate the effect of patterned stimuli.

In this thesis, we designed a patterned TBS delivering at 3 selected sites in EC of our in vitro hippocampal model. The TBS evoked activity is being processed and routing in the network. With specific time intervals and stimulation repetitions, the causal relation between stimulus and response is direct and clear. The axonal activities were recorded in micro tunnels, specified the network level information routing into axon base clarity. We evaluated the significance of involving 4 subregions to comprehending stimulus pattern and interrogated the axonal transmission at each subregion. TBS pattern is shown below (Fig. 1.3). The stimulus train was composed of different numbers (4-6) of trains with the same 150 ms intertrain interval. Each train has 5 biphasic square pulses with each pulse having a 10  $\mu$ amp amplitude, negative phase first for maximum negative to positive current gradient and biphasic for charge balance, and an inter-pulse interval of 10  $\mu$ s. The entire 3-site stimulus takes 1.4 s. Considering the temporal onset delay of evoked activities and propagation of the evoked activities in our engineered 4 compartment networks, we set the recording length to be 2 s.

## Designed Theta burst stimulation (TBS) pattern

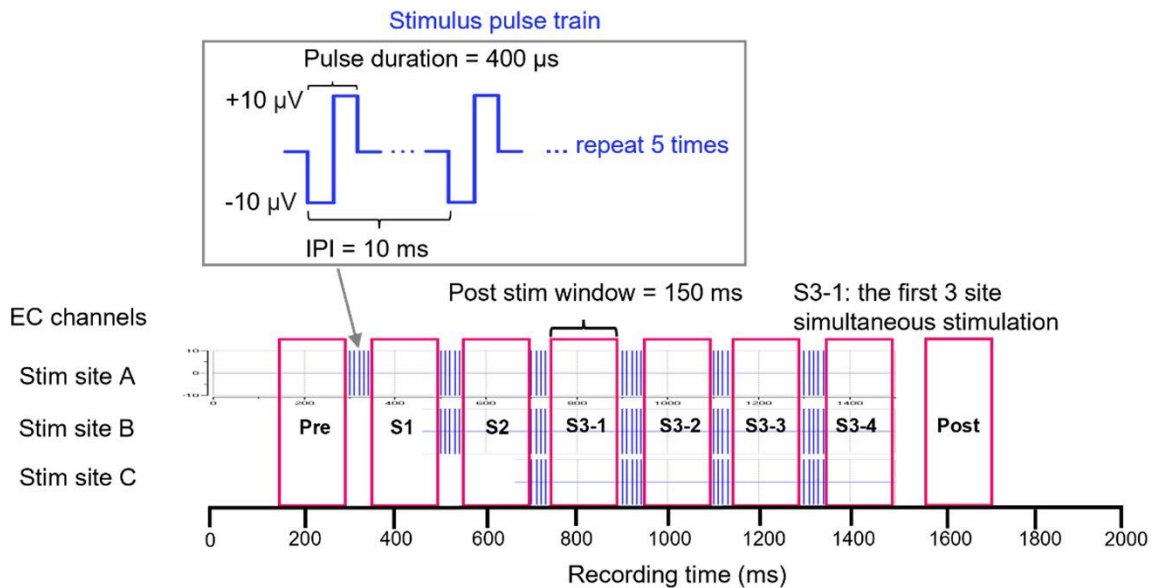


Figure 1.3 Illustration of the patterned TBS

The TBS consists of 4 – 6 trains (blue bars) of high frequency bipolar pulses, which are 10 micro volts amplitude and last for 400 microseconds, negative pulse first and with IPI for 10 milliseconds. The TBS trains are delivered to multiple sites labeled as A, B, C with a delayed manner. The stimulated activities are evaluated at the 150 milliseconds post stim window labeled as 'S1' to 'S3-4'. Two windows of the same length before and after the stimulus train are selected as control labeled as 'Pre' and 'Post'.

### The gaps, 3D neuronal culture

The cell culture system is widely applied to both research and application areas such as neurotherapeutics, drug screening, electrophysiological investigation etc. Instead that two-dimensional (2D) cell culture remains the predominant culture model, three-dimensional

(3D) cell culture system become increasingly promising to support technicians and researchers to resemble the native tissue or cellular environment.

The main goal of 3D cell culture is to bridge the gap between *in vivo* and *in vitro* conditions. Cell-cell, cell-microenvironment interactions are involved in modulations that affect the cell fate. Several 3D cell culture techniques have been developed principally categorized in 1) explant culture, 2) self-assembled aggregate culture and 3) scaffold-based cell culture (Ko and Frampton 2016). Among them, the elevating focus has been put onto establishing complex *in vitro* cell culture with extracellular matrix (ECM) (Nicolas et al. 2020). The importance arises to reproduce certain level complexity and heterogeneity of ECM in the brain. Some native brain ECM 3D cultures have been reported (Crapo et al. 2014; Baiguera et al. 2014; Sood et al. 2016). A variety of biomaterial systems have been developed toward this goal, including multi-layer tissue construct (Frimat et al. 2015), a MEMS-based 3D microbio reactor (Bastiaens et al. 2018). Compared to ECM-based 3D cell culture, the disassociated neuronal culture without any scaffolds has certain advantages such as avoiding disrupting the natural 3D space of connected hippocampal cellular structure, and the dense neuronal culture has an extremely rich repertoire of activity patterns (Wagenaar, Pine, and Potter 2006). However, in a passive diffusion system, the nutrition, oxygen supply and waste removal are not adequate at the bottom layer of the culture of more than x cell layers long term. In addition, because in a reliable electrophysiological study, neuron network matures around 3 weeks to generate stable spontaneous activity, a substrate suitable for supporting healthy neuronal cells growth, and with long-term stability is needed. Therefore, hydrogel-based ECM consisting of water-swollen polymers are being developed for their similar mechanical properties typically reported as elastic modulus (E) of soft

tissues. The support also includes large porosity suitable for neurite extension and network formation in neuronal culture (Tedesco et al. 2018a; Frimat et al. 2015). Therefore, hydrogel techniques emerged as a promising solution to build 3D neuronal network in vitro for studying electrophysiology. The passive diffusion of what in a 3D hydrogel-neuron system with a thickness of 400  $\mu\text{m}$  supports high density neuronal culture survival in the hydrogel encapsulation (Cullen et al. 2007).

Multiple hydrogel-cell systems have been reported. Among them, Matrigel is one of the widely applied candidates. Matrigel is extracted from Engelbreth-Holm-Swarm (EHS) mouse sarcoma tumors and it is composed of ECM proteins as laminin, collagen IV, heparan sulfate proteoglycans, entactin/nidogen, and several growth factors. There are certain drawbacks associated with this natively derived matrix, including batch to batch variation, xenogeneic composition, diverse component variability (Aisenbrey and Murphy 2020; Caliarì and Burdick 2016). The applications also include, MaxGel ECM contains human extracellular matrix components including collagens, laminin, fibronectin, tenascin, elastin and a number of proteoglycans and glycosaminoglycans (Caliari and Burdick 2016). It has been reported to mix and modify the type-IV collagen to successfully realize 3D stem cell and neuron culture (Kim et al. 2017a; Lam et al. 2020). The system provides sufficient integrin binding agent that regulate cell growth, proliferation, and migration. The addition of MaxGel ECM into synthetic scaffold to improve the cell attachment was proposed (Lam et al. 2019). Different volume ratio mixtures were created and applied in 2D cell test and 3D encapsulation cultures. Therefore, there is a need to explore the practical solution dedicated to one's specific platform and research aim. The feasible 3D culture system should be able to integrate into our signaling platform. To address this, we tested and recorded the

neuronal growth encapsulated in 3 different hydrogel candidates, and on micro glass beads. The criteria for evaluation include: the provision of bioenvironment to support neuronal growth as 3D in our platform; the stability to maintain long-term neuronal culture, the evidence of substrate assisting network formation.

## **CHAPTER 2: STUDY OF AXONAL TRANSMISSION DURING PATTERNED STIMULATION ON AN ENGINEERED HIPPOCAMPAL NETWORK**

### **Background**

The human hippocampus plays a central role in the formation of episodic memory (Roy et al. 2017; Rolls 2010) and contributes to profound cognitive functions (Lisman and Redish 2018). In particular, the four main subregions involved in memory formation and consolidation are entorhinal cortex (EC), dentate gyrus (DG), Cornu Ammonis 1 (CA1) and CA3. Anatomical and behavioral studies together with electrophysiological investigation through in-vivo recording consistently show functional distinctions among the subregional layers (Roy et al. 2017; Langston et al. 2010; Masser et al. 2014), such as pattern identification from sparse primary input from EC to DG's large number of neurons (Chavlis, Petrantonakis, and Poirazi 2017; J. K. Leutgeb et al. 2007) and pattern completion in CA3 recurrent collaterals (Poli et al. 2018; S. Leutgeb and Leutgeb 2007). The divergent nature of the perforant path projections suggests that information originating focally in EC is distributed widely along the septotemporal axis (Cappaert, Van Strien, and Witter 2015).

To understand these functioning mechanisms, one must gain access to record the hippocampal neuronal activities at the network level. However, recording and decoding the signal with superb spatial and temporal resolution are not reachable in vivo, particularly in the axons that relay information from one region to the next. Reconstituting the living connections to study the electrophysiology in vitro in a controlled manner is vital for gaining

insight into the functional pathways in memory formation. Extensive works has demonstrated the high accessibility and practicability of cocultured neuronal network (Kim et al. 2017b; Poli et al. 2017). qPCR tests prove that the subregional cells maintain their identity in the reconstructed culture (Brewer et al. 2013). Poli. et al have demonstrated the ability of pattern separation on the 2-compartment co-cultures (Poli et al. 2018). But most of these investigations were limited to a two-compartment system, e.g., CA3-CA1 co-culture. This could lose some of the comprehensive network connections from other subregions that completion the circuit. A more integrated hippocampal network would give more accurate information close to in vivo.

Most of the questions about decoding the hippocampal functions arise from how the network is reacting to outside stimuli. Theta oscillation is a pivotal rhythmic component in hippocampus important for brain inter region communications (Lisman et al. 2017). Theta burst stimulation (TBS) recapitulates natural brain rhythms, and it has been particularly effective in stimulating Schaffer collateral axons into CA1 in hippocampal slice preparations to evoke long-term potentiation (Shimono et al. 2002). Valuable circuit architecture and dynamics could be explored further in this engineered hippocampal network with multisite recording of communicating axon functionally in response to TBS. Giving the fact that memories are distributed across multiple synapses, it is hard to establish clear-cut causal links between plasticity and outside stimulus, when we don't know the actual neurons that were stimulated by a behavior. Using the stimulus input distributed to a limited set of neurons or axons would better emulate one brain region taking information from others.

There is far more uncertainty about the routing of information in the brain circuit and the localized plasticity after the network is subjected to defined stimulus patterns. With our reverse engineered network, 4 subregions of the hippocampal formation are distributed into 4 chambers clockwise. Axonal connections are enabled by the microfluidic tunnels, and the electrical activity is sampled through the embedded electrodes. We designed the patterned TBS that was delivered at 3 sites in EC. Taking the advantages of axonal recordings in the micro tunnels, we specifically studied the axonal transmission between 4 subregions. There are several key questions we are trying to answer: 1) Is this network able to process the patterned stimulus and communicate accordingly between subregions? 2) How do the communications between subregions vary with stimulus and what are the meanings of those variations? 3) How reproducible is axonal transmission with repetition?

We used a simple digital quantification method that directly compare the temporal spiking patterns at the resolution of 3 ms (Poli et al. 2018; Chung and Edwards 2019), to down sample detected spikes recorded at 40  $\mu$ s resolution. We first demonstrated this in vitro hippocampal network uniquely processes the single site and multisite stimuli. Then we present the transmission plasticity changes with single-site stimulus and multisite stimulus. The subregional functionalities are expressed in axonal transmission, where responses in EC-DG were very dissimilar across 10 s repeats consistent with a pattern separation function. In contrast, responses in CA3-CA1 had the highest similarity, indicating pattern completion. Finally, using the defined stimulus and activity pattern, we determined the individual axons finishing pattern completion.

## Methodology

### Device fabrication and assembly

The microfluidic platform for 2D culture consisted of two main components: (1) a commercially available microelectrode array MEA120 (MultiChannel Systems, Reutlingen, Germany) with 120 low impedance electrodes and electrically insulated interconnects serving as the bottom substrate and (2) a custom designed and fabricated 4-compartment culture chamber integrated on top of the MEA120 (Fig. 2.1B). The culture chamber was made from Polydimethylsiloxane (PDMS) (SYLGARD™ 184, Dow, Inc.) with micromolding techniques. The master mold was fabricated with photolithography on two layers of thick photoresist (PR). The supporting substrate was a 4-inch silicon wafer cleaned with a brief dip in hydrofluoric acid (HF) followed by a thorough rinse in deionized (DI) water. In order to align the two PR layers, a set of chrome (Cr) alignment marks was first photolithographically patterned with lift-off technique on the wafer. Shipley 1827 positive PR was spin coated on the wafer with 4500 rpm for 30s to a thickness of 2  $\mu\text{m}$ , followed by a soft bake at 120 °C for 1 min and exposed through the alignment-mark mask in a mask aligner (Karl Suss MA6) under 10 KJ/cm<sup>2</sup> for 20 s. The exposed PR was then developed in MF-319 developer (MICROCHEM) for 45 s, rinsed with DI water and blow dried using a nitrogen gun. A thin layer of Cr (1000 Å) was deposited over the entire wafer in an E-beam evaporator and then lift-off in acetone. After the alignment marks were finished, two sequential PR layers were deposited and patterned. The first layer was 3- $\mu\text{m}$  thick SU-8 2000 negative PR. It was patterned and developed to form 10  $\mu\text{m}$  wide lines that were 3  $\mu\text{m}$  high, which would subsequently form the PDMS microtunnels after molding. In the finished

platform, these microtunnels would be used for isolating axons that would grow from one chamber to the connecting chamber through the microtunnels. The second layer was 500- $\mu\text{m}$  thick SU-8 3500. The photomask for this second layer was used to pattern the parts of the mold for the 4 main culture chambers separated by 400  $\mu\text{m}$  and were 500  $\mu\text{m}$  tall. These two photomasks were aligned to the Cr alignment marks to ensure correct feature definition. After developing the second PR layer, the wafer was hard baked at 150°C for 30 mins to further solidify and stabilize the SU-8 mold. Before the molding process, the mold was first vapor coated with release agent triethoxysilane (Gelest, Inc) for 2 hours. SYLGARD™ 184 Silicone Elastomer Kit (Dow, Inc.) was used at the recommended 10:1 mix ratio of the polymeric base and curing agent. After thorough mixing and degassing under partial vacuum, the mixture was poured over the mold wafer to slightly more than 500  $\mu\text{m}$  depth. A final degassing step was performed until all gas bubbles were visibly dissipated. To ensure a flat and even PDMS top surface, a PET plastic film was applied on top of the PDMS with a 355-gm weight added to make sure the PET film was in contact with the top surface of the SU-8 chamber mold. The PET film would also serve to ease the final demolding step. The entire assembly was then cured at 60°C for 12 hours in an oven on a shelf that had been carefully leveled. Finally, the demolding process involved gently peeling off the PET film, which would carry the PDMS piece with it. Each PDMS device was punched out and aligned onto the MEA120 substrate under a microscope.

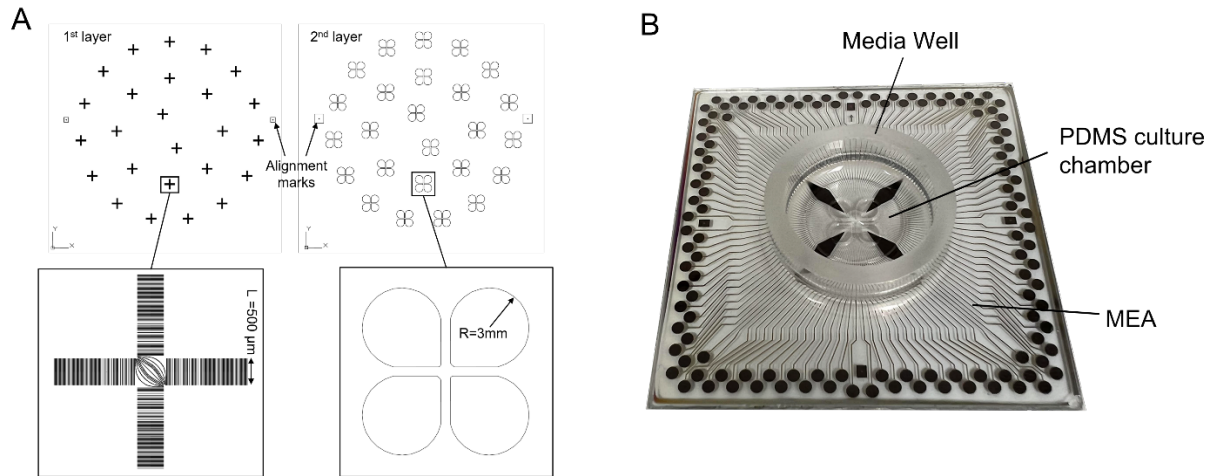


Figure 2.1 SU8 mold masks and the MEA-PDMS culture recording device **A**. Detailed mask design. Each mold wafer contained 28 PDMS devices. The 2-layer process included a thick SU-8 (500  $\mu\text{m}$ ) pattern that precisely defined the chamber height and lateral geometries and a thin SU-8 (3  $\mu\text{m}$ ) layer that defined the 10- $\mu\text{m}$  wide microtunnels that connected neighboring chambers. **B**. The 4-compartment culture chamber was aligned and attached to an MEA (MSC) under a microscope (not shown).

## Cell culture

To ensure device sterilization and the embedded micro tunnels adequately filled with media by capillary force, we performed the following surfaces preparation steps. The assembled MEA and PDMS device was cleaned with 70% ethanol and rinsed with DI water for 2 times. The liquid residue was vacuumed out and device was left dry for 1 hour. Then the device was treated with 35 mA Oxygen plasma for 2 mins to obtain the hydrophilic surface. Poly-D-lysine (PDL) solution (Sigma P6407, 0.1 mg/ml in water) was filled into each of the 4 chambers at room temperature overnight. On the second day, the PDL solution was vacuumed out and rinsed with DI water 1 time. The device was left in bio cabinet 1 hour for drying before dissection and cell plating.

The primary hippocampal cultures procedure is based on established lab protocol (Brewer et al. 2013). To this experiment design specifically, the whole hippocampus was removed from postnatal day 4 (P4) rat, then the 4 subregions (EC, DG, CA3, CA1) are separated respectively. The subregional tissues were processed into neuron suspensions with targeted densities: EC: 800; DG: 2500; CA3: 800; CA1: 1000 cells/ $\mu$ L. Subregional neurons were plated into 4 chambers on MEAs in neural basal media (BrainBits, Springfield, IL) medium (Brewer and Torricelli 2007) or BrainPhys plus SM1 (Stem Cell Technologies) to reach at the final densities of 330/1000/330/410 cells/ $\text{mm}^2$ . The final cell plating density ratio intends to mimic the in vivo anatomical density ratio for the subregions in hippocampus (Braitenberg 1981). Growth factors FGF2 and PDGFbb (Peprotech) were added at 10 ng/mL. Cultures were incubated in a humidified incubator with 5% CO<sub>2</sub>, 9% O<sub>2</sub> at 37 °C. Half of the culture medium was removed and replaced with the same volume of fresh medium every 3-4 days with 2x growth factors to replenish the original concentration during the first week only. Neuron growth was monitored and captured through phase contrast microscopy every 7 days. Cells at each of chamber that are roughly 400  $\mu$ m apart were monitored.

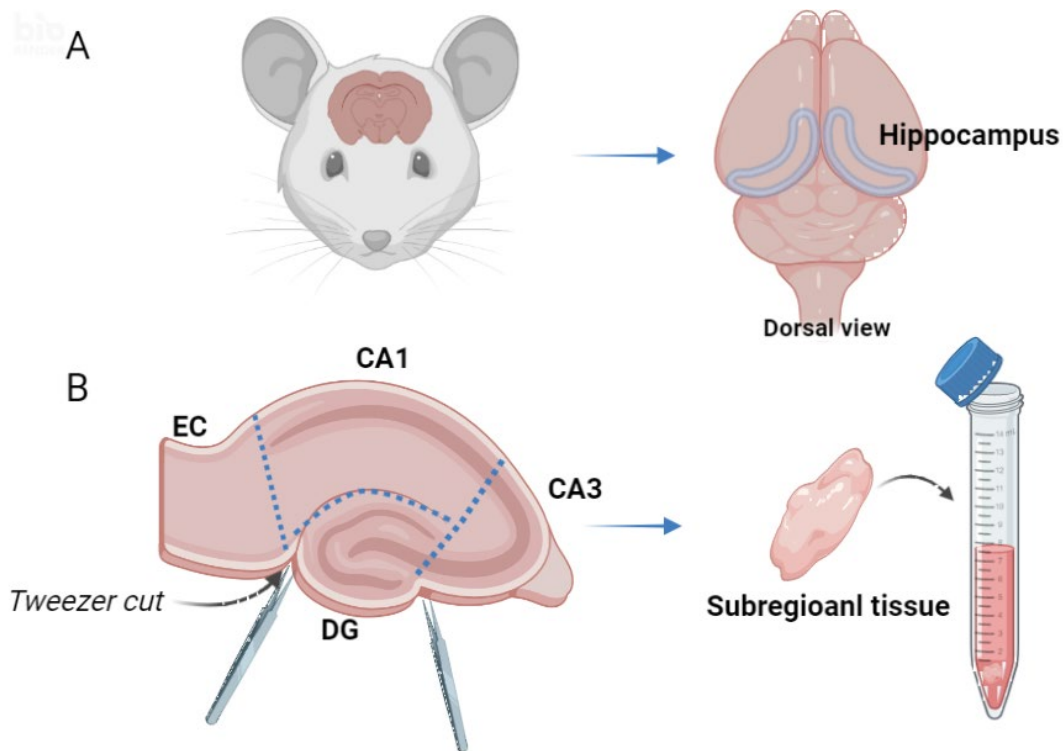


Figure 2.2 Hippocampal dissection illustration A. The whole hippocampus es identified and taken out from postnatal rodent. B. The subregion tissues are directly separated under the microscope as illustrated.

## Fluorescent imaging

To verify the presence of axons in the microfluidic tunnels, Calcein AM (ThermoFisher), a cell-permanent dye that stains the live neuronal cells was used. Approximately 2  $\mu\text{M}$  working solution was added to the cell culture and then incubate for 30 mins. A fresh media wash was done for 15 mins to remove the ester and reduce the background intensity. Bis-Benzamide (NucBlue, Thermo Fisher) that emit blue fluorescence bonds to DNA was used to identify the location of cell bodies and facilitate cell counting. 2 drops of Hoechst 33342 were added to the 1 mL media well, and then incubate for 15 mins. The dyes were excited with GFP and DAPI, respectively. Image acquisition was done on microscope with a Hamamatsu camera

(ORCA-flash 4.0, Hamamastu Photonics) driven by MetaMorph Basic software (Molecular Devices).

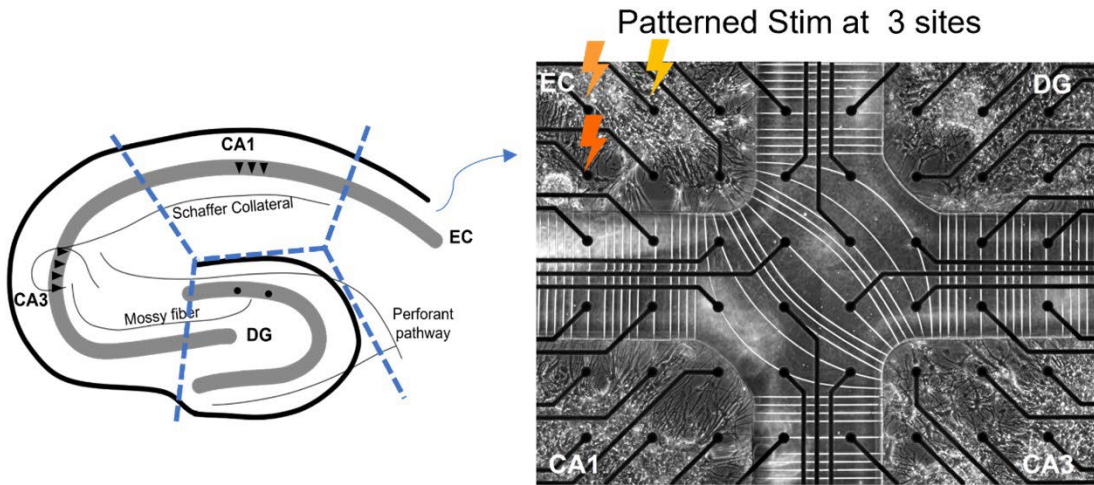
### **Electrophysiology and stimulating protocol**

The cultures were kept in the incubator for 3 weeks, which allows the sufficient differentiation, polarization of the neurons, and formation of the synaptic connections. The mature network ensures the electrophysiological recording with optimal active channel numbers.

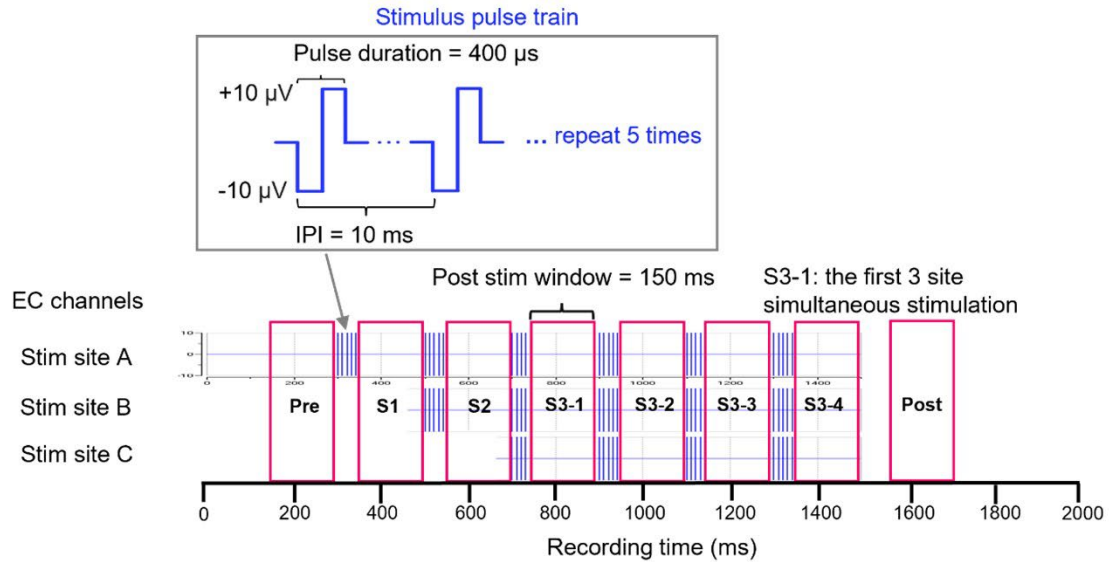
Design of the theta burst stimulation (TBS) pattern. To fully examine the axonal responses in each subregion of the reverse engineered hippocampal network, we delivered the patterned TBS to electrodes in EC chamber (Fig 2.3A). Because entorhinal cortex gates hippocampal formation in brain, the stimuli sent to EC would emulate the information entering the hippocampal network and being processed at downstream subregions. In specific, the high frequency pulse trains have 5 biphasic pulses that has 10 ms inter pulse interval (IPI), 400  $\mu$ s pulse duration (PD) and 10  $\mu$ V amplitude with negative pulse first. The trains are delivered at 5 Hz. 3 TBS are delivered to 3 electrodes (ABC) in a delay manner. The initial training of the network includes repetitions of 3-site stimulations. 3 distinct EC electrode channel combinations were chosen as stimulating sites, respectively. Each set of multisite combinational stimulations has 10 repetitions with 10 s intervals and 2 minutes breaks in-between the sets. To investigate the ability of pattern completion, a “partial-cue” signal is designed as the stimulus train only delivering to 1<sup>st</sup> and 2<sup>nd</sup> site (AB). These sets of stimulations are performed in the same temporal order after 9 minutes of initial training. The different repeats allow us to investigate and understand the ability of network ‘learning’

and axonal transmission plasticity change in different timescales, which are 200 ms, 10 s and 9 mins. The detailed stimulus pattern and recording timeline are in Fig 2.3 B, C.

### A. Hippocampus subregions and in-vitro network



### B. Designed Theta burst stimulation (TBS) pattern



### C. Timeline

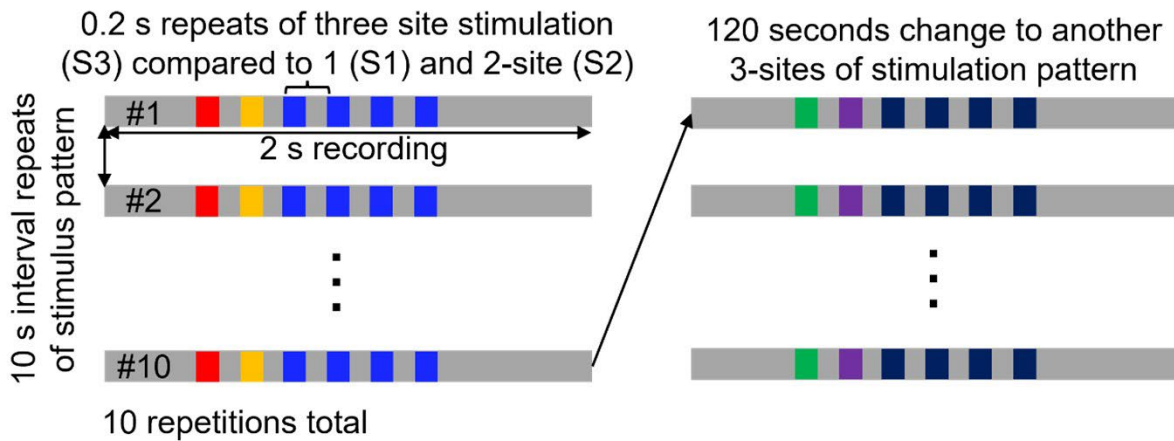


Figure 2.3 Reverse engineered hippocampal network and patterned TBS **A.** The 4 hippocampal subregions are plated into device chambers clockwise. **B.** The details of patterned TBS. **C.** The timelines about 0.2 s, 10 s, and 120 s repeats.

## Data processing

The raw data are collected through MC\_Rack (MultiChannel Systems). Then the files are converted into single channel files (.mat) from McsMatlabDataTools in MATLAB (MathWorks Inc.). Since the spike detection algorithm is based on the threshold detected from biological and thermal noise of the signal in the 200 ms contiguous windows, the artifacts from stimulation have the drawback tricking the algorithm and generate deviated noise level. Therefore, the 50 ms segments during the stimuli delivery are blanked out through all stimulated recordings.

The spikes in single channel were detected after the raw signal is filtered through 300 - 3000 Hz bandpass filter and then applying an optimal amplitude threshold calculated from Wave\_clus MATLAB toolbox (Quiroga, Nadasdy, and Ben-Shaul 2004). Because the axonal couplings and ion environment varied from tunnel to tunnel, the signal amplitudes have big deviations between the tunnels, usually range from tens of micro volts to few thousand micro volts. To optimize the spike detection performance from Wave\_clus, differential thresholds were chosen as 4.5 or 11 times of biological and thermal noise of the signal that was calculated for 200 ms contiguous windows. The spikes were detected with a refractory period setting to 2 ms.

The following processing is based on custom-written MATLAB scripts to realize certain functions. The spikes trains contain the information of how the neurons fires. It represents

the dynamics of neuronal activity. The spike train was used to characterize pattern separation in dentate gyrus (DG) on the scale of millisecond (Madar, Ewell, and Jones 2019a). Spike train synchrony is also an important measurement for in-vitro neuronal networks (Ciba et al. 2020). The detected spike trains are converted into spike vectors that have the number of spikes in the 3 ms bins.

### **Jaccard distance and similarity**

For quantifying the similarity and dissimilarity of the spike patterns, we used Jaccard distance (JD), calculation of the binary vectors derived from temporal response patterns. The activities being evaluated are based on each of the 150 ms post stimulus windows. Also 2 segments of same length before and after the stimulation were picked up as control, respectively (Fig 2.8B). They are labeled as 'Pre' and 'Post'. The binary vector converted from spike train has 50 \* 3 ms bins indicating whether spikes present in the bins. The calculation of JD between 2 vectors is defined in Equation (1). A detailed example is in Fig 2.8B. JD quantizes the dissimilarity between 2 pieces of activity while similarity is represented as 1-JD.

$$JD = \frac{j_{01}+j_{10}}{j_{01}+j_{10}+j_{11}} \quad (1)$$

### **Statistics**

Data analysis was performed using custom-written scripts in MATLAB (2020a), including functions from toolboxes. We performed one and two-tailed t-tests or ANOVA whenever the data were normally distributed. All values are reported as mean  $\pm$  S.E.M. unless otherwise noted. Statistical tests were appropriately used to assess significance (p-value < 0.05).

## **Results and Discussion**

### **Network formation on MEAs and optimization**

The phase contrast image shows the engineered hippocampal networks (Fig 2.4A). The locations and layout of the electrodes are seen as black circular dots. The PDMS chamber contains 279 microfluidic tunnels in total. In each orthogonal connecting subregion, many axons can grow through 67 tunnels, while 2 electrodes in each of 4 tunnels detect axonal activity and enable determination of the direction of propagation. The structure accesses about 6% of the inter-regional axonal activity for analysis. The diagonal EC-CA3 region has 11 curved channels and 5 of them have electrodes. These curved channels connecting EC to CA3 emulates the perforant path that allows direct connection and communication between these two regions (Fig. 2.4A).

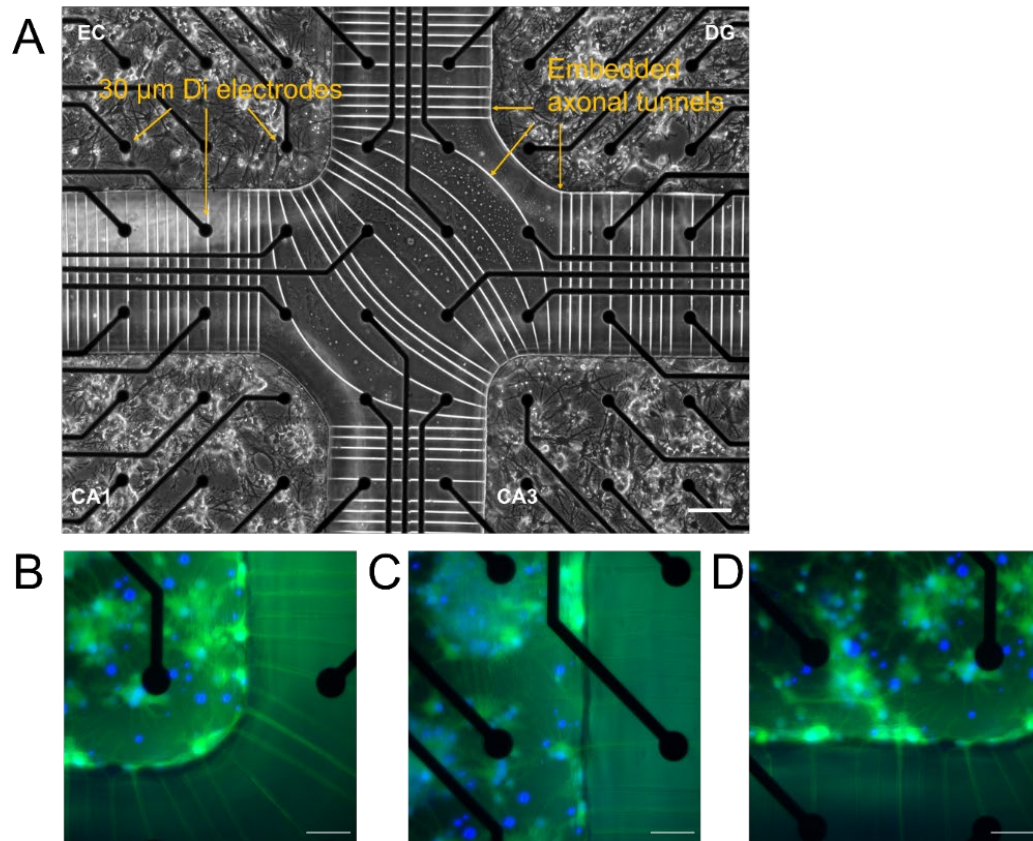


Figure 2.4 Phase contrast and fluorescent images of reverse engineered hippocampal network (Calcein AM (Green) stain for live neurons and processes and Bis-benzamide (blue) for nuclei). **A.** 4-chamber PDMS device is aligned with MEA where subregional neurons grow in corresponding chambers (DIV21). Micro tunnels connect adjacent regions and the electrodes in tunnels record axonal activity (Scale bar: 100  $\mu\text{m}$ ). **B-D.** Pictures show the axons grow into diagonal/horizontal/vertical microfluidic tunnels. While the cell bodies remain in the chambers (Scale bars: 50  $\mu\text{m}$ ).

Fluorescent images were taken to facilitate the final cell density validation and axonal connections demonstration. The initial cell densities plated were 330, 1000, 330, 410 cells/ $\text{mm}^2$  for EC, DG, CA3, CA1 respectively to proportionately represent the in vivo densities. The cell densities were calculated at mature stage by staining with Benzimidazole only (inset Fig 2.5). Results show the final densities for EC, DG, CA3, CA1 are 1580, 2750, 1430, 1900, cells/ $\text{mm}^2$  due to continuous neurogenesis. This density ratio resembles that

found in vivo (Kastellakis et al. 2015). The absolute density was determined empirically to optimize activity. We investigated a media change from current lots of Neurobasal/B27 to promote more activity. The BrainPhys media that changed the concentration of inorganic salts, neuroactive amino acids, and energetic substrate has been reported to improve the neuron synaptic function (Bardy et al. 2015). Neurobasal/B27 was optimized for neuron survival and outgrowth of embryonic neurons (Brewer, 1993). The initial cell culture should be maintained in Neurobasal/B27 for one week and gradually change into BrainPhys. We found that all 4 subregions increased their active channel numbers from day 2 to day 8 (Fig. 2.6). Even though the error bars are relatively high due to array-to-array variation, the active channel numbers are significantly higher than the day at change beginning. The effect of substrate treatments on neural growth has also been examined. We plated same cell suspension at on glass slips with different treatment besides PDL coating, and the cell densities on the slips were monitored at 3 check points. 3-glycidoxypropyl-trimethoxysilane solution (3-GPS) (Boehler et al. 2012), which is a silanizing linker, helps binding polylysine on to glass surface covalently has the highest survival. By comparing the viability on substrates processed with or without O<sub>2</sub> plasma, we confirm that plasma treatment before plating is important to maintain the cell viability (Fig. A1).

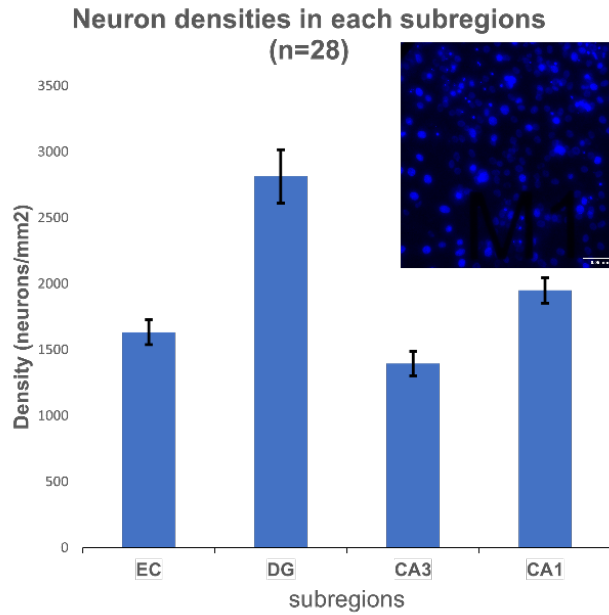


Figure 2.5 Cell densities in the mature hippocampal network (DIV 21)  
 It shows 4-compartment coculture neuronal reconstruction at day 21 maintains the cell densities with physiological ratio approaching 33:100:33:41 (n = 7 arrays \* 4 fields).

### Active Channel Numbers in BrainPhys Media Change

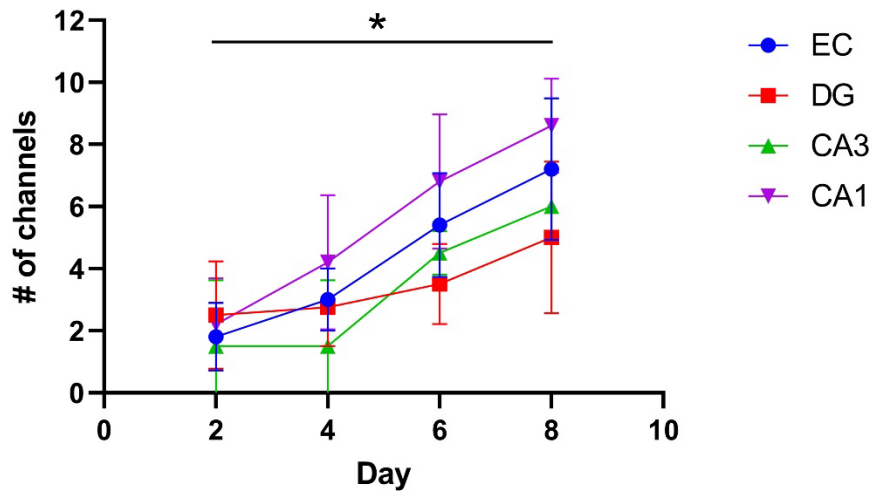


Figure 2.6 The active electrode numbers increased after BrainPhys Media Change  
 T tests show significant difference between day 2 and day 8 at CA1, EC regions (P<0.05), and increased trends for 4 regions.

## **Analysis of axonal activities in response to patterned TBS**

To answer the questions how hippocampal functions such as pattern completion or separation are performed in each of hippocampal subregion, it is critical to investigate and understand what kind of pattern is generated, transferred, and stored. However, it is very difficult to monitor these processes and massive information transfer in vivo. In our experiments, the well-defined structured culture allows us to gain the axonal spiking in each subregional tunnel. Axonal responses in micro tunnels during patterned stimuli are interrogated between four subregions to reveal the information transfer.

The axons growing in micro tunnels fire spikes and cause the electric charge flows. The high impedance in the tunnels give amplifying effect and the potential changes are clearly recorded by the 30  $\mu\text{m}$  diameter electrodes at the bottom of the tunnels. The amplitude of the spikes approached 0.5 mV (Fig. 2.8B). Since the 2 electrodes in the same tunnel record the same 1-3 axons with variation in axon-electrode coupling, the recorded spiking is not independent (Fig. 2.7B), the more active channel between the two was sorted out to represent the tunnel activity. We extensively investigated the single channel signal with tagged detected spikes at different thresholds of detection. The optimized threshold chosen for spike detection was greater than -4.5 or -11-fold times the standard deviation of the noise. The raw analogue signals are the direct evidence to prove the calculations in the following sections.

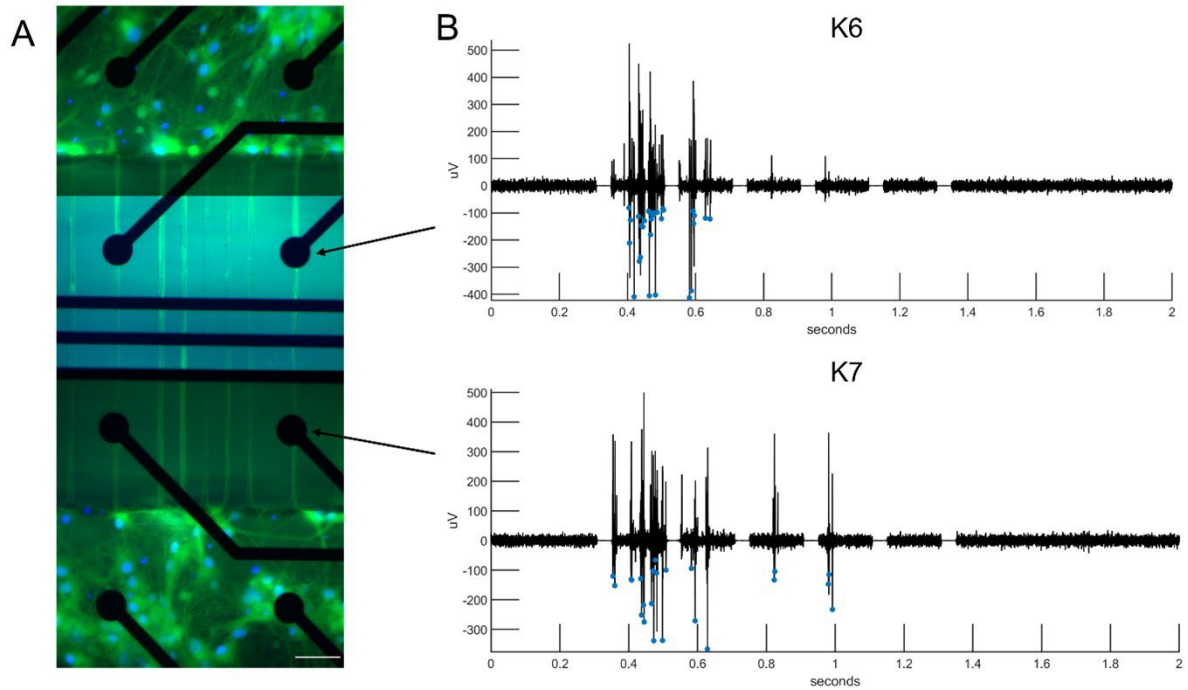


Figure 2.7 Images of tunnel electrodes and recordings of axons connecting adjacent regions **A.** Fluorescent image shows the axons grow into the micro tunnels and connect two subregions. Cell bodies locate only in chambers. **B.** Two electrodes in the same tunnel record activities from same axons. Electrode with more spikes was selected.

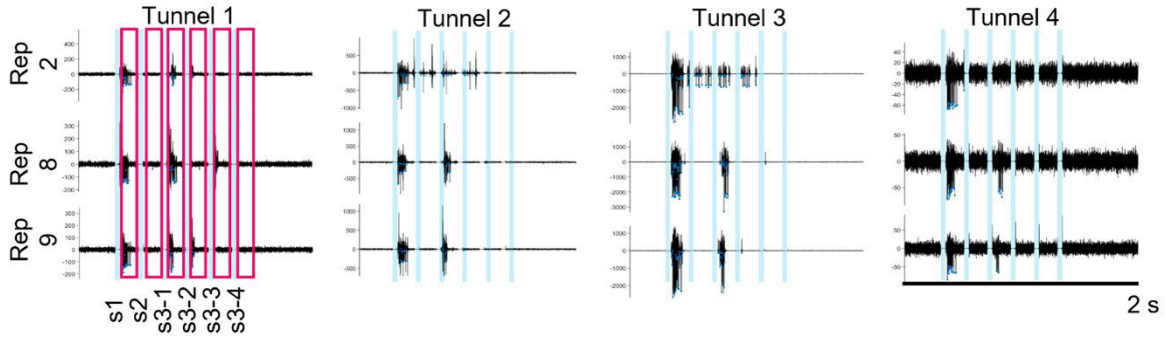
In this work, we used a simple metric to quantify the spiking temporal pattern's similarity level including between-site similarity, between-repeat similarity and between-tunnel similarity. These calculations are interpreted into the understanding of information uniqueness, axonal transmission plasticity at different timescales, and tunnel synchrony.

**Differences in spike patterns evoked by 1,2 and 3-site stimulation using Jaccard distance.**

The stimulus evoked responses are seen in the 150 ms post stimulus window (red box), and site specified stimuli are marked at the blue bar (Fig 2.8A). The selected examples show 4 parallel tunnels in CA3-CA1 that single site S1 to multisite S3 stimuli evoked at 3 repetitions.

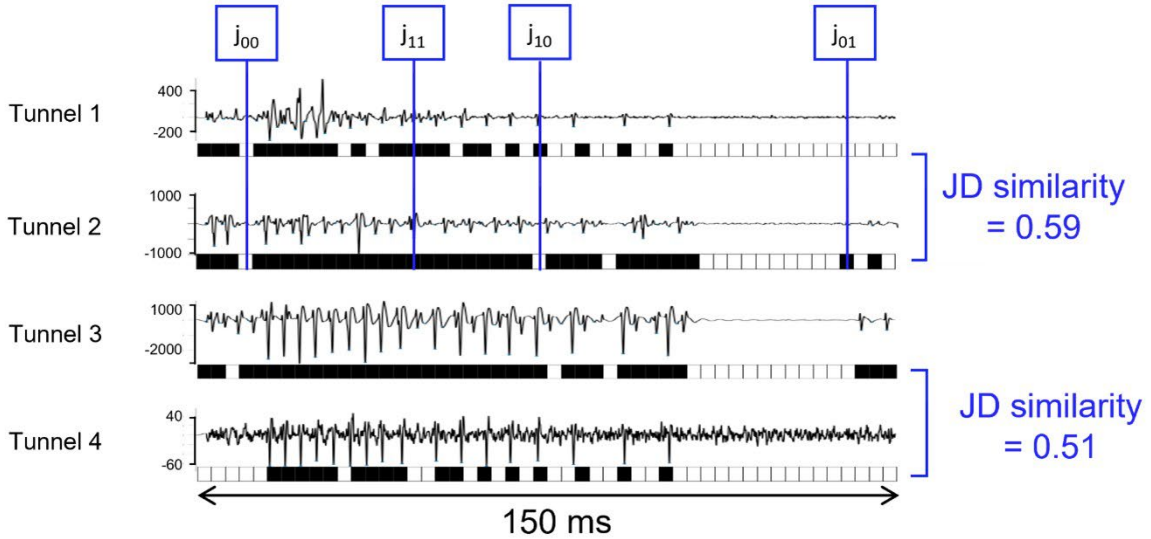
The zoom-in 150 ms analogue signal shows the activity pattern in each individual tunnel. Four tunnels have somewhat synchronized activities with varied amplitudes from tunnel to tunnel, which ranges from  $-50 \mu\text{V}$  to  $-2000 \mu\text{V}$ . That's mainly because the axon-electrode contact varies (Fig 2.8B). In tunnel 2, there is clear evidence of two axons, one with amplitudes around  $-200 \mu\text{V}$  and the other around  $-800 \mu\text{V}$  at their peaks. We quantified these response differences by converting this analogue signal to a binary 'digital' vector. By empirical variation to maximize the Jaccard distance between two tunnels, the optimal bin size was set as 3 ms, while a bin size of 10 ms or larger was not sufficient to resolve differences in temporal pattern variations. This setting would better represent the dynamic diversity of response patterns than those of 50 ms binary window or larger. The example shows the single site stimulation evoked similar patterns of 0.59 across tunnels 1 and 2, while a much less similar response of 0.4 was seen after 3-site stimulation S3-1 for tunnels 1 and 2 (Fig 2.8C), apparently blocking the larger spikes.

### Selected repetitions of 4 tunnels in CA3-CA1



### B. Jaccard distance calculation and zoom-in evoked activities in 4 tunnels (150 ms) Rep 2 S1

$$JD = \frac{j_{01} + j_{10}}{j_{01} + j_{10} + j_{11}} \quad \text{Similarity} = 1 - JD = 1 - \frac{15}{37} = 0.59$$



### C. Rep 2 S3-1

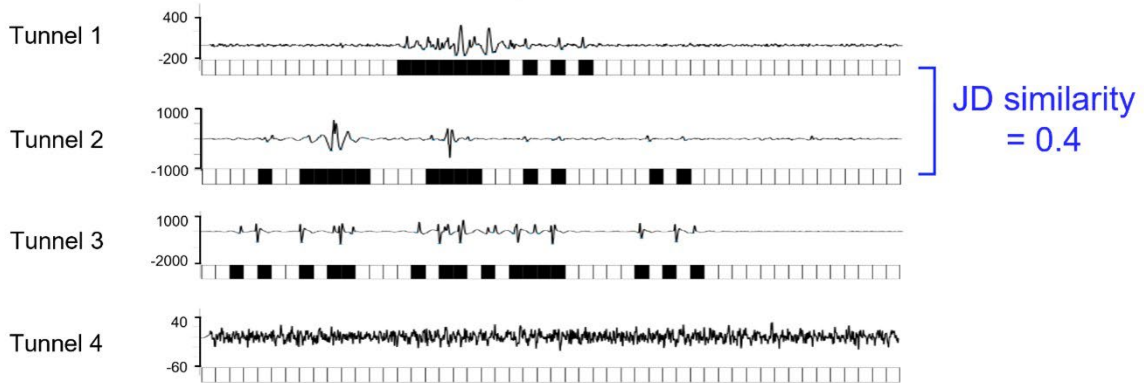


Figure 2.8 Selected examples of analogue data in 4 tunnels and the Jaccard Distance (JD) calculation **A**. The stimulating sites evoked synchronized activities in subregional tunnels with example from array 33152, stimulating sites B3A5C4, region CA3-CA1, repeated recordings (repetitions) 2, 8, 9. Seven out of 10 repetitions have activities. Blue boxes represent the stimulus train timings, red box represents one 150 ms post stimulus window expanded in **B**. **B**. The binary Jaccard vectors are determined from the presence (black boxes) or absence (open boxes) of spikes in 3 ms bins at the thresholds of 4.5 or 11 std noise. Jaccard distance calculation represents the dissimilarity between 2 vectors. Zoom-in 150 ms activity window shows spike patterns in 4 tunnels. Stimulation at a single site evoked distinct patterns of activity in axons between CA3 and CA1. **C**. With the first 3-site stimulation, (S3-1) at Rep 2 the large spikes from S1 are blocked resulting in a less similar pattern of activity in each of the four tunnels from the same axons.

### **Axonal transmission in tunnels between subregions carries unique patterns in response to patterned stimulation in EC.**

We first investigated the spiking patterns of each 150 ms post stimulus window following stimulation at a single site, two sites as controls for the 3-site stimulation. The 3-site stimulation was repeated four times with 0.2 s delays to be able to evaluate the reliability of responses, all compared to the pre-stim and post-stim activity patterns as ground controls. Each of the four subregions has 4 tunnels to sample from activity between the adjacent subregions. For example, in the tunnels between CA3 and CA1 (CA3-CA1), responses evoked by single site stimulation (S1) could be compared between the same axons to indicate somewhat distinct patterns between the two kinds of patterned stimulation (Fig 2.9A). The 2-site stimulation that included the first site produced strong inhibition and no spikes (not shown). Adding the third site, with the two previous sites of preceding stimulation evoked a robustly different response. To evaluate this pattern differences, we applied a digital method of comparing binary temporal spiking using Jaccard distance (JD, see Methodology) for dissimilarity and  $1 - JD$  for similarity. The JD calculations were performed for each tunnel.

Results for this array show 4 tunnels have S1/S3 dissimilarity around 0.8 and dissimilarity close to 1 between S3 and S2 (Fig. 2.9B). Also, neurons code the information in firing rate being widely studied in vivo and different neuron assemble firing can be characterized with different ISI distribution (Vakilna et al. 2021). We applied the ISI computation by log-log scale cumulative distribution and presented the S1/S2/S3 response ISI into 3 lines (Fig. 2.9C). ANOVA test shows their slopes are significantly different.

Since the brain functions as group of neurons, and neuronal ensemble exists functional connectivity (Poli, Pastore, and Massobrio 2015). The patterned stimulus delivered at multiple sites could cause activation of different neuron groups. Thus increased the complexity of presynaptic activities, which contribute to the distinct patterns after S3 compared with S1 or S2. Overall, the 2 quantification methods fully demonstrated that the responses from single, double, and triple EC input sites are unique and prove the engineered network is able to process these stimulus patterns and communicate uniquely between subregions.

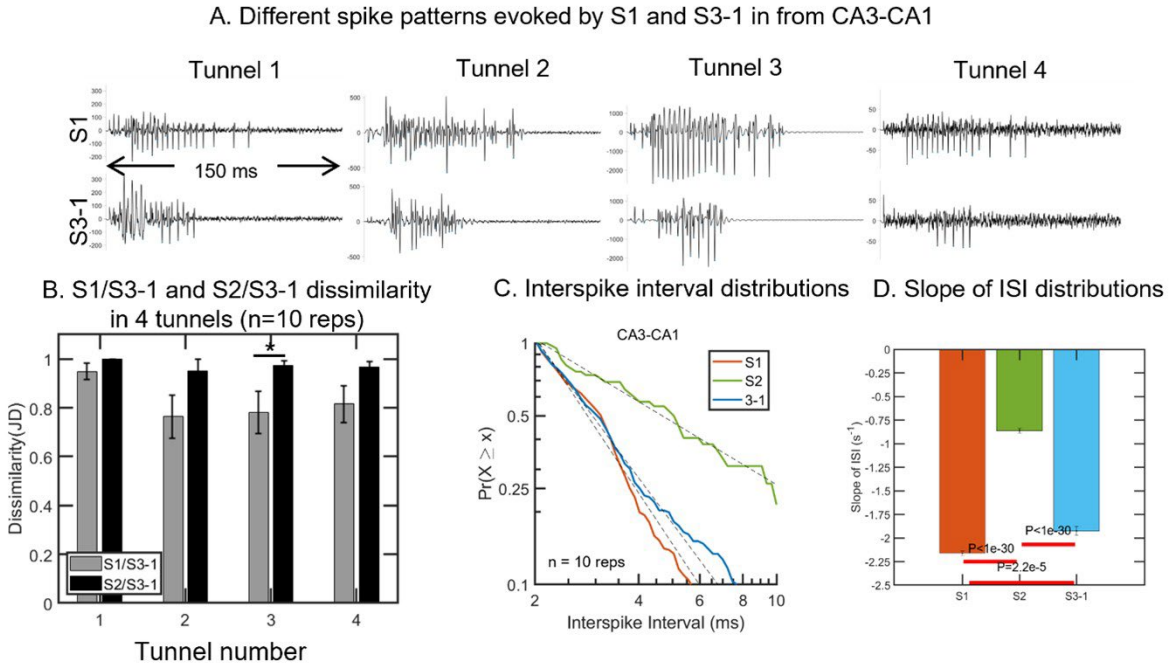


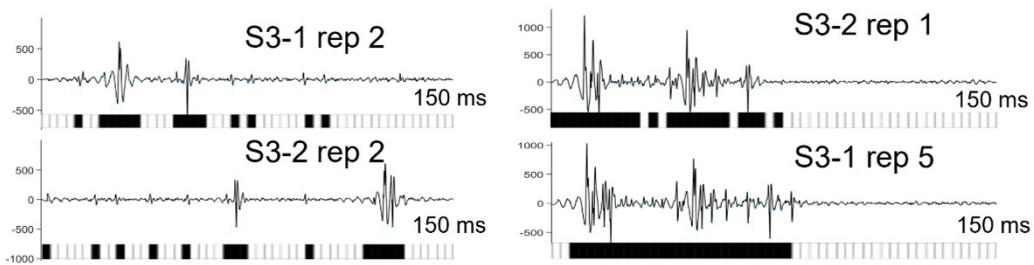
Figure 2.9 Uniqueness of 3 site pattern stimulation **A.** 150 ms raw spike patterns show the differences from the activities caused by S1 and S3-1 in 4 parallel tunnels (F9, F10, G11, G12 of array 33152). **B.** Dissimilarity of S3-1/S1 and S3-1/S2 calculated in 4 tunnels. The subregional mean is calculated from 10 repetitions. 3 ms bin size. One tail t test show that the 4 tunnels all have S1/S3-1, S2/S3-1 dissimilarity greater than 0 ( $p < 0.001$ ). t-test shows only tunnel 3 was significantly different between S1/S3-1 and S2/S3-1 dissimilarity (zero bins were redacted). Add S1/S3-1 as third bar for each tunnel **C.** Cumulative interspike interval log-log distributions of the activities from S1/S2/S3-1 reveal large differences in slopes of the distributions. **D.** The slopes of fitted lines on cumulative ISI distributions showing differences with significant p values from ANOVA for each kind of stimulation.

**Short-term (0.2 s) repeated stimulation patterns do not replicate patterns of spike responses but cause dissimilar responses.**

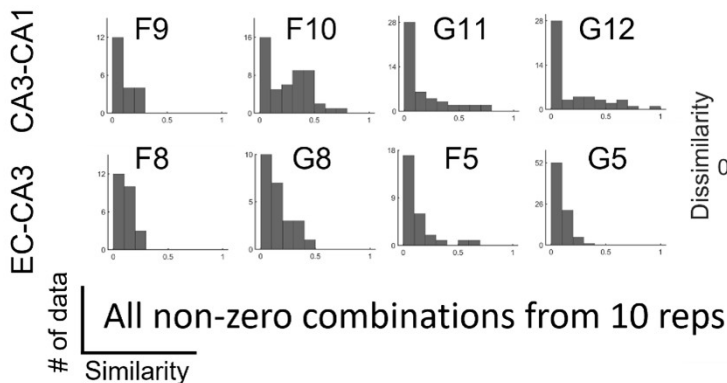
The designed theta burst stimulation was repeated at three sites four times (S3-1, S3-2, S3-3, S3-4), which allows us to investigate response reliability and short-term plasticity associated with identical stimulation repeats. We computed the similarity (1-JD) between the responses by S3-1 and S3-2 pair wise. Examples show a low similarity pair case (0.17) and high similarity pair case (0.74) (Fig. 2.10A). Using all non-zero combinations from 10

repeated recordings, we plotted the similarity distribution histogram based on single tunnels in regions. Result shows a large population of low similarity (0-0.1), and there also exists variations of distributions from the 4 tunnels in the same region (Fig. 2.10B). The dissimilarity of same site repeats has been calculated for all regions, and the result shows subregional bars are over 0.7 with small errors. High dissimilarities are also seen in comparison between S3-2/S3-3 and S3-4/S3-3 (Fig A2). The results indicate the successive same stimulus evoked a strong different pattern than the previous.

A. Representative activities (G11) showing limited similarity evoked by sites repetitions  
 Similarity = 0.17 example      Similarity = 0.74 example



B. Variation in similarity between S3 site repetition in different subregions have different distributions



C. Short timescale site repetitions evoked dissimilar activities (n = all non-zero combinations)

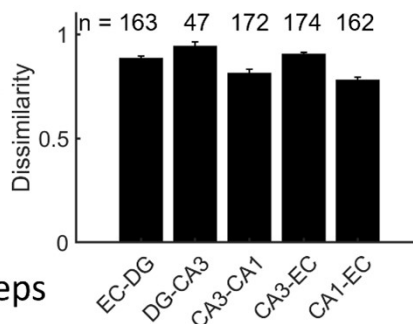


Figure 2.10 Dissimilar responses from 3-site stimulation presented at 0.2 s repeats **A.** Representative activities (electrode G11, array 33152) showing limited similarity evoked by sites repetitions. **B.** Variation in similarity between S3 site repetition in different

subregions (EC-CA3, CA3-CA1) have different distributions. **C.** Short timescale site repetitions evoked dissimilar spike time distributions of activity (n = Pairwise combinations of 4 tunnels/subregion times 10 repeats (S3-1) times 10 repeats (S3-2)). Unresponsive stimulations were excluded.

### **Spiking patterns from 10 s stimulus repeats express subregional functionalities.**

To evaluate the effect of repeated stimulation and axonal persistence of plasticity of spiking patterns, the same S1/S2/S3 stimuli was repeated 10 times at 10 s intervals. We found the complex of spiking patterns varied with repetitions, which is consistent with well-known trial-to-trial variability (Madar, Ewell, and Jones 2019a; Sasaki et al. 2006). To evaluate the chance level of the response similarity, we performed a Monte Carlo simulation with 1000 trials. In the simulation, similarity between randomly picked channels are pairwise computed. For both single site and three site responses, the chance levels are  $0.13 \pm 0.001$ , and the similarities in same tunnel between repeats are  $0.48 \pm 0.03$ , clearly above the Monte Carlo chance (t-test above chance,  $p=8e-10$ ) (Fig. 2.11A). Compared to single-site stimulation, similarity dramatically decreased to  $0.24 \pm 0.05$  for multisite stimulation (t-test above chance,  $p=8e-7$ ; t-test against S1,  $p=0.027$ ). By examining the row signals of the 10 repeats, EC-DG had relatively unique patterns in each repeat (Fig. 2.11C), compared to CA3-CA1, which had more similar patterns (Fig. 2.11D). Compared to responses from single site stimulation (S1), three-site stimulation in EC evoked lower similarity responses in the same CA3-CA1 tunnel (Fig. 2.11E).

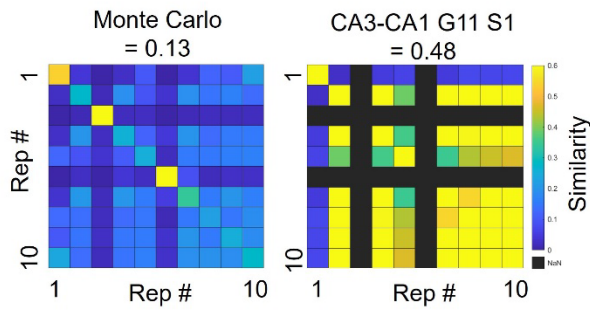
Next, we examined the reproducibility of responses in each of the subregional axon communications in the trisynaptic circuit based on their responses to the 10 s repeat stimulations. For the group of data from the four tunnels in the same subregion, we found

that for single site S1, EC-DG had a significantly lower similarity than chance ( $p < 1e-10$ ). CA3-CA1, CA3-EC and CA1-EC were significantly higher ( $p < 1e-20$ ,  $p < 1e-6$ ,  $p < 1e-9$ , respectively) (Fig 2.11F). The similar patterns evoked by 10 s repeats at these three regions indicate some degree of persistent change or plasticity. The differences in similarity between subregions demonstrates different degrees of output persistent similarity between subregional processing. The multisite stimulation 10 s repeats have lower similarities in DG-CA3, CA3-CA1, CA3-EC compared to single site. It is likely these regions participated in functional input discrimination. Moreover, CA3-CA1 and CA1-EC have similarities are over chance ( $p < 1e-4$ ,  $p < 1e-9$ ), indicating higher levels of persistence to three-site stimulation than single site.

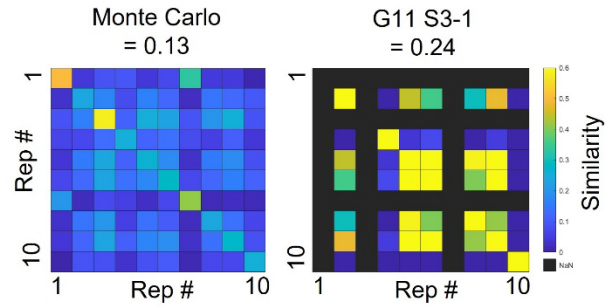
One way to interpret these results is in terms of opposing features. Two features of neural networks could contribute to the properties of this system: deterministic and stochastic contributions to trial-to-trial variation (Faisal, Selen, and Wolpert 2008). Compared to the unique responses from 0.2 s stimulus repeats, we do find axons persist in firing similar spiking patterns at 10 s repeats (Fig. 2.11D, F), suggestive of enduring plasticity changes for a probabilistic determinism. However, the least similar pattern at EC-DG renders a similarity lower than the chance level (Fig. 2.11F), implying subregional intrinsic properties for generating less overlap patterns, contributing to pattern separation (Yassa and Stark 2011; Madar, Ewell, and Jones 2019b; Poli et al. 2018; Chavlis, Petrantonakis, and Poirazi 2017). Pattern separation is thought to extract a subset of features from a complex input to aid downstream significance testing for principal components and novelty in CA1. This could seem stochastic, but also could represent deterministic selection of specific features.

The highest similarity seen in CA3-CA1 could be reasoned from the anatomical fact that CA3 neurons prominently reconnect to themselves through recurrent collaterals. Therefore, the outputs of CA3-CA1 are more similar across repeats. These results imply that different subregion endogenous properties could be expressed in our heterogenous network to demonstrate subregional functionality. Applying JD metrics, the temporal pattern robustly demonstrates enduring plasticity in the inputs to CA3-CA1 axons and the completion of the loop through CA1-EC. Yet the levels of similarity in spike patterns here are far below deterministic standards of computers.

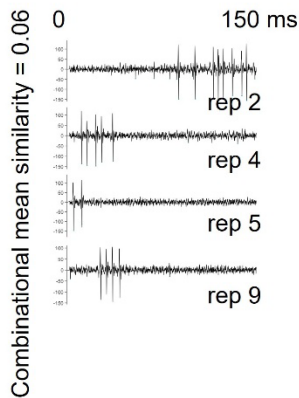
A. Similarity between repeats chance level and S1



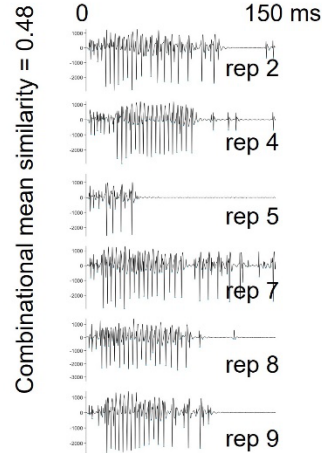
B. Similarity between repeats chance level and S3-1



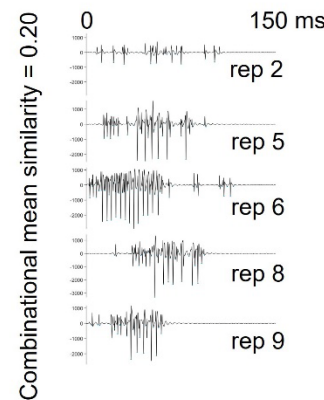
C. EC-DG channel G3 S1



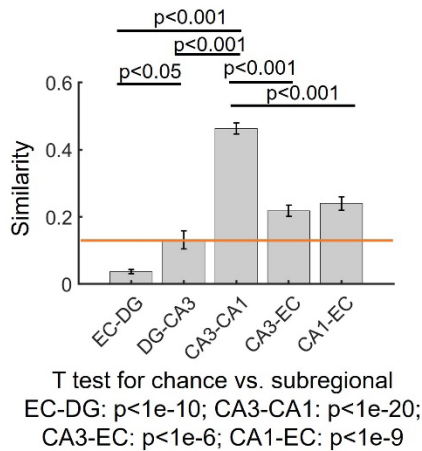
D. CA3-CA1 channel G12 S1



E. CA3-CA1 channel G12 S3-1



F. S1 10s stimulus repeats similarity at 5 subregions



G. S3-1 10s stimulus repeats similarity at 5 subregions

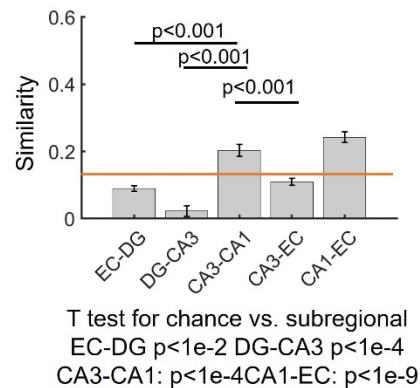


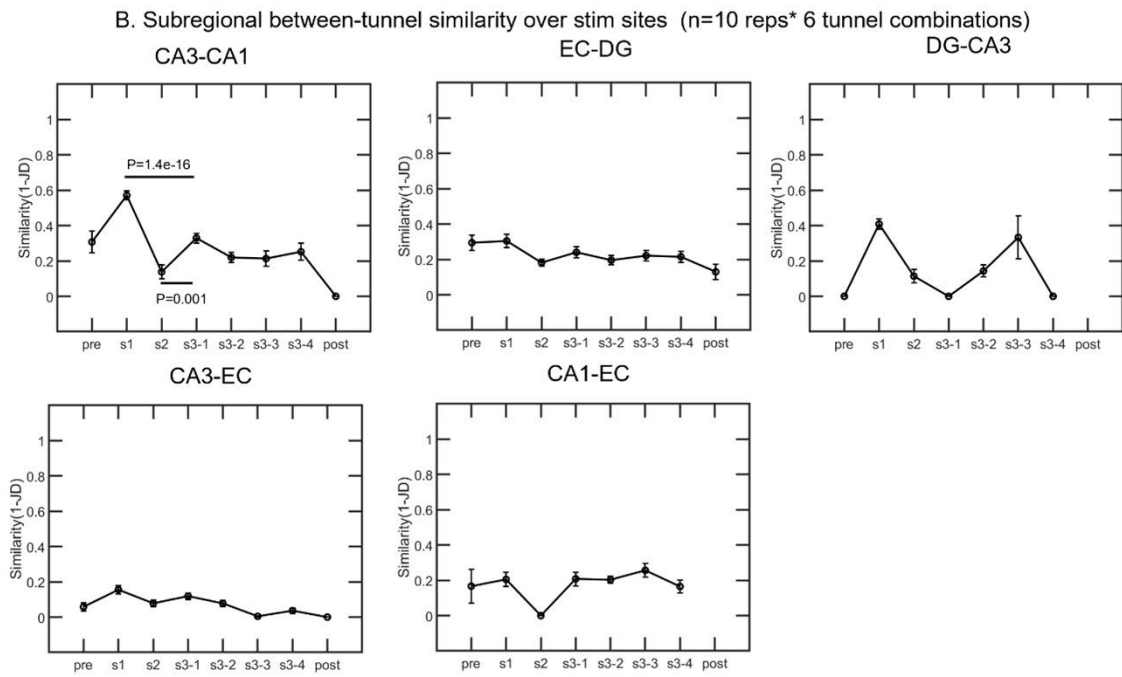
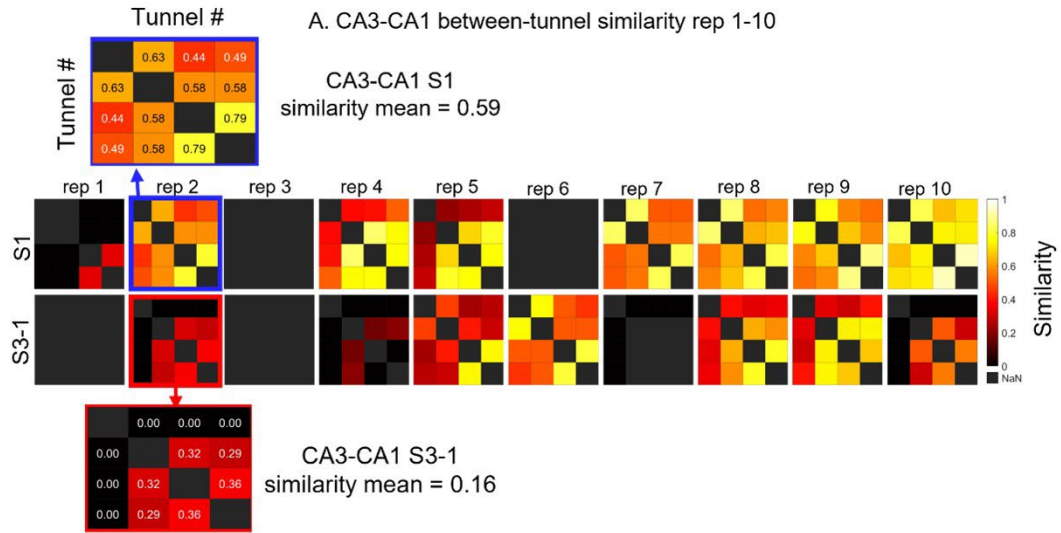
Figure 2.11 Comparison of axon-to-axon activity from 10 s repeats between subregions reveals major differences in CA3-CA1, EC-DG **A**. An example of S1 similarity chance level and single tunnel (G11, Array 33152) has greater between-rep similarity. **B**. Same comparison as a, notice the chance level keeps same but multisite has lower repeatability. **C-D**. Analogue signal shows S1 activities at EC-DG and CA3-CA1: almost totally different patterns in each repeat at EC-DG. More similar patterns at CA3-CA1. **E**. Multisite S3-1 has

lower level of similarity at CA3-CA1. **F.** Single site 10 s repeats similarity varied from region to region ( $n = 4$  tunnels \* 10 reps \* 10 reps combinations), with EC-DG significantly lower (t test:  $p < 1e-10$ ) and CA3-CA1, CA3-EC, CA1-EC significant higher (t test:  $p < 1e-20$ ,  $p < 1e-6$ ,  $p < 1e-9$ , respectively). Orange line: chance level. Stars and bars show ANOVA significant level between regions. **G.** Multisite S3-1 10 s repeats similarity level is lower while CA3-CA1 and CA3-EC are significant above chance (t test:  $p < 1e-4$ ,  $p < 1e-9$ ).

**Between-tunnel similarity indicates different information transmitted between tunnels. Most similar output in CA3-CA1 is reduced by patterned multisite stimulus.**

Brain function is partly realized through synchronized activities (Nikolić et al. 2012)(Gollo et al. 2014). Measuring the synchrony is enabled in our system by comparing activity between individual axons sampled in the tunnels between subregions. In our design, 4 tunnels with electrodes that structurally connect adjacent regions. The similarity of activities in these tunnels indicates how synchronized outputs are with each other. The similarity between two tunnels was assessed by pairwise tunnel similarity using the Jaccard distance (Methods, 1-JD). The averages from all tunnel combinations are used as subregional similarity. In the results, the S3-1 has less similar output at CA3-CA1 than S1 as color coded (Fig. 2.12A) in most of the repeats. Averages for each of the five subregions showed distinct variations in synchrony among axons (Fig. 2.12B), suggesting each subregion transmits information in a unique fashion. In CA3-CA1, each kind of pattern stimulation (single, two-site or three-site) evoked distinct between-tunnel similarities, further indicating that this output distinguishes different kinds of input as would be needed for novelty detection. In EC-DG, the stimulus evoked between-tunnel similarity didn't change much from the 'pre' control and overall showing a decreasing trend, indicating a relatively stable synchrony. Interestingly, for the output of DG-CA3, the synchrony levels by different sites start to

express distinguishment, where S1 increased the synchrony a lot (0.4), then S3-1 reached 0 synchrony, meaning a much less correlated output. The similar stable and decreasing trend is seen in CA3-EC where S1 slightly increased the between-tunnel similarity, then it kept the level at 0-0.1, might be the evidence that EC directly innervates CA3 with less synchronized activities instead of having the output from CA3 which can have relatively higher synchrony for specific sites. As for CA1-EC, there was a drop on S2, which might be caused by sparse data from S2. But the other sites evoked activities at a similar level of tunnel synchrony as the 'pre' and 'post' control, implying a stable finish of the circuit. In the parallel comparison of S1 and S3-1 (Fig. 2.12C), four subregions show strong tunnel synchrony at S1 is significantly higher than S3-1 replace stars on graph with these p values (EC-DG  $p < 0.05$ , DG-CA3  $p < 0.001$ , CA3-CA1  $p < 0.001$ , CA3-EC  $p < 0.05$ ). CA3-CA1 axon outputs in response to single site stimulation were most correlated at 0.6. While at DG-CA3, multisite S3-1 causes zero similarity, indicating unique axonal transmission. For CA1-EC, the synchrony with S1 and S3-1 have no significant difference compared to EC-DG and CA3-EC have the differences. These results support the within tunnel repetition similarities in the previous section, that the network processes single site stimulation with less uniqueness both temporally and spatially, compared with multisite stimulus. The auto-associative network in CA3 contributes to the highest CA3-CA1 similarity.



**C. S1/S3-1 Similarity in 5 subregions (n = 10 reps)**

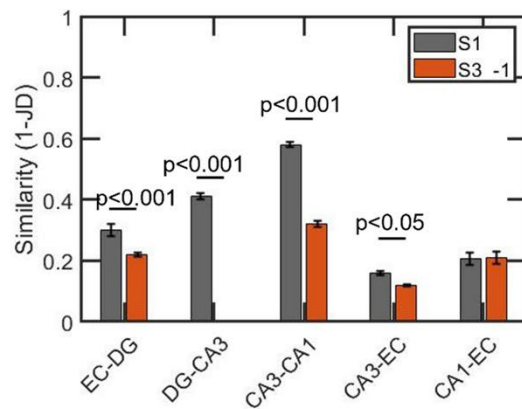


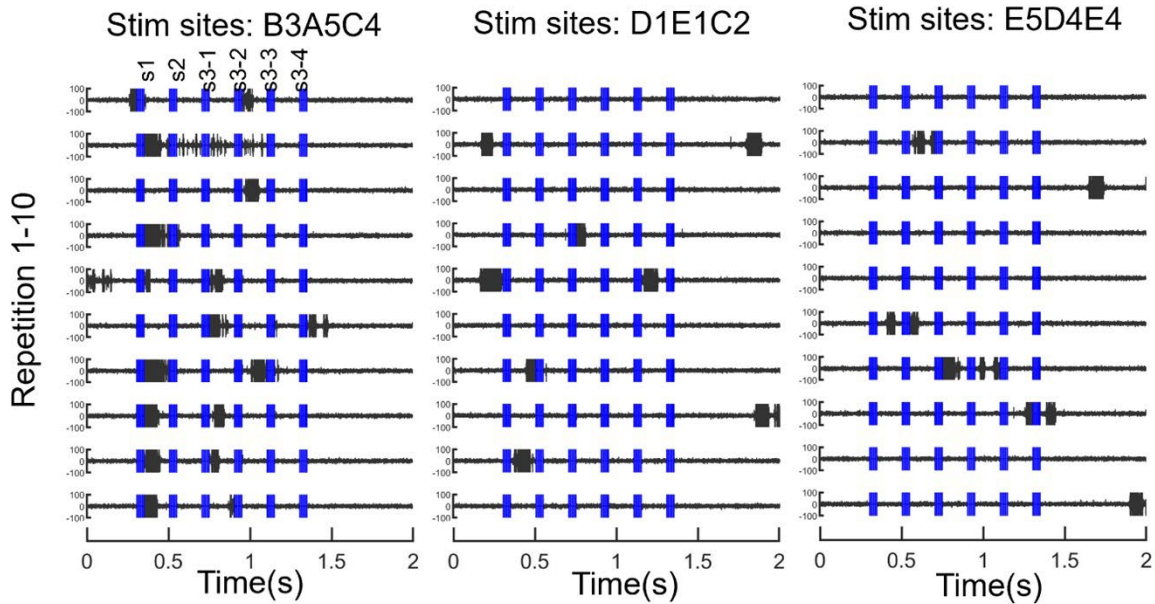
Figure 2.12 Between tunnel similarity and subregional differences to assess synchrony **A.** Between-tunnel similarity for the activities evoked by S1 and S3-1 are calculated as the pairwise combinations among each of the four tunnels for each repetition, respectively. S3-1 has less similar output at CA3-CA1 than S1. **B.** Stim sites S1/S2/S3-1 evoked distinct similarities ( $p=2.9e-16$ ,  $p=0.001$ , respectively). Different similarity trends are seen in different subregions. **C.** S1/S3-1 activities have different levels of between-tunnel similarity across subregions, CA3-CA1 creates the highest similarity (synchrony). (Array 33152)

### **Evoked patterns of axonal activity discriminate stimulation at different sites**

Following the first set of 10 repeats of 3-site stimulation, 2 more stimulation repeats were performed involving totally different site combinations in EC. The burst patterns vary greatly in an example of CA3-CA1 channel F11 spiking patterns from 3 different stimulation sites for 10 repeats (Fig. 2.13A 1, 2, 3). The 150 ms analogue signal further emphasizes differences of spiking patterns of S1 from different stimulation sites (Fig. 2.13B). Upon pairwise dissimilarity calculation, a large portion of the data falls into the high dissimilarity range of 0.9 to 1. Specifically, 60% S1, 77% S2 and 51% S3-1 activity metrics were above 0.9 dissimilarity, meaning unique patterns of activity from different stimulation site combinations (Fig. 2.13C). The statistics further confirmed the similarity differences caused by single site to multisite (S1, S2, S3-1) (Fig. 2.13C).

As Hebbian theory stated, neurons fire together wire together, with groups of neurons being the process unit. When different patterns of input stimuli enter the network, different neuronal ensembles are recruited for transmitting and processing that input. Therefore, the variability seen between different stimulation sites likely reflect engagement of different ensembles of neurons. Despite being potentiated by the TBS stimulating protocol at 2 min interval, the axons between subregions are still capable to transmit unique information.

A. CA3-CA1 channel F11 2s raw data from 3 stimulating site combinations



B. Zoom-in CA3-CA1 F11 S1 150 ms activity from different stim sites showing distinct patterns



C. Distribution of pair-wise calculation on site response similarity between different stimulating site combinations for S1, S2, S3-1 (example of CA3-CA1)

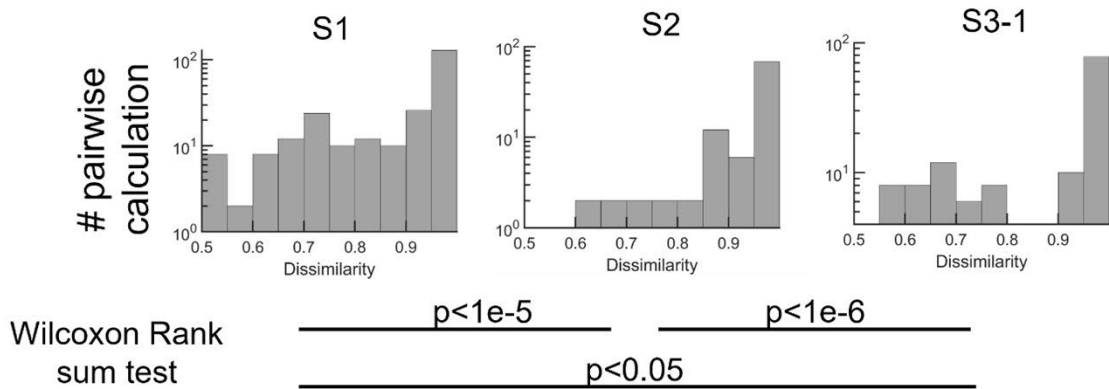


Figure 2.13 CA3-CA1 responds substantially different to each of three different stimulation site combinations A. Overview of channel CA3-CA1 G11 burst activities from

three different stimulation sites in EC. number 1 B3A5C4, 2 D1E1C2, 3 E5D4E4 (array 33152) **B.** 150 ms window shows very dissimilar spiking pattern of single site (S1) stim from 3 sites combinations (Rep 9, 9, 6 respectively). **C.** Dissimilarity histogram of activities from stimulating site combination showing large portion of the pair-wise calculations are above 0.9 dissimilarity for S1, S2 and S3-1.

### **Partial stimulus evokes pattern completion in CA3 and unique response in DG axons after training with three-site stimulation.**

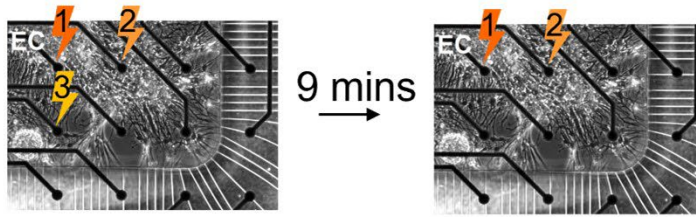
Pattern completion refers to the ability to complete or recognize a previously learned pattern when presented with a partial cue (Rolls 2010). By determining the pattern of the response to three-site stimulation followed by a delay and the response to two-site stimulation, we hypothesize that evidence for pattern completion will be evident from a two-site response with similar patterns with only this 'partial-cue' stimulus to patterns from the three-site training response. Temporal pattern decorrelation has been used as to prove separation that is realized at single granule cells (Madar, Ewell, and Jones 2019a).

The 'partial cue' is represented by delivery of the patterned theta burst stimulation to only two of the original three sites (Fig. 2.14A). We found EC-DG channels present responses with two-site partial-cue stimulation were similar to the three-site stimulation delivered nine minutes earlier even though the third site was missing (Fig. 2.14B). Pair-wise combinations were computed for similarity between the evoked responses from each site at 10 reps (3-site/2-site) yielding 10\*10 measures for EC-DG, tunnel 2, S1 (Fig. 2.14C). The subregional tunnel-site heatmaps show that even a single site can reproduce activities with a certain level of similarity at different regions (black arrow column, Fig. 2.14D). Interestingly, in the absence of third site stimulation, the delayed two-site partial stimulus, 4 individual axons in EC-DG and CA3-EC (Blue triangles) evoked patterns similar to training on three-site

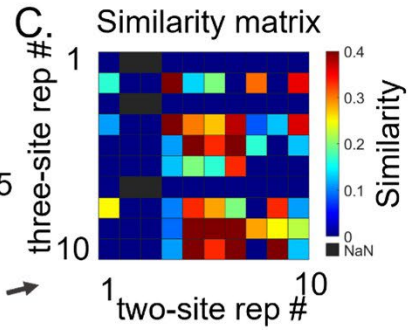
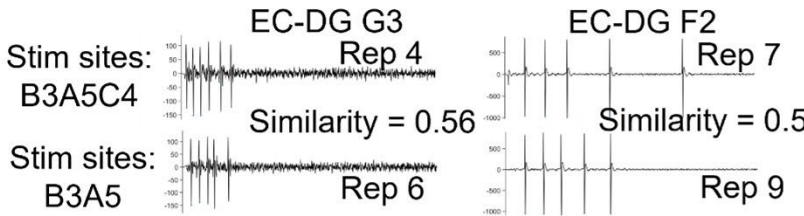
stimulation (Fig. 2.14D). The S1 caused similarity was evaluated at those 5 subregions (dashed line, Fig. 2.14E). We found for S1, CA3-CA1 and CA1-EC subregions have averages around 0.22 and 0.19 which are significantly higher than Monte-Carlo chance dashed line of 0.13 ( $p < 1e-9$ ,  $p < 1e-3$ , respectively). For S2 evoked activity similarity, we were able to discern some 'active' channels (blue triangles) showing similar activities with the lack of S3 stimulus. The subregional statistics shows EC-DG has significantly higher similarity than chance ( $p < 1e-5$ ), while other regions are significantly lower, except for CA3-EC (N.S.) (Fig. 2.14F).

The single site similarity between 3-site and 2-site serves as a measurement to examine if the axons plasticity changes at longer (9 minutes) stimulation interval, and the statistical result confirms that the CA3-CA1 and CA1-EC can maintain plasticity at a low degree. Even though the similarity of the activities in those 'active' channels are not high (0.17), it is above the randomized baseline (0.095,  $p < 0.001$ ). On the contrast, other channels presented response but with extremely low similarity approaching 0, and that is significantly lower than randomized baseline ( $p < 0.001$ ). In fact, memory is often distributed to multiple axons and synapses (Haberly and Bower 1989; Nabavi et al. 2014). It could be possible that the integrative effects from these active channel axons carry better pattern completion information. Results also suggest a small distinct neural population, not all, codes for specific pattern completion.

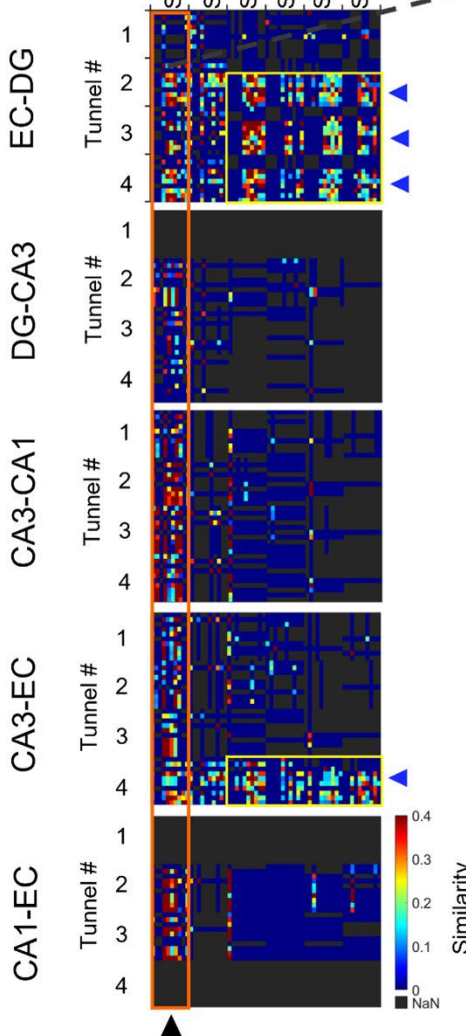
A. three-site stimulation for trainings and two-site cue probe



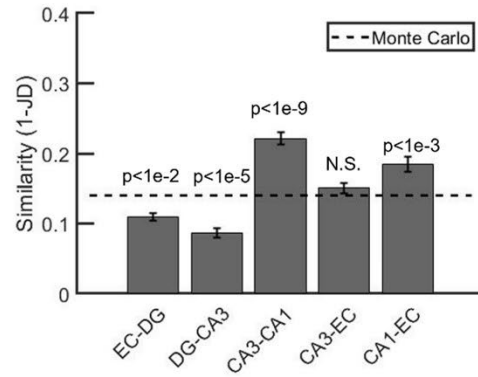
B. Similar pattern from training S3-1 and cued two-site response



D. Similarity activities to training



E. S1 evoked similarity activities to training, CA3-CA1, CA3-EC levels are above chance



F. S2 evoked similarity activities to training, EC-DG level is above chance

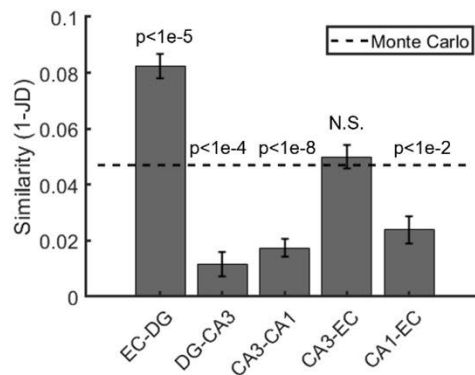


Figure 2.14 Individual axons carry similar patterns in response to partial two-site stimulus nine minutes after training with three-site stimulation as a test of pattern completion. **A.** 3-site and 2-site stimulation for a partial pattern. **B.** Examples of similar patterns S3-1 from 3-site and 2-site stim at electrodes G3 (3-site rep 4, 2-site, rep 6) and F2 (3-site rep 7, 2-site rep 9). **C.** An example of pairwise similarity calculation between 3-site and 2-site; EC-DG tunnel F2. **D.** The subregional heatmap of similarity shows persistence of single site activity similarity (black triangle, first column) after 9 mins and individual axons (blue triangles) in response to two-site partial stimulus. **E.** The subregional statistics of single site activity similarity between 3-site and 2-site. T tests show significant difference between subregional data and chance data (EC-DG  $p < 1e-2$ , DG-CA3  $p < 1e-5$ , CA3-CA1  $p < 1e-9$ , CA1-EC,  $p < 1e-3$ ). **F.** S2 evoked activity similarity to training at each subregion. EC-DG has significantly higher similarity than chance (t test:  $p < 1e-5$ ) (Array 33152).

## **CHAPTER 3: DESIGN, FABRICATION, & CHARACTERIZATION OF A 3D ELECTROPHYSIOLOGICAL SYSTEM**

### **Background**

Electrophysiology is for the main approach to understand neuronal activities and mapping the cognitive connection in the neuronal circuits (Poli, Pastore, and Massobrio 2015; Poli et al. 2017; Aebersold et al. 2016; Graziane and Dong 2015; Palop and Mucke 2016). The advent of microelectromechanical systems (MEMS) technologies has enabled minimally invasive neural implants for in-vivo neural interface (HajjHassan, Chodavarapu, and Musallam 2008; C. Xie et al. 2015) and microfluidic platforms for in-vitro (Gribi et al. 2018; Kim et al. 2017b; Forró et al. 2018) neuronal recordings and stimulations. However, in-vivo recordings are limited by the number of electrodes that can be safely implanted and connected to the outside world with typically fewer than 100 independent channels (Mankodiya et al. 2009; HajjHassan, Chodavarapu, and Musallam 2008; Xiang, Liu, and Lee 2016). Also, it is difficult and time-consuming to interpret the spike trains collected in vivo with the extreme complexity of neural activities in the natural brain. Lastly, in-vivo recordings must be done with humane treatment of the animal subjects with Institutional Review Board (IRB) approvals and oversights on human subjects. These procedural requirements render in-vivo recordings expensive and restrictive. In contrast, in-vitro electrophysiology offers higher spatial resolution and broader coverage with as many as 26,000 sites (Ballini et al. 2014; Müller et al. 2015; Obien et al. 2015) and possibly more in the future. It allows freedom in selecting and isolating certain brain regions and subnetworks for targeted studies in a well-

controlled environment (Brewer et al. 2013; Kim et al. 2017b; Aebersold et al. 2016; Wheeler and Brewer 2010; Eytan and Marom 2006). Finally, it does not require expensive facilities and labor for the care of live animals or human subjects. Examples include the use of microelectrodes array (MEA) in a small culture chamber to study specific cognitive function (Wheeler and Brewer 2010; Poli et al. 2018; 2017), information transmission between subregions, and neural circuit plasticity in a controlled experiment (Brewer et al. 2013).

However, there are also valid concerns about in-vitro recordings, including the likely possibility that neuronal activities of tissues isolated from the brain may not represent what would happen in the natural 3D environment. In particular, the well-established culture and recording approaches are typically based on 2D rigid surfaces, which lack the intrinsic properties of the in vivo environment such as the natural extracellular matrix in 3D, natural supplies of nutrients and oxygen, specific gene expression (Nicolas et al. 2020; Edmondson et al. 2014) and constant cell-cell and cell-matrix interaction (Bosi et al. 2015; Aebersold et al. 2016; Murphy et al. 2017; Caliari and Burdick 2016). To better mimic the natural environment, researchers have built 3D in vitro models to study network activities and dynamics (Frega et al. 2014; Bosi et al. 2015; Tedesco et al. 2018b; Su et al. 2010; J. Xie et al. 2019; Shmoel et al. 2016). However, a comprehensive electrophysiological study in 3D neuronal network constructs has not been reported due to the lack of a 3D electrode array for long-term culture and cell growth monitoring that allows fluorescent imaging and spike detection.

This chapter discusses the investigation on constructing such an in vitro system from both engineering and biological application aspects. First, we successfully developed the complete

process of fabricating the 3D signaling system and demonstrated the functionality of performing in vitro neuronal recording. Second, multiple substrates for constructing the 3D primary neuron culture have been investigated, and it was found that stacking multiple layers of micro glass beads was the most effective scaffold to support 3D neuronal network. The platform was designed with both a top and a bottom array of electrodes that could stimulate or detect neuronal activities with any of the electrodes. The top electrode array consisted of 60 electrode sites and transparent conductors made of indium tin oxide (ITO) supported on a polyethylene terephthalate (PET) film, which was also transparent to facilitate visual imaging and monitoring of the neuronal tissues. With both electrode arrays in use simultaneously, the neuronal communications in all 3 dimensions (x, y, and z) could be detected (Fig 3.1A). Further, the platform was designed with 4 compartments within the culture chamber, with micron-sized tunnels connecting the compartments to facilitate controlled axonal connections among different subregions of the hippocampus (Fig 3.1 B). This represented a significant advance over our previous 2-compartment chamber design, which demonstrated the self-wired connection between subregions (Brewer et al. 2013). The integrated platform would provide better insights into the trisynaptic circuits of the hippocampus not attainable with the previous 2D dual-compartment platforms.

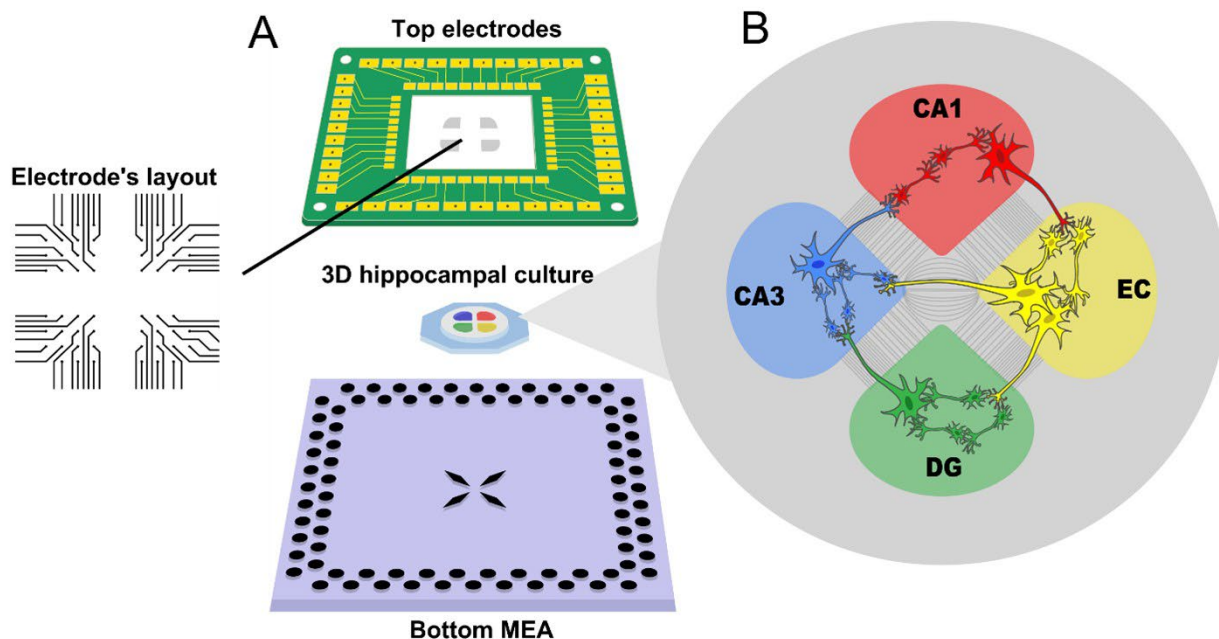


Figure 3.1 Schematic of designed 3D hippocampal culture and signaling platform **A**. The sandwich structure consists of top electrode, 3D hippocampal culture and bottom MEA. Zoom-in showing the top electrodes layout. **B**. In-vitro hippocampal subregional culture to mimic the anatomic order and micro tunnels between each subregion.

### Material choice

Indium tin oxide (ITO) consists of indium oxide ( $\text{In}_2\text{O}_3$ ) and tin oxide ( $\text{SnO}_3$ ) typically in a 10:1 ratio of  $\text{In}_2\text{O}_3:\text{SnO}_3$ . It is both transparent and electrically conductive and can be made into thin layers. Due to its excellent mechanical and electrical properties, it is widely used as a conducting material in numerous applications, such as flexible displays, transparent circuit, biomedical device platform, etc. (Singh, Suman, and Kumar 2006; Rogers et al. 2001) ITO film has relatively high transmittance from the visible to infrared range and relatively low resistivity. It can be deposited and patterned into transparent electrical compartments to facilitate the transmission of light while serving as interconnects for electrical circuit. Therefore, ITO is one of the ideal interconnect materials for stimulation and recording

electrodes where transparency is required. Moreover, it is amenable to be included into a microfabrication process flow, allowing several deposition methods to form thin films on different substrates. Several well-established deposition methods include E-beam deposition, DC sputtering and RF sputtering. Thin film ITO has been deposited on hard substrate to quantify cellular adhesion (Choi et al. 2008) and for optogenetic research (Kwon et al. 2013).

Conventional microelectrode arrays (MEA) are fabricated on rigid substrates such as silicon and glass. These substrates are flat and can withstand high temperatures during subsequent processing steps, which are necessary properties for a variety of photolithographic MEMS deposition and etching processes. However, in consideration for a transparent substrate for the top electrode array, glass is not suitable. Although transparent, glass slides cannot be easily perforated, which is a requirement to allow exchanges of oxygen, nutrients, and metabolic waste for the neuronal tissues cultured underneath it.

PDMS thin film was also investigated as a potential candidate as the substrate for the top electrode. It is transparent and can be made porous easier than glass with molding techniques. However, the traditional deposition by evaporation for thin-film ITO usually involve heating the substrate up to several hundred Celsius. PDMS thin films will very likely crack during the subsequent cool down step, destroying the array. Huck et al. have taken this feature as an advantage to form aligned buckles of thin film metal structures on the elastomer using photolithography (Huck et al. 2000). An alternative deposition process for ITO is sputtering, which can be performed at temperatures lower than 100 °C. The finished thin film is sufficiently transparent and flat with sputtering power at 60 W resulting in a

thickness of 150 nm (Figure 3.2). However, these sputtered ITO thin films are ceramic in nature, and thus exhibit significant mechanical mismatch with PDMS, rendering the device too fragile to sustain any subsequent patterning process. Polycarbonate (PC) materials have been considered as transparent substrates with reasonably similar stiffness as ITO. However, the significant mismatch in thermal expansion coefficients would lead to serious fractures in the ITO thin film even with low-temperature sputtering. In the end, patterned ITO electrodes on PET appears to be the only viable alternative among all these choices given their reasonable similarities in Young's moduli and thermal expansion coefficients. These two mechanical properties for the material candidates are summarized in Table 3.1.

Table 3.1 Mechanical properties for material candidates of making the electrodes

Material	Young's modulus	Thermal expansion coef.	Reference
ITO (sputtered)	100 Gpa	7.6E-6	(Nasr Saleh and Lubineau 2014; Tien and Lin 2021)
PDMS	3 Mpa	265	(Gupta, Lee, and Labouriau 2021)
polycarbonate (PC)	2.4 Gpa	65	EngineeringToolBox
PET	4 Gpa	2.0E-05	(Nasr Saleh and Lubineau 2014)

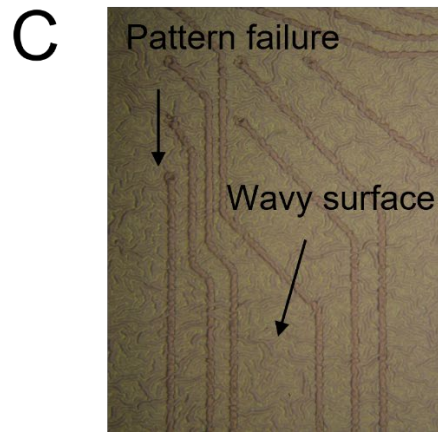
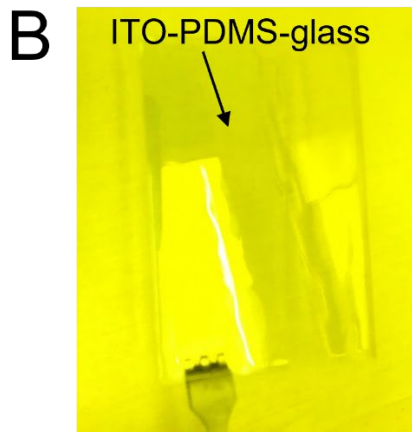
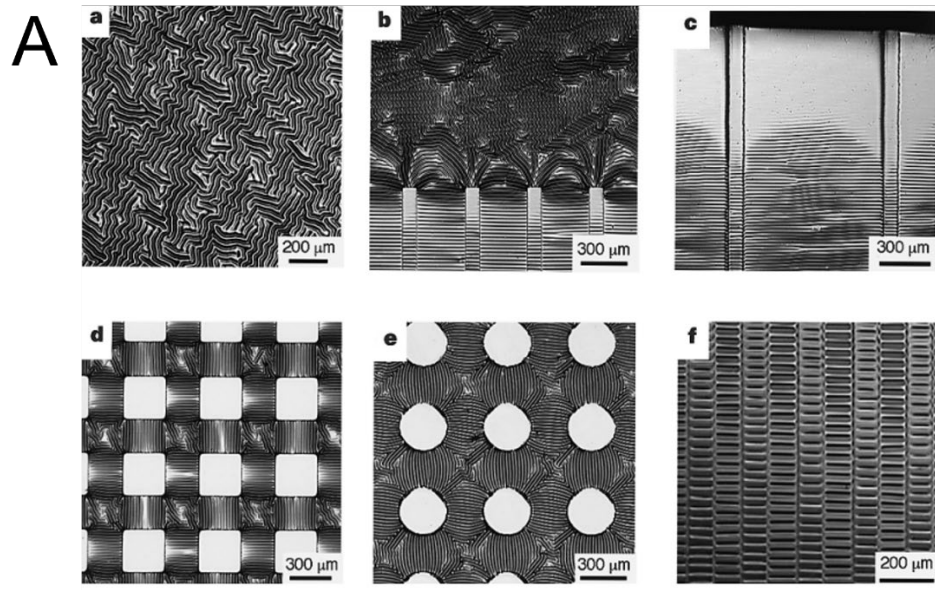


Figure 3.2 Patterned metal thin film on PDMS and 150 nm ITO pattern on PDMS **A.** buckled metal thin film on PDMS (Huck et al. 2000) Reprinted with permission from Springer Nature © 1998. **B** 150 nm ITO with metallic tent is sputter deposited on PDMS/glass. **C** Pattern failure was observed after PR is patterned on the wavy ITO/PDMS surface.

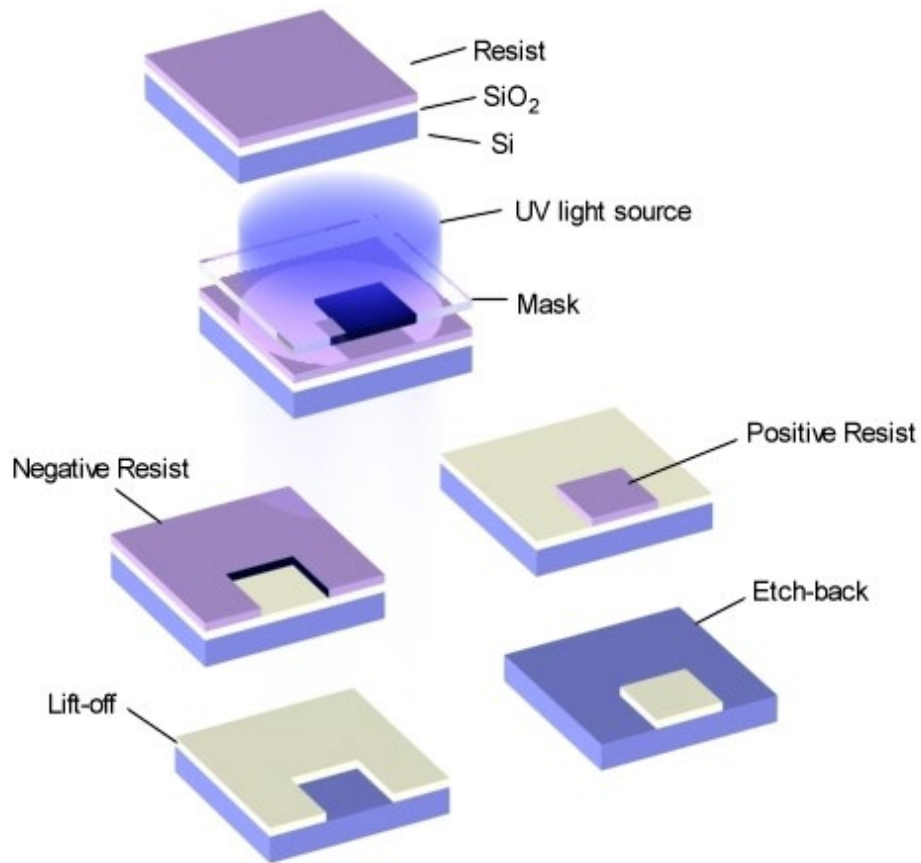


Figure 3.3 A typical photolithography process (S-Cubed. Inc)

## Methodology

### Fabrications

The proper fabrication methods should be chosen to fulfill compatibility of the materials and functionalities of the design. Even though PET has much lower heat conduction and tolerance than traditional silicon wafer, it takes the advantages of capable being CNC and laser machined. To prevent deformation of PET due to temperature (<120 °C), we used RF power sputters, chemical vapor depositions and oxygen plasma etchings etc. Focused laser beam

was used to perforate and release the substrate fast and precisely. In this chapter, we developed the full fabrication path, where the platform is built based on common clean room MEMS instrumentations and is assembled with convenience.

The key fabrication steps were based on soft-lithography using a thick negative photoresist (SU-8) photolithographically defined on a silicon wafer to serve as the mold for polydimethylsiloxane (PDMS) molding. The resulting PDMS piece was structured with 4 clover-leaf shaped compartments separated with 400  $\mu\text{m}$ -wide walls. At the base of the walls were 279 micro-tunnels measuring 10  $\mu\text{m}$  wide and 3  $\mu\text{m}$  tall each connecting the adjacent compartments. A set of micro-tunnels was used to connect two of the compartments diagonally. This PDMS piece was aligned and bonded onto a Multi-Electrode Array (MEA) (MultiChannelSystems, 120MEA200/30iR-Ti). The transparent top electrode array was fabricated with the use of indium tin oxide (ITO), a transparent conductive material, lithographically patterned onto a transparent substrate, polyethylene terephthalate (PET) film. A printed circuit board (PCB) was designed to support the top electrode array while providing the interconnects to the MEA chip on the bottom. The processing steps are detailed below:

#### *ITO electrode fabrication*

A 1300 Å ITO-PET film (Sigma-Aldrich co.) was cut into 3-inch squares. Positive photoresist (Shipley 1827 MICROCHEM) photolithography (similar to above) defined the pattern of contacting pads and connection leads followed by a hard bake under 120 °C for 20 min. 3M HCl solution was used for etching of ITO for 30 s. The residual photoresist after acid etching was removed by ultrasonic cleaning in acetone for 5 min. and sample piece was rinsed by

IPA and DI water successively and dried in room temperature. Second layer photoresist patterned the passivation layer. 0.3  $\mu\text{m}$   $\text{SiO}_2$  was RF power sputter deposited (DV-502M Denton Vacuum, LLC). The  $\text{SiO}_2$  layer was finished by lift-off. A self-designed alignment chamber was used to work with a laser cutting machine (S36 Trotec Laser Inc.) Low-power  $\text{CO}_2$  laser was used to perforate the electrodes and release them from the film (illustrated in Fig. 3.5).

#### *Printed Circuit Board (PCB) and bonding with ITO electrodes*

PCB design. An important aspect is connecting the neural electrodes to outside amplifier. To achieve ease the use, the PCB connection layout has been designed same as MEA60 chip (MSC). And the electrodes recording can be directly visualized through MC\_Rack (MCS), 60 channel interface. For better electrical connection, a 68-channel contact pin board was designed (Eagle Autodesk Inc.) and fabricated (Xinfeng Huihe Circuits CO., LTD). 60 0.68 mm D 14 mm length spring loaded pin probes (MultiChannelSystems) were assembled into PCB sockets. A 68-channel PCB D-Sub connector (TE Connectivity) was soldered onto the board and connected directly to a coaxial cable connected to the signal amplifier (MEA60, Multichannel Systems). The detailed designs are seen in Figure 3.4.

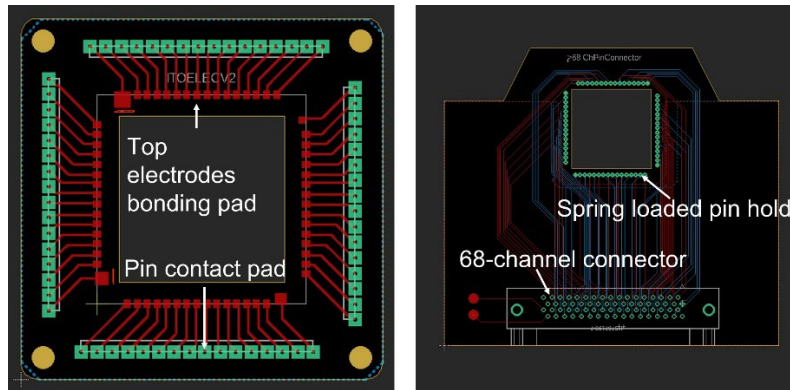


Figure 3.4 PCB designs for connecting top electrodes  
 Left: PCB for holding top electrode; Right: 68-pin connectors to amplifier

Interconnecting printed circuit board design and details: 0.8 mm FR4 double sides, 20  $\mu\text{m}$  Cu, 3  $\mu\text{inch}$  gold immersion PCB was designed (Eagle Autodesk Inc.) and fabricated (Xinfeng Huihe Circuits CO., LTD). The PCB and released ITO electrodes were cleaned in acetone and IPA for 5 mins each bath then rinsed with DI water, dried in vacuum oven under 90  $^{\circ}\text{C}$  for 1 hour before bonding. Anisotropic conductive film (ACF) serves as an excellent flex-to-board or flex-to-flex conductive bonding adhesive. 30  $\mu\text{m}$  thick ACF (TGP5010UB 3T Frontiers Pte Ltd) (Baek et al. 2011) was applied to PCB contacting area and ITO electrodes were aligned with it under microscope. Nanoimprint machine (HEX3 Jenoptic, LLC) was used to perform ACF final binding for better controlling the contacting pressure and temperature. Two-step process had the conditions of 1 Mpa/60  $^{\circ}\text{C}$  for 3 s and 3 Mpa/150  $^{\circ}\text{C}$  for 30 s.

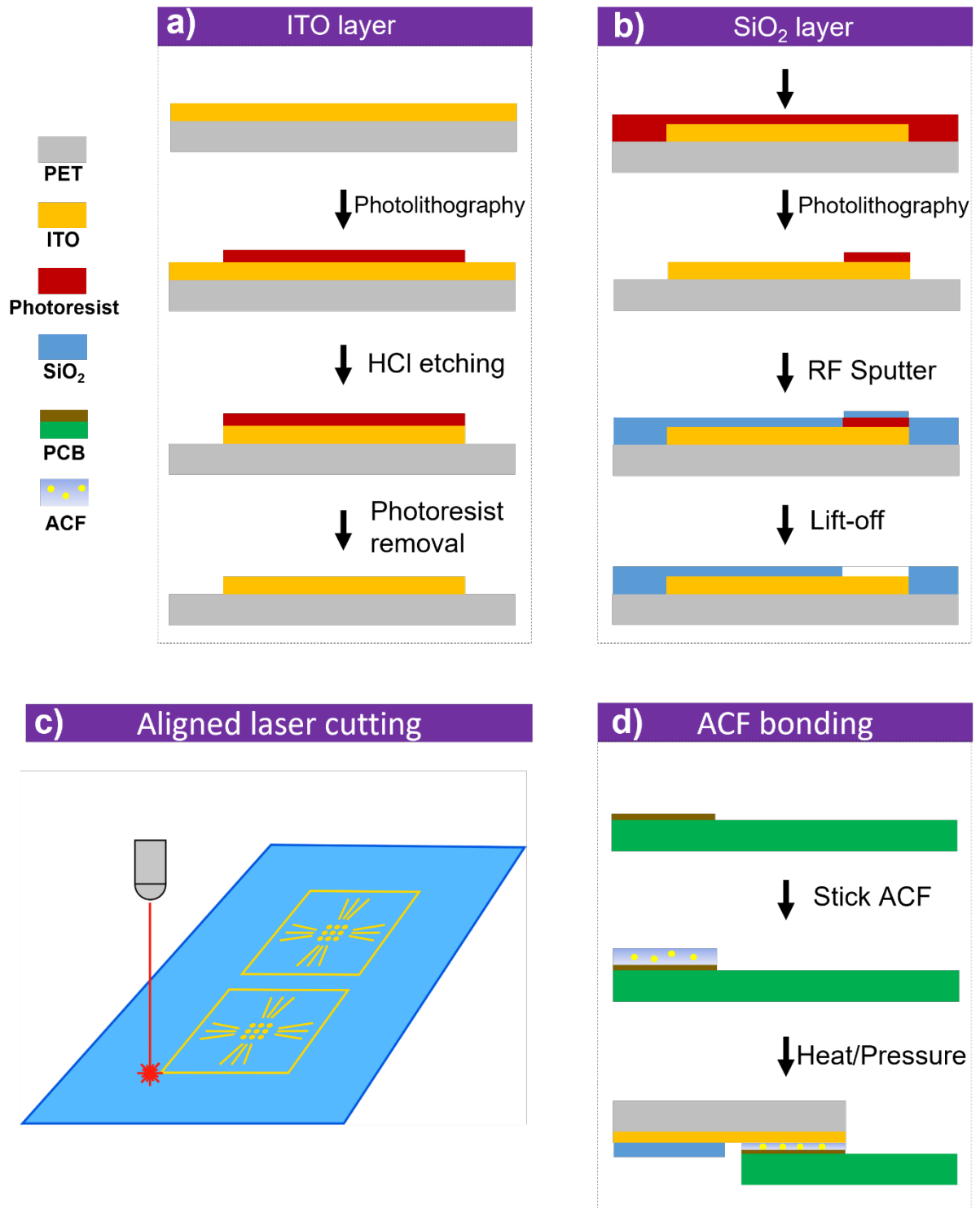


Figure 3.5 Fabrication process flow for top ITO electrode **A.** Photolithography define the ITO leads and contact pads. **B.** Lift-off process patterns the RF power sputter deposited silicon oxide isolation layer. **C.** Use custom-designed alignment chamber to perform laser cutting and release the electrode. **D.** ACF bond ITO electrode on designed PCB.

### *Alternative Parylene C isolation*

Parylene is a common polymer consists of para-benzenediyl rings backbone that often applied as electrical insulation. In chemical vapor deposition process, the dimer was decomposed into monomer and formed a layer of uniform coating on the substrate at room temperature. Parylene-C is USP class VI implantable plastic material and conforms the Biological Evaluations for Medical Applications. Besides being used on biomedical devices, it has been applied as isolations on electrophysiological probe (Rajaraman et al. 2007). Parylene demonstrates good stability in biological environment. Therefore, the Parylene isolated electrodes were also fabricated and tested. After ITO electrodes were constructed, 0.5  $\mu\text{m}$  Parylene was deposited (SCS PDS 2010, Specialty Coating System, Inc) on the substrate as an insulation layer. Then, the Parylene covering the contact pads and electrodes was removed completely by Oxygen ash under 300 W, 2 minutes.

### *PEDOT:PSS coating*

PEDOT:PSS is one of the prevalent conductive organic. It is sufficiently flexible to be used as thin film architecture in organic semiconductor. PEDOT:PSS has high biostability and excellent biocompatibility (Broski, Wu, and Fan 2018; Kayser and Lipomi 2019). Therefore, it has been applied as a coating layer on electrodes to enhance the electrochemical conductance and charge storage capacity (Broski et al. 2017). After insulation layer patterning was finished, the electrodes were patterned with PR again and left the contact pads exposed. The electrodes were O<sub>2</sub> cleaned at 100 W 60s. Then PEDOT:PSS (768650, Sigma-Aldrich) was spin coated on substrate with 4000 rpm for 2 minutes. The coated

electrodes were baking on the hot plate at 120 °C for 30 minutes. The PR mask was removed in acetone.

### **Functional Characterization**

Electrode impedance measurement: The electrical behavior of microelectrodes was studied in PBS (1X, pH 7.4) under room temperature by an LCR meter (EXTECH instruments). An Ag-AgCl electrode served as the reference electrode. The impedance was measured under the typical spiking frequency which is 1 kHz.

Transmittance measurement: to characterize the optical performance of our fabricated electrodes, a spectrometer (Cary-60 UV-vis spectrometer) was used to measure the light transmittance through the electrodes film at the range of 200 – 800 nm.

### **Surface preparation**

Bonded ITO electrodes and PDMS devices were cleaned with acetone and rinsed with IPA, DI water successively for 2 times before assembly. The compartments were dried with nitrogen gas and then were well aligned under the microscope and examined visually with evidence of contact seal. Subsequently, the platform was treated with Oxygen plasma for 2 mins to obtain the hydrophilic surface. PDL solution (Sigma P6407, 0.1 mg/ml in water) was filled into the chamber and ITO top electrodes was immersed under the liquid surface at room temperature overnight. On the second day before cell plating, the PDL solution is sucked out and rinsed with DI water 1 time. The entire device is put in bio cabinet 1 hour for drying before dissection and cell plating.

### **3D primary neuron culture**

3 substrates were used and evaluated in this thesis. The detailed methods are listed below.

**Matrigel (9.6 mg/mL, 356231, Corning, United States):** hippocampal cell suspension at a density of 11,000 cells/ $\mu$ L was obtained through standard cell culture protocol in previous chapter. The Matrigel (9.6 mg/mL, 356231, Corning) experiment was conducted in at 4° C on ice to prevent gelation before mixing. Using pre-chilled pipet tips, 100  $\mu$ L Matrigel was added with 28  $\mu$ L prepared cell suspension for a final cell density of 2500 cell/ $\mu$ L (Final Matrigel concentration 7.5 mg/mL). 6  $\mu$ L cell-gel mixture is injected into each chamber (as in Chapter 2). Then the plate was incubated at 37 °C for 30 to 45 minutes for matrix gelation. 1 mL culture media was added to the media well afterwards. The cultures were kept in 37 °C and 5% CO<sub>2</sub>, 9 % O<sub>2</sub> – 95% humidified air incubator, with half of media changed every 3 days.

**VitroGel (VHM01, TheWell Bioscience, United States):** similar to Matrigel mixing method, the cell suspension was first prepared with cells at a density of 6000 cells/ $\mu$ L. Supplements including B27, GlutaMax, growth factors in the suspension media were adjusted as 3 times as original concentrations. 100  $\mu$ L warmed VitroGel (VHM01, TheWell Bioscience) mixed with 50  $\mu$ L cell suspension. The mixture was injected into the chamber quickly and the plates were left at room temperature 15 minutes for gelation. Prewarmed and CO<sub>2</sub>-equilibrated culture media was added to the well and plates were incubated kept in 37 °C and 5% CO<sub>2</sub>, 9 % O<sub>2</sub>– 95% humidified air incubator. Media change was done in the same manner. Micro glass beads (9040, Thermo Scientific, United States): the methods for constructing 3D neuronal cultures on glass beads were described previously (Frega et al. 2014; Brofiga et al. 2020). Specifically, 40  $\mu$ m diameter glass beads (9040, Thermo Scientific) were sterilized with 70% Ethanol for 10 minutes, then washed with sterile water for 3 times. dried? Then they were submerged into 0.1 mg/mL PDL solution (P6407, Sigma-Aldrich) overnight. On

the dissection day, the PDL was removed, and glass beads were washed with sterile water once. Then they were left to dry in the biohood for 1 hour. Microbeads were then pipetted onto Transwell (353095, Corning) inserts to self-assemble into single mono layer. A total number of 20,000 beads were estimated being assembled on the porous membrane. A freshly isolated neuronal cell suspension was prepared at a density of 800 cells/ $\mu\text{L}$ . Next, the Transwell and microbeads were submerged in culture media, 100  $\mu\text{L}$  of cell suspension was added to each well. At the same time, 4  $\mu\text{L}$  of cell suspension was plated into each electrodes' subregion chamber to form the bottom 2D culture. The microbead-cell mixture was incubated for 10 hours and then pipetted into the electrode chamber. The stable culture was maintained in the incubator and the growth monitored. Half media was changed every 3-4 days (first week with Neurobasal.B27/GlutaMAX/growth factor media, then change half to BrainPhys/SM1/GlutaMAX/growth factors each time).

## **Results and discussion**

### **3D platform design and ITO electrodes fabrication**

The 3D signaling platform was designed for both ease of use and performance, which is compatible with current cell culture, microscopic monitoring protocol and commercial electrophysiology instrumentation (Multichannel System MEA120 (bottom) and MEA60 (top) headstages). The neuron cultures sandwiched between the top ITO electrodes and bottom MEA is divided into 4 chambers. Each chamber has an area of 9  $\text{mm}^2$  with the height

of 0.4 mm in clover leaf shape (Fig. 3.7A). The 4 hippocampal subregions are deposited into each chamber clock-wisely in the manner of anatomical layered structure of hippocampus. The axonal tunnels with a size of 3 x 10 x 400  $\mu\text{m}$  connect adjacent compartments mimicking the axonal connections between each cell layers and the cross tunnel which emulate the perforant pathway from EC to CA3 render an architecture approaching biological reality (Fig. 3.1B). The ITO electrode system combined with existing multichannel system to retrieve signal from both top and bottom of the 3D neuronal culture through two signal cables to different amplifiers which minimizing the signal interference and reduce the processing complexity.

Specifically, the ITO electrodes contacting pads have a diameter of 30  $\mu\text{m}$  and a contact area around 1000  $\mu\text{m}^2$ . Each electrode is separated by 200  $\mu\text{m}$  like the bottom MEA (Fig. 3.6A). The high wavelength transmittance of the film in visible light allowed observation through the electrodes from either neuronal culture on top or bottom. A book page is clearly read under the fabricated electrodes film before release (Fig. 3.6B).

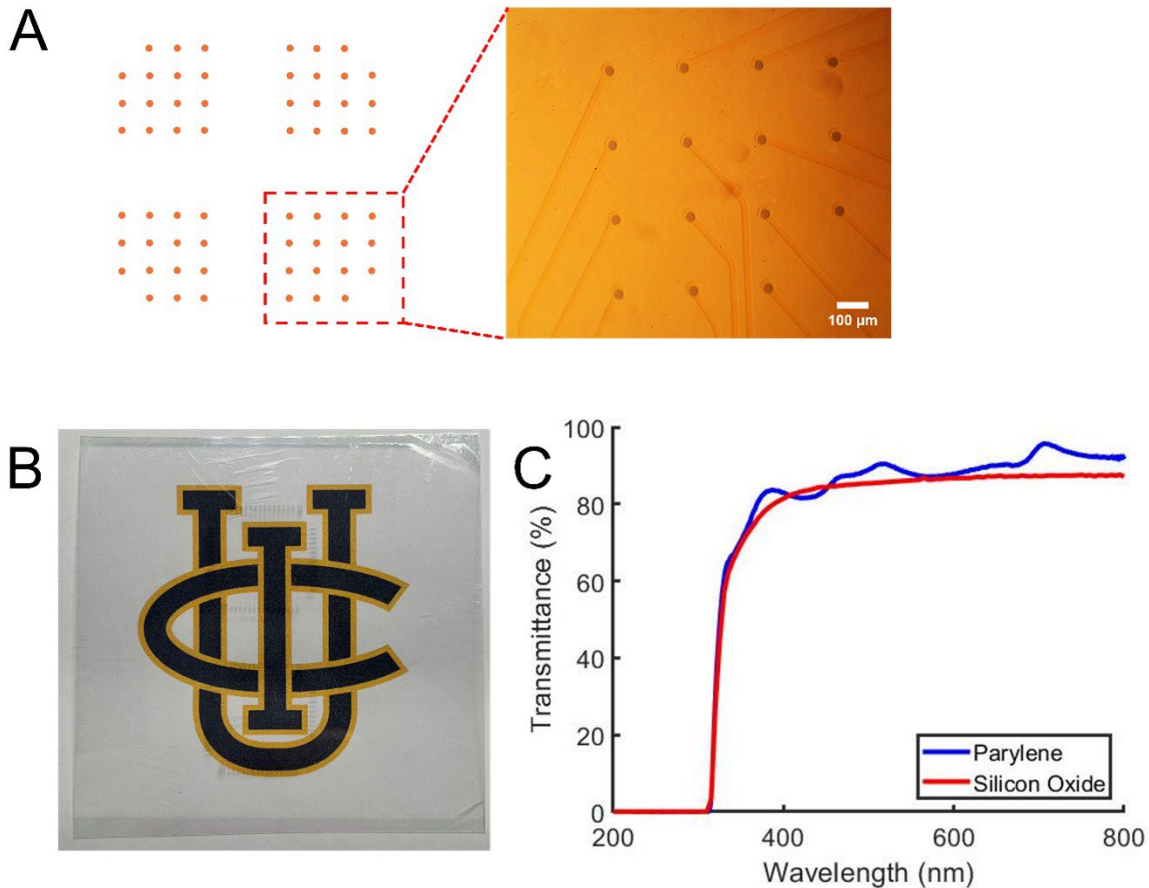


Figure 3.6 Photos and transmittance measurements of finished ITO electrode **A.** 30  $\mu\text{m}$  diameter electrode layout with connecting leads under 10X microscope. **B.** Top electrode on top of UCI logo shows excellent transmittance. **C.** UV-vis transmittance measurement

### Characterization of top electrodes

Neuronal spiking has a typical frequency of 1 kHz. Therefore, an electrode's impedance at 1 kHz in a saline solution is regularly evaluated (Won et al. 2018). We performed the same impedance measurement on both bare ITO electrodes and PEDOT:PSS coated ITO electrodes, and the electrodes are imaged in Fig 3.7A. In the results average ITO electrode impedances of 375 kohm are shown in Fig. 3.7B. After surface coating of PEDOT:PSS, we found that the impedance per electrode reduced to about 150 kohm under same measurement condition (Fig. 3.7B) The large reduction on impedance is mainly attributed to the enlarged surface

roughness (Broski, Wu, and Fan 2018). From the image (Fig. 3.7A) we can see the uneven light reflection of PEDOT:PSS coated electrodes compared with bare ITO electrodes. From the impedance measurement, we conclude that our fabrication yielded electrodes with comparable impedance for recording multiple and single unit activity compared with a value of 100 kohm from commercial MEA electrodes with same contacting area (Multichannel System). In the biological environment, an electrode interfacing with neuronal tissue and picking up single unit action potentials, local field potentials (LFP) from contacting neurons and background noise (Rivnay et al. 2017; Recording 2004). The quality of neuronal signal with respect to electrodes' impedance level were broadly investigated (Rajaraman et al. 2007; Zhao et al. 2016), suggesting lower impedance electrodes are able to improve signal-to-noise ratio (SNR) for both LFP and spikes (Neto et al. 2018). Nevertheless, by taking advantages of complex spike sorting algorithm, neuroscientists are able to determine single unit waveform from overlaid signal from multiple sources after conducting more complicated analysis(Quian Quiroga and Nadasdy 2004). The ITO electrode is designed to have 60 channels, and we found that in average of 6 arrays, 50 channels per device are electrically connected well. The remaining dead electrodes are possibly caused by incomplete removal of insulating silicon dioxide during the lift-off process, or the misalignment of the PCB and ITO electrodes contacts during the anisotropic conductive film bonding. Reducing the hard bake time to have less photoresist reflow will help to improve the lift-off process. A better design with bigger tolerance for misalignment may also reduce the percent of dead electrodes. However, the current successful rate renders a fair number of electrodes per device that enabled us to record hippocampal network electrophysiology.

We also measured light transmittance in the range of UV-vis for both Silicon oxide coated and Parylene isolated electrodes. We can see that over 80 % light passing through the electrodes at visible light range (380-700 nm) (Fig. 3.6C). Even though there is a sharp drop at 300 nm which may block some fluorescent excitation. But it can still provide sufficient transmittance for the excitation spectra used for common probes, such as rhodamine, GFP and DAPI.

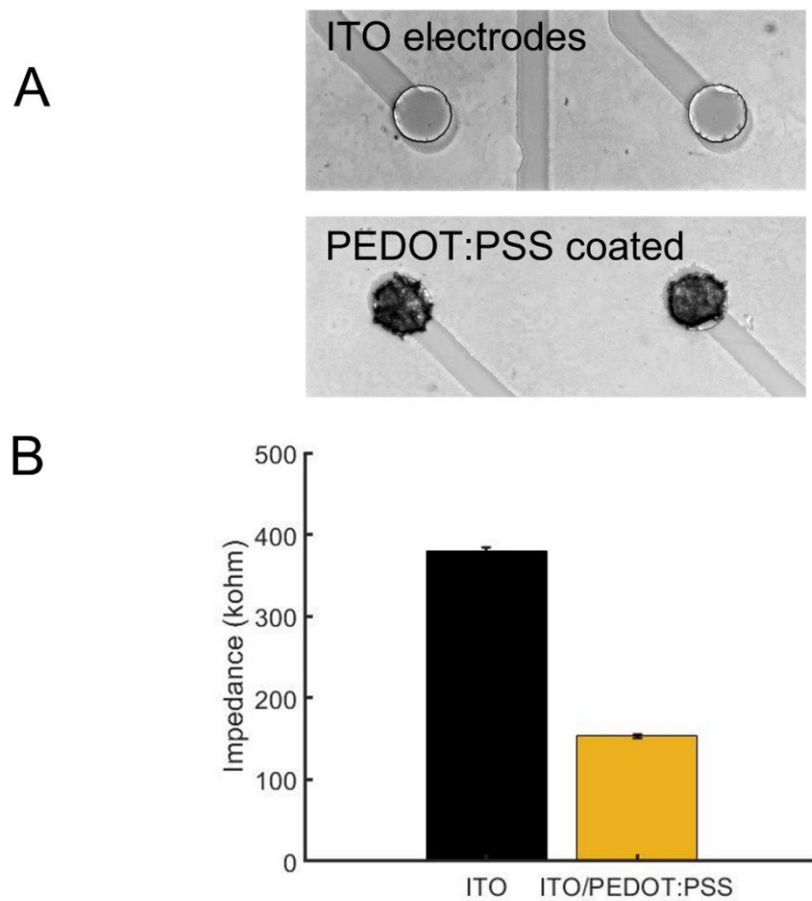


Figure 3.7 Impedance measurements of the electrodes **A.** Images of ITO electrodes with and without PEDOT:PSS coating. **B.** The impedance measurements for ITO electrodes and PEDOT:PSS coated electrodes show PEDOT:PSS coating largely reduce the impedance (n= 4 devices \* 60 electrodes).

### Platform set-up and actuation

ITO electrode mounted PCB is manually aligned with PDMS culture chamber under the microscope (Fig. 3.8A), ensures all electrodes are assigned to 4 chambers. The PDMS chamber has 4 compartments and connected with microfluidic tunnels (same design as Chapter 2) (Fig. 3.8B). Finally, the bottom MEA is assembled to top electrode and culture chamber. The configuration with schematic of cross-sectional view of how platform retrieves activities from hippocampal culture is presented in Fig. 3.8C. The platform is designed and assembled with the intention of ease of use, compatibility, and maintenance. The spring-loaded pin generates force and gap tolerances which allows electrodes on the bonded printed circuit board to connect with the external amplifier smoothly and ensures a good quality of recording. Moreover, the integrated platform (Fig. 3.8D) maintains free standing like a sole MEA chip that can be plugged in headstage for electrophysiological recording and unplugged for neural culture incubation.

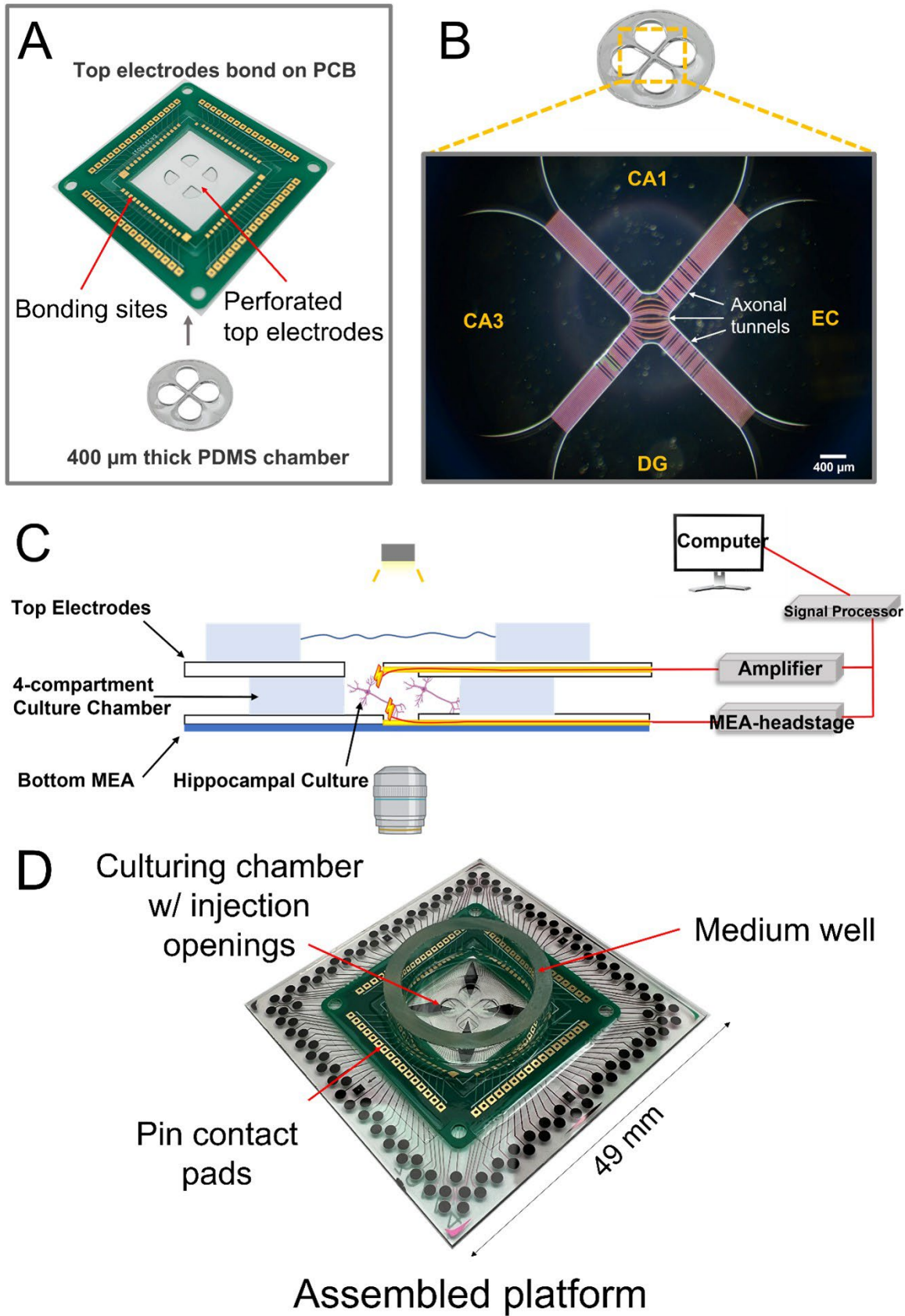


Fig. 3.8 Photos of device setup and schematic of cross-sectional view to explain how the platform works **A.** PCB board with gold connectors bonded with ITO electrodes with ACF (see Fabrication) align with 4-compartment PDMS culture chamber. **B.** Four-chambered PDMS device with micro-fluidic tunnels that connect hippocampal subregions (400 x 10 x 3  $\mu\text{m}$ ) **C.** Illustration of cross-section view of platform. Gray box represents PDMS confinement and wavy line above emulates the culture media. **D.** The final assembled platform for culture and recording in 3D.

## Planar Culture and Recordings

To demonstrate the feasibility of ITO electrodes picking up high-quality signals from neuronal culture and evaluate the overall biocompatibility of materials from microfabrication process, we firstly utilized 2D planar culture of the rat hippocampal neurons on top of the ITO electrodes. The culture on the device was optically observed and electrophysiological recording was performed on day 21 in vitro (21 DIV). A photo in Fig. 3.9A shows the bare electrodes before culture. A plating concentration of 50,000 cells/cm<sup>2</sup> yielded a dense neuronal network and covered electrodes contacting pads well (Fig. 3.9B). Through cell counting, we found there was no significant cell density difference between the electrode substrate and a control glass slips (Fig. 3.9C). These results demonstrate the high level of biocompatibility of our devices over 21 days. An ideal situation was observed when there is a single neuronal soma over the center of the recording electrode, which maximizes the signal of the specific single unit. To assess the ability of the top electrodes to monitor the electrical activity of a neuronal culture system, recordings were performed on postnatal rat hippocampal neuronal cultures at DIV 21. Using our established electrophysiology protocol, all devices with cultures have been connected to preamplifiers and activity recorded via computer software. Raw data with 25 kHz sampling rate were recorded via MC-Rack. In the 300 s spontaneous recording, several electrodes constantly showed active neuronal signals. An example of action potentials after applying a 300 Hz high pass filter is shown in Fig. 3.10A.

The electrode layout and raster plot present active channels during a 3 min recording (Fig. 3.10B). The limited active channel numbers could be attributed to several reasons, the inhibitory effect in the network (Boehler, Wheeler, and Brewer 2007), dead electrodes caused by any steps of fabrication failure stated in above section, and single cell coupling, which is normal to see in open chamber versus in micro tunnels (Narula et al. 2017; Dworak and Wheeler 2009). The recordings were also processed through MATLAB with the 30 s raw data trace shown in Fig. 3.10C. An example of action potentials waveform sorted on one electrode is shown in Fig. 3.10D. The calculated inter spike interval (ISI) histogram present in Fig. 3.10E. Optical observation of live neurons, along with recorded neuronal activities up to 21 days verify the electrodes' compatibility and capability of long-term neuronal culture, monitor and electrophysiology.

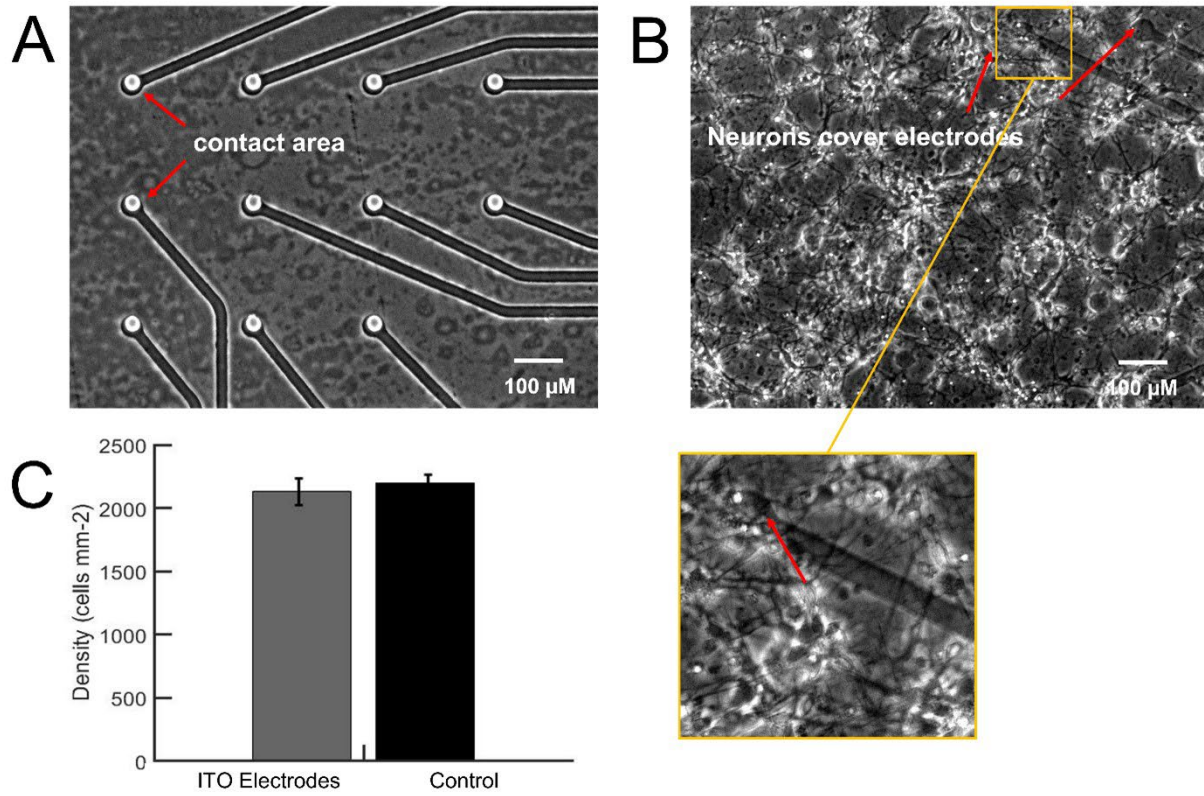


Figure 3.9 2D planar neuron culture demonstrates good biocompatibility **A**. Phase contrast photo of ITO contact pads. **B**. Neurons grow on top of electrodes covering the contact area. **C**. Cell density on ITO electrodes is similar to glass cover slip control (DIV 21,  $n = 4$ ).

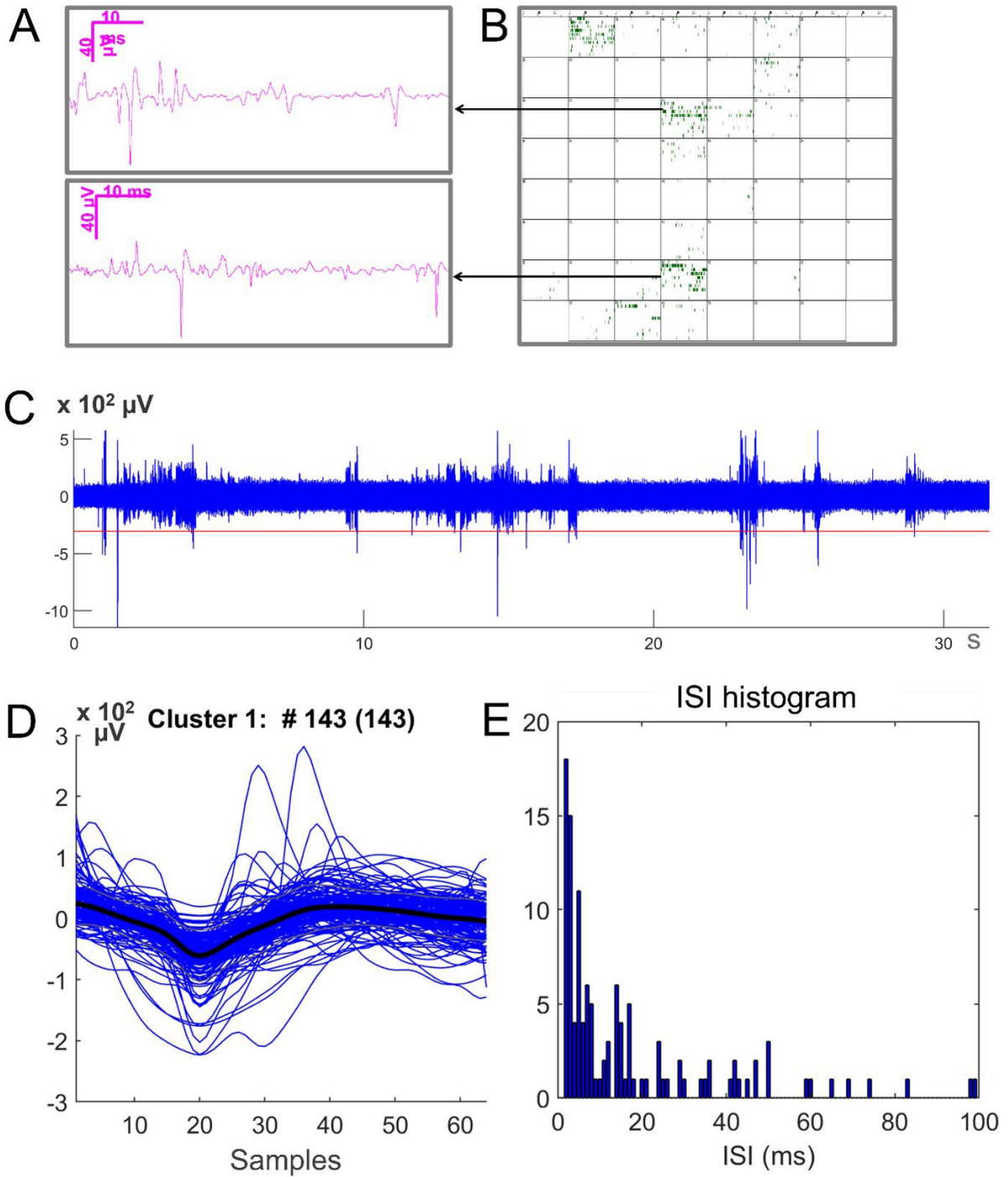


Fig. 3.10 ITO electrodes recordings and single channel data processed by MATLAB based algorithm Wave\_clus **A**. Recorded signals from 2 channels show spikes clearly. **E**. Raster plot of spikes from a 300 s recording taken from the commercial software interface. Each dot is a spike; each box is an electrode; each row is 30 s. **A**. 30 s long filtered raw data with detection threshold set  $4.5 \times \text{S.D.}$  of the noise (red line). **B**. Overlay of 143 detected spikes

wave forms. Each sample is 25  $\mu$ s. C. Inter spike interval (ISI) distribution for detected spikes.

### **3D culture construction**

In vitro 3D neuronal construction has long been discussed. The basic purpose is to recreate an environment that neurons could grow and form the connections in the way approaching in vivo (Frimat et al. 2015; Lam et al. 2020; Jang et al. 2015; Murphy et al. 2017). Especially in electrophysiology area, substantial network dynamic changes have been observed after the neural networks have been formed in 3D (Bourke et al. 2018; Brofiga et al. 2020). In this work, we investigated the potential solutions that allow us to integrate the 3D culture into our platform. The goal is to have stable 3D neuronal structure with network formation (requires viability). The structure and culture must be stable for 3 weeks of development.

Hydrogels have proven useful for 3D in vitro applications (Caliari and Burdick 2016). Multiple hydrogel candidates have been tested and evaluated as the cell encapsulation substrates. Depending on the type of the hydrogel scaffold, the gelation mechanisms are different. In general, gelation can be achieved by either covalent or noncovalent crosslinking. Typically, two initiations for natural peptide or protein-based systems are temperature and salt concentration. In the first case, like Matrigel, it undergoes gelation at temperature ranges 22 to 37 °C. In the gelation process, the entactin acts as a crosslinker between laminin and collagen IV. In charge interaction gelation, the physical interaction happens between positive and negative charge ionic groups. For example, the VitroGel, it can be maintained at room temperature, and gel formation is induced by ionic solution such as culture media. Nevertheless, chemical crosslinking of polymers can also be used for hydrogel, which is

beyond the discussion in this thesis. Therefore, when applying different hydrogels to the platform, the protocol varied. The detailed descriptions are in Methods.

**Matrigel:** As Matrigel contains rich extracellular matrix protein, it provides good biophysical binding sites for cell bodies and neurite extension. We seeded the neurons in Matrigel to form the encapsulation culture and observed the growth progress through DIV 1 to 21. The results show hippocampal neurons have healthy growing progress and begin to form a network around DIV 8. Through the photos taken at different layers of the 3D structure, the cell bodies and neurites are clearly seen connecting adjacent neurons. We observed small low levels of cell density variations at different layers. But this difference is not uniformly seen at different fields, and it might be caused by the mixing procedure before gel gelation, the step where we want to minimize the shear stress introduced to neurons at their sensitive state (Fig. 3.11A). However, we observed the severe Matrigel degradation starting around DIV 19, where about 90% of the Matrigel at the well center degraded, leaving the neurons in clumped groups with some evidence of connections. While about 40% of height loss happens at the edge of the well. This gradient of degradation can be seen by the layered photos losing focus on centripetal direction (Fig. 3.11B).

As mentioned above, gelation for Matrigel comes from component entactin acting as a crosslinker between the laminin and collagen IV. And it mainly contains ECM proteins. The Matrigel degradation with metalloproteinases from cancer cells have been studied (Dolo et al. 1999). Since substantial evidence is seen for degradation in x experiments, it is possible that proteinases secreted from neurons cause this degradation. Even though Matrigel has demonstrated excellent feasibility for short-term applications (Usui et al. 2017; Jang et al.

2015; Karahuseyinoglu et al. 2020) and different cell types (Novin and Nouri 2007; Grefte et al. 2012), it is not practical to use Matrigel as 3D scaffold for reliable 3D electrophysiological recording in our platform.

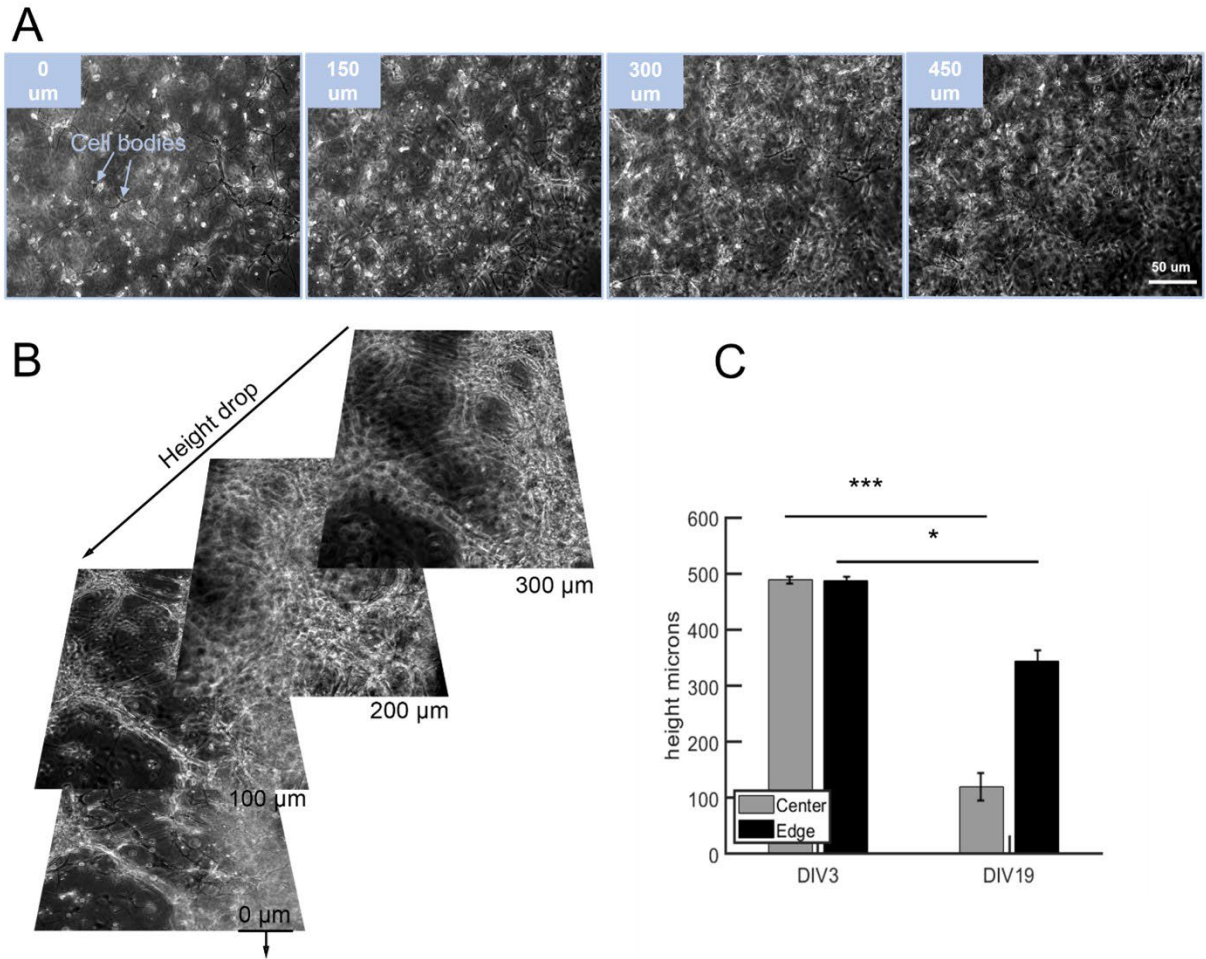


Figure 3.11 3D cell culture on Matrigel and the hydrogel degradation **A.** Photos of cell at different layers of the 3D encapsulated culture (DIV 8). **B.** A stack of images showing the gel degradation at day 19. **C.** Bar plot showing the significant height drop both at center of the well and edge of the well (n= 4 wells \* 4 fields).

**The synthetic hydrogel:** Synthetic hydrogel will reduce the complications associated with Matrigel application, including the drawbacks of batch-to-batch variation, unpredictable degradation, and xenogeneic composition. Since the focus of this thesis is not for

bioenvironment modulation, we intend to incorporate commercially available options that provide the feasible solutions on supporting neuronal growth to meet our research goal. A synthetic hydrogel named VitroGel was tested. This hydrogel is a xeno-free synthetic polysaccharide-based hydrogel system. VitroGel provides a bioenvironment which supports the survival of primary hippocampal neurons. After 6 hours of seeding, the culture was stained with 4.6 ug/mL PI, and we didn't discern a large dead population at any depth (Fig. 3.12 A). Through day 21, we observed distribution of ball-shape tissue pieces throughout different depths of the culture with no obvious structure collapse (Fig 3.12B). By using Calcein AM as a vital dye, we found that most of the round particles are live cells, and the viabilities at different layers are around 76%. Interestingly, we found that neurons at the very bottom of the chamber formed a single layer network, and the neurites extension and connections are clearly seen (Fig. 3.12 C). This would be evidence that VitroGel supports the cell viability but does not provide enough attachments for neurite extension. The passive diffusion system is sufficient for neurons growing under the specific depth. However, for studying of electrophysiology, an in vitro network formation is needed. Poly-D-lysine is frequently used in 2D culture to promote cell attachment. It is positively charged amino acid that has electrostatic interaction with negatively charged ions of the cell membrane. Therefore, we assume that using some chemistry to modify the hydrogel surface with polycationic groups will help the prosthesis attachment and neural network formation.

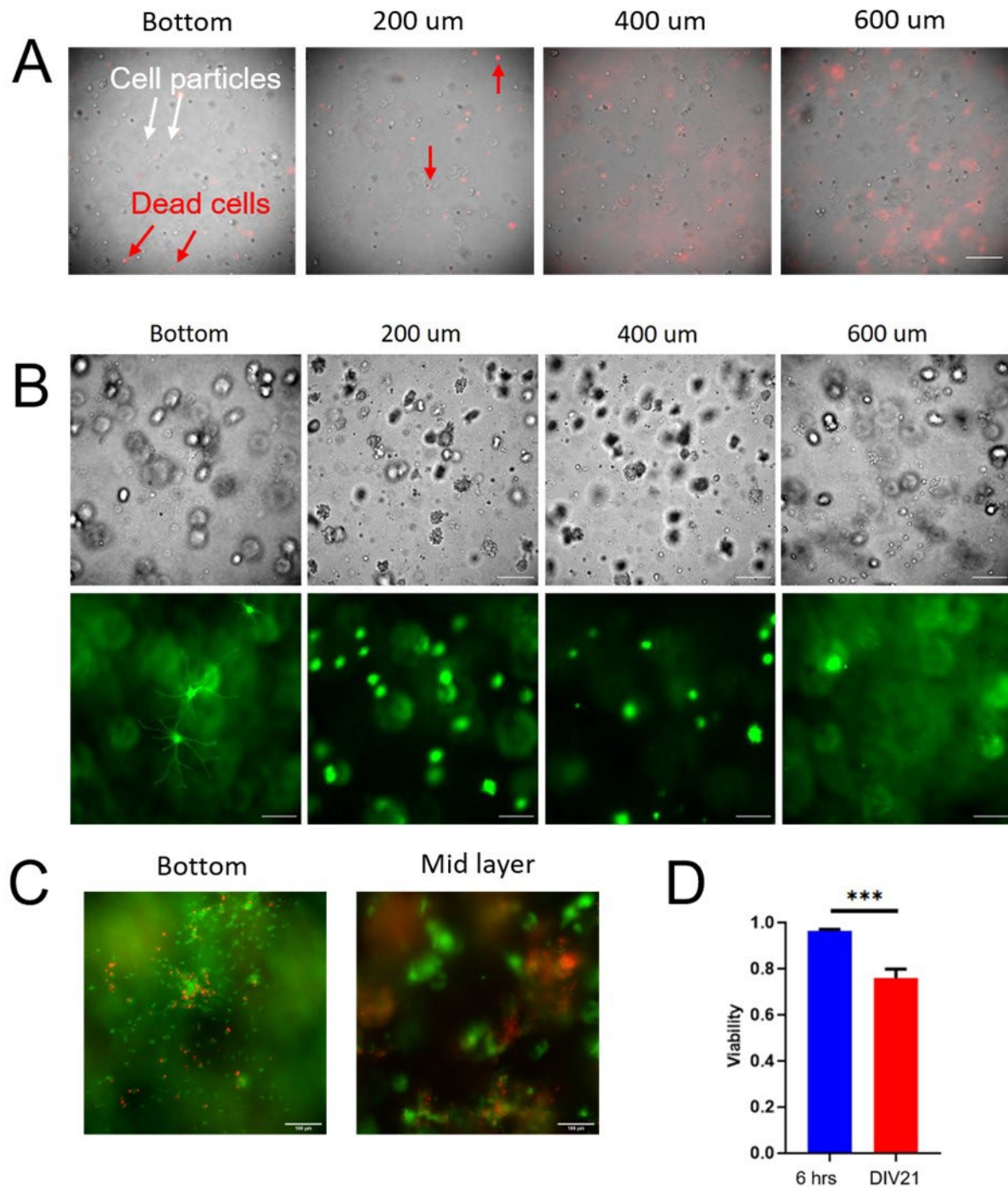


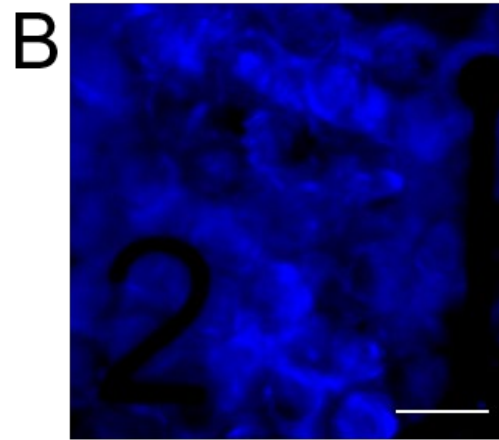
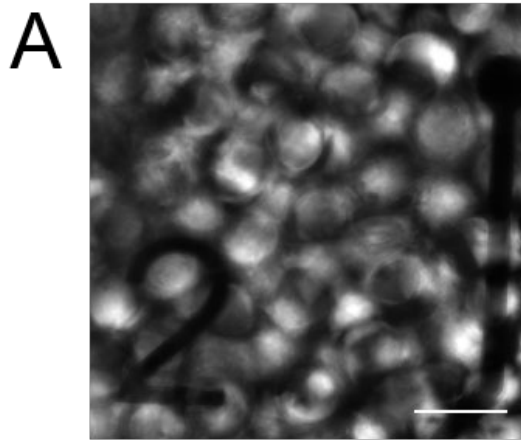
Figure 3.12 3D encapsulated culture with VitroGel **A**. Limited dead cells were seen at different layers of the culture after 6 hours in vitro with Propidium Iodide (PI) staining (scale bar: 50  $\mu\text{m}$ ) **B**. 3D neuron culture DIV18 Top row: Phase contrast image showing neurons at different layer of the 3D structure; Bottom Calcein AM staining for live cells (scale bar: 50  $\mu\text{m}$ ). **C**. Fluorescent imaging VitroGel culture at bottom and mid layer. Red:

PI; Green: Calcein AM (scale bar: 100  $\mu\text{m}$ ). **D.** Cell viability test performed at 6 hours and day 21 in vitro.

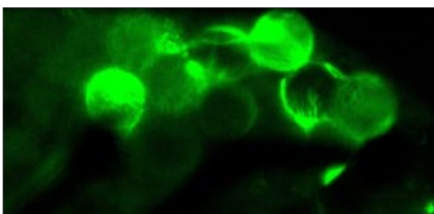
### **Network formation on micro glass beads scaffold**

From the observations of VitroGel culture, we found that neurons in our system preferred a hard surface to grow and form the network connections. A hard scaffold to form 3D network and perform in vitro electrophysiology has been investigated using 40 micro glass beads (Frega et al. 2014; Brofiga et al. 2020). Glass has highly stable chemical and physical properties, therefore, the micro glass beads self-assembled into layered structure that can maintain both physical structure and chemical stability for a long term. We took advantages of our platform being easily assembled and disassembled; the hydrogel-cell mixture can be injected into the chamber by pipette. While applying micro beads, the top ITO electrodes were taken off before we pipette the glass beads into the chamber. The cell attached micro beads are stacking from the bottom of the well, the ideal hexagonal packaging results in a void ratio of 0.74. After the 3D stack of  $\sim 10$  layers of the glass beads, the ITO electrodes were attached and sealed on top of the chamber. The flexibility of film allows the electrodes to get close contact with the glass beads top. At day 7, the neuronal tissues are filling into the gaps between micro beads (Fig 3.13A). Nuclear staining on live culture at DIV 7 shows more than one cell are attached to each bead (Fig 3.13B). To identify the neuronal connections at 21 DIV, fixed cultures were immunostained with MAP2 to specifically label neurons with dendrites. Instead of sticking to flat surface, the cell bodies attach to glass beads and form the intricate connections through the gaps between micro beads (Fig 3.13C). We also included a 2D control as shown in Fig. 3.13D. The spread 2D connections are seen from the

camera underneath, while in 3D the connections are formed in 3D with varied fluorescent intensities.



Cell bodies attach to glass beads



Neurites extend to adjacent cells

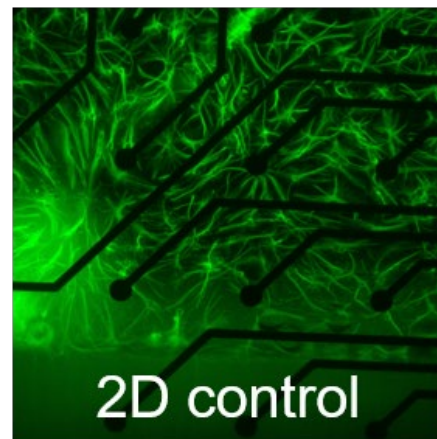


Figure 3.13 3D culture on glass beads **A.** Phase contrast image of 3D neuron culture shows the stack of micro beads (Scale bars: 50  $\mu\text{m}$ ) **B.** Bis-benzamide staining of nuclei at live status (DIV7). **C.** DIV21 culture with immunostaining MAP2 to show the neuron cell body attached to glass beads spreading across gaps between beads in the z direction; Neurites are extending from a cell on one glass bead to another. **D.** 3D network built on micro glass beads compared with 2D (MAP2).

The micro glass beads demonstrated outstanding practicability towards facilitating 3D neuronal model. Cells were first plated on single layer micro beads on the porous membrane. After settling down and incubating overnight, the cells attached to the beads which allowed stacking viable cells into a 3D layer about 10 beads high (400  $\mu\text{m}$  high). This easy operation to pipette cell attached beads into the platform will increase the rate of successful operations. This work presents the possibility of micro beads working as the substrate to be tested for network electrical activity for comparison of 3D spike dynamics to 2D dynamics.

## CHAPTER 4: CONCLUSION AND FUTURE PERSPECTIVES

To summarize, in the first part of thesis, we have reverse engineered the hippocampal formation as a 2D network in a novel 4-compartment device. The system is also novel in being able to monitor the axons that transmit information between subregions, which was the focus of this analysis. The network has the subregional cell density ratio approaching the in vivo densities with a large fan-out from EC to DG and fan in from DG to CA3. The diagonal micro tunnels for feed-forward connection from EC to CA3 to mimic the perforant path (PP) is an improvement from the four-chamber device without this path(Vakilna et al. 2021).

There are 280 micro-fluidic tunnels embedded between the subregions that allow axonal transmission to be sampled for recording by the four pairs of microelectrodes in the tunnels. By delivering patterned theta burst stimulation into EC, to emulate an LTP-capable input into the hippocampus, the routing of information as axonal transmission between subregions was evaluated. Specific site responses were examined individually in the 150 ms post stimulus window, at 10 s repetitions and after a 9 min delay. A simple Jaccard distance metric was used to quantify the temporal pattern similarity at 3 ms resolution.

We found that the network first responds to the stimulus in EC around the sites of stimulation, processes the stimulus and then transmits activity to the other subregions. From the analyses, the axonal responses caused by single site stimulus and multisite stimulus have substantial differences, suggesting the processing involves of different neuronal units. In short-term (0.2 s) stimulus repeats, the network has most unique responses to each of the

stimuli, without inducing plasticity. Also, despite the variability of the network, in which the same stimulus was delivered to the same network, the responses from each time are not the same, we found that network maintains a certain level plasticity for single site stimulus that decreases for multisite stimuli during the 10 s repeats. Specifically, CA3-CA1 has the highest retention effect at this timescale. In contrast, EC-DG transmitted much less overlapping spiking patterns at the repeats. Compared to single site, multisite stimulation had lower similarity of the spiking patterns, but CA3-CA1 and CA1-EC were able to demonstrate some persistence with repetition. After a 9 mins, CA3-CA1 and CA1-EC transmissions are still able to persist in similar activity caused by single sites. The theta burst stimulation delivered at different sites in EC was discriminated by the network as highly dissimilar patterns of activity transmitted between subregions. For activity synchrony calculated from between-tunnel similarity, the highest synchronized CA3-CA1 output by single site stimulus was reduced by the multisite stimulus. Through defining the temporal patterns and partial cue stimulus we found a small group of individual axons that performed pattern completion at EC-DG.

The innovation of this work includes measurement of single axon responses to the application of patterned stimuli with which we are able explore the unique processing properties in subregions and to each kind of input. Simultaneous recording of the diverging effect at EC-DG and converging effect at CA3-CA1 verified the engineered network integrates the abilities of pattern separation and pattern completion. Our findings in the transmission features reflected from temporal spiking form are of concord with the subregional functionalities proposed by computational models (Rolls 2010). The relatively low but over baseline similarity from temporal patterns is reflects the stochastic feature of neural

processing that contributes to feature extraction and novelty detection. Beyond the current work, future integration of propagation directionality or temporal delay information could help to confirm the axonal direction better as well as establishing the inhibitory nature of the feedback axons by disinhibition with a GABAergic blocker. A longer recording and stimulating regime could help to sort the spikes and determine the source and target of the transmission.

An important aspect of in vitro electrophysiology is to resemble the natural environment. In the second part of this thesis, we were able to extend 2D network culture into 3D with electrical access. The integral pathway of constructing this in vitro system has been investigated from both engineering and biological aspects. Firstly, we designed and fabricated an ITO/PET based film electrodes and packaged it onto PCB. The electrodes have 60 contact pads which are arranged into 15 per chamber. A sophisticated design enables direct connection to a 60-channel amplifier and computer interface to read out the network activity. The impedance of the ITO electrodes was reduced to improve the signal to noise with performance with a biocompatible conductive organic PEDOT:PSS patterned on the electrodes.. In functionality tests, we plated hippocampal neurons on the electrodes to establish excellent biocompatibility and the electrodes successfully measured the neuronal signals. However, we found corrosion after several repeated uses of the Silicon Oxide insulation, which greatly reduced the durability of a single device. Therefore, the alternative insulator Parylene has been deposited and patterned. The optical transmittance measure shows equal performance for SiO and Parylene isolated electrodes. The culture pictures taken verify the feasibility of live optical observation from platform.

Secondly, three substrates were evaluated as 3D scaffolds. The results show Matrigel, a prevalent hydrogel used on cell cultures, degraded dramatically around day 19 in primary cell construction rendering it unable to support long-term 3D culture. The synthetic hydrogel VitroGel was not sufficient to support neurite extension and network formation. Compared with the hydrogel candidates, micro glass beads demonstrated excellent practicality in supporting the 3D neural growth and network formation as verified with live cell fluorescent imaging.

As stated in the introduction, a well-engineered platform is needed to support in vitro culture and access electrical activity in the 3D model, the engineering investigation in this work will extend neuroscience investigation for comparisons of 3D vs. 2D. Further exploration on how the information routing in the 3D network based on this well characterized platform is needed.

## BIBLIOGRAPHY

- Aebersold, Mathias J., Harald Dermutz, Csaba Forró, Serge Weydert, Greta Thompson-Steckel, János Vörös, and László Demkó. 2016. "Brains on a Chip': Towards Engineered Neural Networks." *TrAC - Trends in Analytical Chemistry* 78: 60–69.  
<https://doi.org/10.1016/j.trac.2016.01.025>.
- Aisenbrey, Elizabeth A., and William L. Murphy. 2020. *Synthetic Alternatives to Matrigel*. *Nature Reviews Materials*. Vol. 5. <https://doi.org/10.1038/s41578-020-0199-8>.
- Amaral, D. G., and M. P. Witter. 1989. "The Three-Dimensional Organization of the Hippocampal Formation: A Review of Anatomical Data." *Neuroscience* 31 (3): 571–91.  
[https://doi.org/10.1016/0306-4522\(89\)90424-7](https://doi.org/10.1016/0306-4522(89)90424-7).
- Amin, Hayder, Thierry Nieus, Davide Lonardoni, Alessandro Maccione, and Luca Berdondini. 2017. "High-Resolution Bioelectrical Imaging of A $\beta$ -Induced Network Dysfunction on CMOS-MEAs for Neurotoxicity and Rescue Studies." *Scientific Reports* 7 (1): 1–13. <https://doi.org/10.1038/s41598-017-02635-x>.
- Andersen, Per. 1975. "Organization of Hippocampal Neurons and Their Interconnections." In *The Hippocampus: Volume 1: Structure and Development*, edited by Robert L Isaacson and Karl H Pribram, 155–75. Boston, MA: Springer US.  
[https://doi.org/10.1007/978-1-4684-2976-3\\_7](https://doi.org/10.1007/978-1-4684-2976-3_7).
- Baek, Dong Hyun, Ji Soo Park, Eun Joong Lee, Su Jung Shin, Jin Hee Moon, James Jungho Pak, and Sang Hoon Lee. 2011. "Interconnection of Multichannel Polyimide Electrodes Using Anisotropic Conductive Films (ACFs) for Biomedical Applications." *IEEE*

*Transactions on Biomedical Engineering* 58 (5): 1466–73.

<https://doi.org/10.1109/TBME.2010.2102020>.

Baiguera, Silvia, Costantino Del Gaudio, Elena Lucatelli, Elena Kuevda, Margherita Boieri, Benedetta Mazzanti, Alessandra Bianco, and Paolo Macchiarini. 2014. “Electrospun Gelatin Scaffolds Incorporating Rat Decellularized Brain Extracellular Matrix for Neural Tissue Engineering.” *Biomaterials* 35 (4): 1205–14.

<https://doi.org/https://doi.org/10.1016/j.biomaterials.2013.10.060>.

Baker, Brendon M., and Christopher S. Chen. 2012. “Deconstructing the Third Dimension—How 3D Culture Microenvironments Alter Cellular Cues.” *Journal of Cell Science* 125 (13): 3015–24. <https://doi.org/10.1242/jcs.079509>.

Ballini, Marco, Jan Muller, Paolo Livi, Yihui Chen, Urs Frey, Alexander Stettler, Amir Shadmani, et al. 2014. “A 1024-Channel CMOS Microelectrode Array with 26,400 Electrodes for Recording and Stimulation of Electrogenic Cells in Vitro.” *IEEE Journal of Solid-State Circuits* 49 (11): 2705–19. <https://doi.org/10.1109/JSSC.2014.2359219>.

Bardy, Cedric, Mark Van Den Hurk, Tameji Eames, Cynthia Marchand, Ruben V. Hernandez, Mariko Kellogg, Mark Gorris, et al. 2015. “Neuronal Medium That Supports Basic Synaptic Functions and Activity of Human Neurons in Vitro.” *Proceedings of the National Academy of Sciences of the United States of America* 112 (20): E2725–34. <https://doi.org/10.1073/pnas.1504393112>.

Bastiaens, Alex J., Jean-Philippe Frimat, Teun van Nunen, Bart Schurink, Erik F. G. A. Homburg, and Regina Luttge. 2018. “Advancing a MEMS-Based 3D Cell Culture System for in Vitro Neuro-Electrophysiological Recordings.” *Frontiers in Mechanical*

*Engineering* 4 (December): 1–10. <https://doi.org/10.3389/fmech.2018.00021>.

Boehler, Michael D., Stathis S. Leondopoulos, Bruce C. Wheeler, and Gregory J. Brewer. 2012.

“Hippocampal Networks on Reliable Patterned Substrates.” *Journal of Neuroscience Methods* 203 (2): 344–53. <https://doi.org/10.1016/j.jneumeth.2011.09.020>.

Boehler, Michael D, Bruce C Wheeler, and Gregory J Brewer. 2007. “Added Astroglia

Promote Greater Synapse Density and Higher Activity in Neuronal Networks.” *Neuron Glia Biology* 3 (2): 127–40. <https://doi.org/10.1017/S1740925X07000440>.

Bosi, Susanna, Rossana Rauti, Jummi Laishram, Antonio Turco, Davide Lonardoni, Thierry

Nieus, Maurizio Prato, Denis Scaini, and Laura Ballerini. 2015. “From 2D to 3D: Novel Nanostructured Scaffolds to Investigate Signalling in Reconstructed Neuronal Networks.” *Scientific Reports* 5: 1–11. <https://doi.org/10.1038/srep09562>.

Bourke, Justin L., Anita F. Quigley, Serena Duchi, Cathal D. O’Connell, Jeremy M. Crook,

Gordon G. Wallace, Mark J. Cook, and Robert M.I. Kapsa. 2018. “Three-Dimensional Neural Cultures Produce Networks That Mimic Native Brain Activity.” *Journal of Tissue Engineering and Regenerative Medicine* 12 (2): 490–93.

<https://doi.org/10.1002/term.2508>.

Braitenberg, Valentino. 1981. “ANATOMICAL BASIS FOR DIVERGENCE, CONVERGENCE,

AND INTEGRATION IN THE CEREBRAL CORTEX.” In , edited by E Grastyán and P B T - Sensory Functions Molnár, 411–19. Pergamon.

<https://doi.org/https://doi.org/10.1016/B978-0-08-027337-2.50052-3>.

Brewer, Gregory J., Michael D. Boehler, Stathis Leondopoulos, Liangbin Pan, Sankaraleengam

- Alagapan, Thomas B. DeMarse, and Bruce C. Wheeler. 2013. "Toward a Self-Wired Active Reconstruction of the Hippocampal Trisynaptic Loop: DG-CA3." *Frontiers in Neural Circuits* 7 (October): 1–8. <https://doi.org/10.3389/fncir.2013.00165>.
- Brewer, Gregory J., and John R. Torricelli. 2007. "Isolation and Culture of Adult Neurons and Neurospheres." *Nature Protocols* 2 (6): 1490–98. <https://doi.org/10.1038/nprot.2007.207>.
- Brofiga, Martina, Marietta Pisano, Mariateresa Tedesco, Roberto Raiteri, and Paolo Massobrio. 2020. "Three-Dimensionality Shapes the Dynamics of Cortical Interconnected to Hippocampal Networks." *Journal of Neural Engineering* 17 (5). <https://doi.org/10.1088/1741-2552/abc023>.
- Broski, Allison, You Guo, Wasif A. Khan, and Wen Li. 2017. "Characteristics of PEDOT:PSS Thin Films Spin-Coated on ITO." *2017 IEEE 12th International Conference on Nano/Micro Engineered and Molecular Systems, NEMS 2017*, 243–47. <https://doi.org/10.1109/NEMS.2017.8017016>.
- Broski, Allison, Jiajia Wu, and Qi Hua Fan. 2018. "Characteristics of Transparent, PEDOT:PSS-Coated Indium-Tin-Oxide (ITO) Microelectrodes" 17 (4): 701–4.
- Caliari, Steven R., and Jason A. Burdick. 2016. "A Practical Guide to Hydrogels for Cell Culture." *Nature Methods* 13 (5): 405–14. <https://doi.org/10.1038/nmeth.3839>.
- Cappaert, Natalie L.M., Niels M. Van Strien, and Menno P. Witter. 2015. *Hippocampal Formation. The Rat Nervous System: Fourth Edition*. Fourth Ed. Elsevier Inc. <https://doi.org/10.1016/B978-0-12-374245-2.00020-6>.

- Chavlis, Spyridon, Panagiotis C. Petrantonakis, and Panayiota Poirazi. 2017. "Dendrites of Dentate Gyrus Granule Cells Contribute to Pattern Separation by Controlling Sparsity." *Hippocampus* 27 (1): 89–110. <https://doi.org/10.1002/hipo.22675>.
- Choi, Chang K., Chuck H. Margraves, Seung I. Jun, Anthony E. English, Philip D. Rack, and Kenneth D. Kihm. 2008. "Opto-Electric Cellular Biosensor Using Optically Transparent Indium Tin Oxide (ITQ) Electrodes." *Sensors* 8 (5): 3257–70. <https://doi.org/10.3390/s8053257>.
- Chung, Bryce P., and Donald H. Edwards. 2019. "Discrimination of Bursts and Tonic Activity in Multifunctional Sensorimotor Neural Network Using the Extended Hill-Valley Method." *Journal of Neurophysiology* 122 (3): 1073–83. <https://doi.org/10.1152/jn.00206.2018>.
- Ciba, Manuel, Robert Bestel, Christoph Nick, Guilherme Ferraz De Arruda, Thomas Peron, Comin César Henrique, Luciano Da Fontoura Costa, Francisco Aparecido Rodrigues, and Christiane Thielemann. 2020. "Comparison of Different Spike Train Synchrony Measures Regarding Their Robustness to Erroneous Data from Bicuculline-Induced Epileptiform Activity." *Neural Computation* 32 (5): 887–911. [https://doi.org/10.1162/neco\\_a\\_01277](https://doi.org/10.1162/neco_a_01277).
- Crapo, Peter M., Stephen Tottey, Peter F. Slivka, and Stephen F. Badylak. 2014. "Effects of Biologic Scaffolds on Human Stem Cells and Implications for CNS Tissue Engineering." *Tissue Engineering - Part A* 20 (1–2): 313–23. <https://doi.org/10.1089/ten.tea.2013.0186>.
- Cullen, D. Kacy, Jelena Vukasinovic, Ari Glezer, and Michelle C. LaPlaca. 2007. "Microfluidic

Engineered High Cell Density Three-Dimensional Neural Cultures.” *Journal of Neural Engineering* 4 (2): 159–72. <https://doi.org/10.1088/1741-2560/4/2/015>.

Daniele Poli<sup>1,2,\*</sup>, Bruce C. Wheeler<sup>3,4</sup>, Thomas B. DeMarse<sup>5</sup>, and Gregory J. Brewer<sup>1,6,\*</sup>. 2017. “Pattern Separation and Completion of Distinct Axonal Inputs Transmitted via Micro-Tunnels between Co-Cultured Hippocampal Dentate, CA3, CA1 and Entorhinal Cortex Networks.” *Neural Eng.* 176 (10): 139–48. <https://doi.org/10.1016/j.physbeh.2017.03.040>.

Dolo, Vincenza, Sandra D’Ascenzo, Stefania Violini, Lorena Pompucci, Claudio Festuccia, Angela Ginestra, M. Letizia Vittorelli, Silvana Canevari, and Antonio Pavan. 1999. “Matrix-Degrading Proteinases Are Shed in Membrane Vesicles by Ovarian Cancer Cells in Vivo and in Vitro.” *Clinical and Experimental Metastasis* 17 (2): 131–40. <https://doi.org/10.1023/A:1006500406240>.

Dranias, Mark R., Han Ju, Ezhilarasan Rajaram, and Antonius M.J. VanDongen. 2013. “Short-Term Memory in Networks of Dissociated Cortical Neurons.” *Journal of Neuroscience* 33 (5): 1940–53. <https://doi.org/10.1523/JNEUROSCI.2718-12.2013>.

Dworak, Bradley J, and Bruce C Wheeler. 2009. “Novel MEA Platform with PDMS Microtunnels Enables the Detection of Action Potential Propagation from Isolated Axons in Culture.” *Lab Chip* 9 (3): 404–10. <https://doi.org/10.1039/B806689B>.

Edmondson, Rasheena, Jessica Jenkins Broglie, Audrey F. Adcock, and Liju Yang. 2014. “Three-Dimensional Cell Culture Systems and Their Applications in Drug Discovery and Cell-Based Biosensors.” *Assay and Drug Development Technologies* 12 (4): 207–18. <https://doi.org/10.1089/adt.2014.573>.

- Eytan, D., and S. Marom. 2006. "Dynamics and Effective Topology Underlying Synchronization in Networks of Cortical Neurons." *Journal of Neuroscience* 26 (33): 8465–76. <https://doi.org/10.1523/JNEUROSCI.1627-06.2006>.
- Faisal, A. Aldo, Luc P.J. Selen, and Daniel M. Wolpert. 2008. "Noise in the Nervous System." *Nature Reviews Neuroscience* 9 (4): 292–303. <https://doi.org/10.1038/nrn2258>.
- Forró, Csaba, Greta Thompson-Steckel, Sean Weaver, Serge Weydert, Stephan Ihle, Harald Dermutz, Mathias J. Aebersold, Raphael Pilz, László Demkó, and János Vörös. 2018. "Modular Microstructure Design to Build Neuronal Networks of Defined Functional Connectivity." *Biosensors and Bioelectronics* 122 (May): 75–87. <https://doi.org/10.1016/j.bios.2018.08.075>.
- Frega, Monica, Mariateresa Tedesco, Paolo Massobrio, Mattia Pesce, and Sergio Martinoia. 2014. "Network Dynamics of 3D Engineered Neuronal Cultures: A New Experimental Model for in-Vitro Electrophysiology." *Scientific Reports* 4: 1–14. <https://doi.org/10.1038/srep05489>.
- Frimat, Jean-Philippe, Sijia Xie, Alex Bastiaens, Bart Schurink, Floor Wolbers, Jaap den Toonder, and Regina Luttge. 2015. "Advances in 3D Neuronal Cell Culture." *Journal of Vacuum Science & Technology B, Nanotechnology and Microelectronics: Materials, Processing, Measurement, and Phenomena* 33 (6): 06F902. <https://doi.org/10.1116/1.4931636>.
- Gage, Fred H. 2019. "Adult Neurogenesis in Mammals Neurogenesis in Adulthood Has Implications for Sense of Self, Memory, and Disease." *Science* 364 (6443): 827–28. <https://doi.org/10.1126/science.aav6885>.

- Gollo, Leonardo L., Claudio Mirasso, Olaf Sporns, and Michael Breakspear. 2014. "Mechanisms of Zero-Lag Synchronization in Cortical Motifs." *PLoS Computational Biology* 10 (4). <https://doi.org/10.1371/journal.pcbi.1003548>.
- Graziane, Nicholas, and Yan Dong. 2015. "Extracellular Recordings." *Neuromethods* 112: 249–57. [https://doi.org/10.1007/978-1-4939-3274-0\\_22](https://doi.org/10.1007/978-1-4939-3274-0_22).
- Grefte, S, S Vullinghs, A M Kuijpers-Jagtman, R Torensma, and J W Von den Hoff. 2012. "Matrigel, but Not Collagen I, Maintains the Differentiation Capacity of Muscle Derived Cells in Vitro." *Biomedical Materials (Bristol, England)* 7 (5): 55004. <https://doi.org/10.1088/1748-6041/7/5/055004>.
- Gribi, Sandra, Sophie du Bois de Dunilac, Diego Ghezzi, and Stéphanie P. Lacour. 2018. "A Microfabricated Nerve-on-a-Chip Platform for Rapid Assessment of Neural Conduction in Explanted Peripheral Nerve Fibers." *Nature Communications* 9 (1): 1–10. <https://doi.org/10.1038/s41467-018-06895-7>.
- Gupta, Nevin Stephen, Kwan Soo Lee, and Andrea Labouriau. 2021. "Tuning Thermal and Mechanical Properties of Polydimethylsiloxane with Carbon Fibers." *Polymers* 13 (7). <https://doi.org/10.3390/polym13071141>.
- Guzman, Segundo Jose, Alois Schlögl, Michael Frotscher, and Peter Jonas. 2016. "Synaptic Mechanisms of Pattern Completion in the Hippocampal CA3 Network." *Science* 353 (6304): 1117–23. <https://doi.org/10.1126/science.aaf1836>.
- Haberly, Lewis B., and James M. Bower. 1989. "Olfactory Cortex: Model Circuit for Study of Associative Memory?" *Trends in Neurosciences* 12 (7): 258–64.

[https://doi.org/10.1016/0166-2236\(89\)90025-8](https://doi.org/10.1016/0166-2236(89)90025-8).

Habibey, Rouhollah, Shahrzad Latifi, Hossein Mousavi, Mattia Pesce, Elmira Arab-Tehrany, and Axel Blau. 2017a. "A Multielectrode Array Microchannel Platform Reveals Both Transient and Slow Changes in Axonal Conduction Velocity." *Scientific Reports* 7 (1): 1–14. <https://doi.org/10.1038/s41598-017-09033-3>.

———. 2017b. "A Multielectrode Array Microchannel Platform Reveals Both Transient and Slow Changes in Axonal Conduction Velocity." *Scientific Reports* 7 (1): 1–14. <https://doi.org/10.1038/s41598-017-09033-3>.

HajjHassan, Mohamad, Vamsy Chodavarapu, and Sam Musallam. 2008. "NeuroMEMS: Neural Probe Microtechnologies." *Sensors* 8 (10): 6704–26. <https://doi.org/10.3390/s8106704>.

Hassabis, Demis, Dharshan Kumaran, Christopher Summerfield, and Matthew Botvinick. 2017. "Neuroscience-Inspired Artificial Intelligence." *Neuron* 95 (2): 245–58. <https://doi.org/10.1016/j.neuron.2017.06.011>.

Henstridge, Christopher M., Spires-Jones, Tara L. 2018. "Modeling AD Brains in Vitro" 21 (July). <https://doi.org/10.1038/s41593-018-0176-3>.

HODGKIN, A L, and A F HUXLEY. 1939. "Action Potentials Recorded from Inside a Nerve Fibre." *Nature* 144 (3651): 710–11. <https://doi.org/10.1038/144710a0>.

———. 1952. "A Quantitative Description of Membrane Current and Its Application to Conduction and Excitation in Nerve." *The Journal of Physiology* 117 (4): 500–544. <https://doi.org/10.1113/jphysiol.1952.sp004764>.

- Huck, Wilhelm T S, Ned Bowden, Patrick Onck, Thomas Pardoën, John W. Hutchinson, and George M. Whitesides. 2000. "Ordering of Spontaneously Formed Buckles on Planar Surfaces." *Langmuir* 16 (7): 3497–3501. <https://doi.org/10.1021/la991302l>.
- Jang, Jae Myung, Si Hoai Trung Tran, Sang Cheol Na, and Noo Li Jeon. 2015. "Engineering Controllable Architecture in Matrigel for 3D Cell Alignment." *ACS Applied Materials and Interfaces* 7 (4): 2183–88. <https://doi.org/10.1021/am508292t>.
- Kafkas, Alex, and Daniela Montaldi. 2018. "How Do Memory Systems Detect and Respond to Novelty?" *Neuroscience Letters*. <https://doi.org/10.1016/j.neulet.2018.01.053>.
- Kanagasabapathi, Thirukumaran T., Davide Ciliberti, Sergio Martinoia, Wytse J. Wadman, and Michel M.J. Decré. 2011. "Dual-Compartment Neurofluidic System for Electrophysiological Measurements in Physically Segregated and Functionally Connected Neuronal Cell Culture." *Frontiers in Neuroengineering* 4 (OCTOBER): 2. <https://doi.org/10.3389/fneng.2011.00013>.
- Karahuseyinoglu, Sercin, Emine Sekerdag, Mohammad Mohammadi Aria, Yagmur Cetin Tas, Sedat Nizamoglu, Ihsan Solaroglu, and Yasemin Gürsoy-Özdemir. 2020. "Three-Dimensional Neuron–Astrocyte Construction on Matrigel Enhances Establishment of Functional Voltage-Gated Sodium Channels." *Journal of Neurochemistry*, no. April: 1–19. <https://doi.org/10.1111/jnc.15185>.
- Kastellakis, George, Denise J Cai, Sara C Mednick, Alcino J Silva, and Panayiota Poirazi. 2015. "Synaptic Clustering within Dendrites: An Emerging Theory of Memory Formation." *Progress in Neurobiology* 126: 19–35. <https://doi.org/https://doi.org/10.1016/j.pneurobio.2014.12.002>.

- Kayser, Laure V., and Darren J. Lipomi. 2019. "Stretchable Conductive Polymers and Composites Based on PEDOT and PEDOT:PSS." *Advanced Materials* 31 (10): 1–13. <https://doi.org/10.1002/adma.201806133>.
- Kim, So Hyun, Sun Kyoung Im, Soo Jin Oh, Sohyeon Jeong, Eui Sung Yoon, C. Justin Lee, Nakwon Choi, and Eun Mi Hur. 2017a. "Anisotropically Organized Three-Dimensional Culture Platform for Reconstruction of a Hippocampal Neural Network." *Nature Communications* 8. <https://doi.org/10.1038/ncomms14346>.
- . 2017b. "Anisotropically Organized Three-Dimensional Culture Platform for Reconstruction of a Hippocampal Neural Network." *Nature Communications* 8: 1–16. <https://doi.org/10.1038/ncomms14346>.
- Ko, Kristin Robin, and John P. Frampton. 2016. "Developments in 3D Neural Cell Culture Models: The Future of Neurotherapeutics Testing?" *Expert Review of Neurotherapeutics* 16 (7): 739–41. <https://doi.org/10.1586/14737175.2016.1166053>.
- Kwon, Ki Yong, Brenton Sirowatka, Arthur Weber, and Wen Li. 2013. "Opto-MECoG Array: A Hybrid Neural Interface With Transparent MECoG Electrode Array and Integrated LEDs for Optogenetics." *IEEE Transactions on Biomedical Circuits and Systems* 7 (5): 593–600. <https://doi.org/10.1109/TBCAS.2013.2282318>.
- Lam, Doris, Heather A. Enright, Jose Cadena, Sandra K.G. Peters, Ana Paula Sales, Joanne J. Osburn, David A. Soscia, Kristen S. Kulp, Elizabeth K. Wheeler, and Nicholas O. Fischer. 2019. "Tissue-Specific Extracellular Matrix Accelerates the Formation of Neural Networks and Communities in a Neuron-Glia Co-Culture on a Multi-Electrode Array." *Scientific Reports* 9 (1): 1–15. <https://doi.org/10.1038/s41598-019-40128-1>.

- Lam, Doris, Heather A. Enright, Sandra K.G. Peters, Monica L. Moya, David A. Soscia, Jose Cadena, Javier A. Alvarado, Kristen S. Kulp, Elizabeth K. Wheeler, and Nicholas O. Fischer. 2020. "Optimizing Cell Encapsulation Condition in ECM-Collagen I Hydrogels to Support 3D Neuronal Cultures." *Journal of Neuroscience Methods* 329 (September 2019): 108460. <https://doi.org/10.1016/j.jneumeth.2019.108460>.
- Langston, Rosamund F., Cassie H. Stevenson, Claire L. Wilson, Ian Saunders, and Emma R. Wood. 2010. "The Role of Hippocampal Subregions in Memory for Stimulus Associations." *Behavioural Brain Research* 215 (2): 275–91. <https://doi.org/10.1016/j.bbr.2010.07.006>.
- Leutgeb, Jill K., Stefan Leutgeb, May Britt Moser, and Edvard I. Moser. 2007. "Pattern Separation in the Dentate Gyrus and CA3 of the Hippocampus." *Science* 315 (5814): 961–66. <https://doi.org/10.1126/science.1135801>.
- Leutgeb, Stefan, and Jill K. Leutgeb. 2007. "Pattern Separation, Pattern Completion, and New Neuronal Codes within a Continuous CA3 Map." *Learning and Memory* 14 (11): 745–57. <https://doi.org/10.1101/lm.703907>.
- Lisman, John, and György Buzsáki. 2008. "A Neural Coding Scheme Formed by the Combined Function of Gamma and Theta Oscillations." *Schizophrenia Bulletin* 34 (5): 974–80. <https://doi.org/10.1093/schbul/sbn060>.
- Lisman, John, György Buzsáki, Howard Eichenbaum, Lynn Nadel, Charan Rangananth, and A. David Redish. 2017. "Viewpoints: How the Hippocampus Contributes to Memory, Navigation and Cognition." *Nature Neuroscience* 20 (11): 1434–47. <https://doi.org/10.1038/nn.4661>.

- Lisman, John, and A David Redish. 2018. "How the Hippocampus Contributes to Memory, Navigation and Cognition." *Nature Neuroscience* 20 (11): 1434–47.  
<https://doi.org/10.1038/nn.4661.Viewpoints>.
- Macis, Elisabetta, Mariateresa Tedesco, Paolo Massobrio, Roberto Raiteri, and Sergio Martinoia. 2007. "An Automated Microdrop Delivery System for Neuronal Network Patterning on Microelectrode Arrays." *Journal of Neuroscience Methods* 161 (1): 88–95.  
<https://doi.org/https://doi.org/10.1016/j.jneumeth.2006.10.015>.
- Madar, Antoine D., Laura A. Ewell, and Mathew V. Jones. 2019a. "Pattern Separation of Spiketrains in Hippocampal Neurons." *Scientific Reports* 9 (1): 1–20.  
<https://doi.org/10.1038/s41598-019-41503-8>.
- . 2019b. *Temporal Pattern Separation in Hippocampal Neurons through Multiplexed Neural Codes*. *PLoS Computational Biology*. Vol. 15.  
<https://doi.org/10.1371/journal.pcbi.1006932>.
- Mankodiya, K., D. Krapohl, S. Hammad, Y. Xie, M. Klinger, and U. G. Hofmann. 2009. "A Simplified Production Method for Multimode Multisite Neuroprobes." *2009 4th International IEEE/EMBS Conference on Neural Engineering, NER '09*, 211–14.  
<https://doi.org/10.1109/NER.2009.5109271>.
- Masser, Dustin R., Georgina V. Bixler, Robert M. Brucklacher, Han Yan, Cory B. Giles, Jonathan D. Wren, William E. Sonntag, and Willard M. Freeman. 2014. "Hippocampal Subregions Exhibit Both Distinct and Shared Transcriptomic Responses to Aging and Nonneurodegenerative Cognitive Decline." *Journals of Gerontology - Series A Biological Sciences and Medical Sciences* 69 (11): 1311–24.

<https://doi.org/10.1093/gerona/glu091>.

Morris, Richard. 1984. "Developments of a Water-Maze Procedure for Studying Spatial Learning in the Rat." *Journal of Neuroscience Methods* 11 (1): 47–60.

[https://doi.org/10.1016/0165-0270\(84\)90007-4](https://doi.org/10.1016/0165-0270(84)90007-4).

Müller, Jan, Marco Ballini, Paolo Livi, Yihui Chen, Milos Radivojevic, Amir Shadmani, Vijay Viswam, et al. 2015. "High-Resolution CMOS MEA Platform to Study Neurons at Subcellular, Cellular, and Network Levels." *Lab on a Chip* 15 (13): 2767–80.

<https://doi.org/10.1039/c5lc00133a>.

Murphy, Ashley R., Andrew Laslett, Carmel M. O'Brien, and Neil R. Cameron. 2017.

"Scaffolds for 3D in Vitro Culture of Neural Lineage Cells." *Acta Biomaterialia* 54: 1–20.

<https://doi.org/10.1016/j.actbio.2017.02.046>.

Musk, Elon. 2019. "An Integrated Brain-Machine Interface Platform with Thousands of Channels." *Journal of Medical Internet Research* 21 (10): 0–11.

<https://doi.org/10.2196/16194>.

Nabavi, Sadegh, Rocky Fox, Christophe D. Proulx, John Y. Lin, Roger Y. Tsien, and Roberto Malinow. 2014. "Engineering a Memory with LTD and LTP." *Nature* 511 (7509): 348–52. <https://doi.org/10.1038/nature13294>.

Narula, Udit, Andres Ruiz, McKinley McQuaide, Thomas B. DeMarse, Bruce C. Wheeler, and Gregory J. Brewer. 2017. "Narrow Microtunnel Technology for the Isolation and Precise Identification of Axonal Communication among Distinct Hippocampal Subregion Networks." *PLoS ONE* 12 (5): 1–15.

<https://doi.org/10.1371/journal.pone.0176868>.

Nasr Saleh, Mohamed, and Gilles Lubineau. 2014. "Understanding the Mechanisms That Change the Conductivity of Damaged ITO-Coated Polymeric Films: A Micro-Mechanical Investigation." *Solar Energy Materials and Solar Cells* 130: 199–207.

<https://doi.org/10.1016/j.solmat.2014.07.011>.

Neto, Joana P., Pedro Baião, Gonçalo Lopes, João Frazão, Joana Nogueira, Elvira Fortunato, Pedro Barquinha, and Adam R. Kampff. 2018. "Does Impedance Matter When Recording Spikes with Polytrodes?" *Frontiers in Neuroscience* 12 (OCT): 1–9.

<https://doi.org/10.3389/fnins.2018.00715>.

Nicolas, Julien, Sofia Magli, Linda Rabbachin, Susanna Sampaolesi, Francesco Nicotra, and Laura Russo. 2020. "3D Extracellular Matrix Mimics: Fundamental Concepts and Role of Materials Chemistry to Influence Stem Cell Fate." *Biomacromolecules* 21 (6): 1968–94. <https://doi.org/10.1021/acs.biomac.0c00045>.

Nikolić, Danko, Raul C. Mureşan, Weijia Feng, and Wolf Singer. 2012. "Scaled Correlation Analysis: A Better Way to Compute a Cross-Correlogram." *European Journal of Neuroscience* 35 (5): 742–62. <https://doi.org/10.1111/j.1460-9568.2011.07987.x>.

Nirenberg, S, and P E Latham. 1998. "Population Coding in the Retina." *Current Opinion in Neurobiology* 8 (4): 488—493. [https://doi.org/10.1016/s0959-4388\(98\)80036-6](https://doi.org/10.1016/s0959-4388(98)80036-6).

Novin, Marefat Ghaffari, and Mohammad Nouri. 2007. "Effect of Matrigel on Function and Morphology of Human Endometrial Epithelial Cell in Vitro." *Iranian Biomedical Journal* 11 (2): 87–94.

- Obien, Marie Engelene J., Kosmas Deligkaris, Torsten Bullmann, Douglas J. Bakkum, and Urs Frey. 2015. "Revealing Neuronal Function through Microelectrode Array Recordings." *Frontiers in Neuroscience* 9 (JAN): 423. <https://doi.org/10.3389/fnins.2014.00423>.
- Palop, Jorge J., and Lennart Mucke. 2010. "Amyloid-B-Induced Neuronal Dysfunction in Alzheimer's Disease: From Synapses toward Neural Networks." *Nature Neuroscience* 13 (7): 812–18. <https://doi.org/10.1038/nn.2583>.
- . 2016. "Network Abnormalities and Interneuron Dysfunction in Alzheimer Disease." *Nature Reviews Neuroscience* 17 (12): 777–92. <https://doi.org/10.1038/nrn.2016.141>.
- Pan, Liangbin, Sankaraleengam Alagapan, Eric Franca, Stathis S. Leondopoulos, Thomas B. DeMarse, Gregory J. Brewer, and Bruce C. Wheeler. 2015. "An in Vitro Method to Manipulate the Direction and Functional Strength between Neural Populations." *Frontiers in Neural Circuits* 9 (JULY): 1–14. <https://doi.org/10.3389/fncir.2015.00032>.
- Pastalkova, Eva, Vladimir Itskov, Asohan Amarasingham, and György Buzsáki. 2008. "Internally Generated Cell Assembly Sequences in the Rat Hippocampus" 321 (September): 1322–28.
- Patel, Jagdish, Shigeyoshi Fujisawa, Antal Berényi, Sébastien Royer, and György Buzsáki. 2012. "Traveling Theta Waves along the Entire Septotemporal Axis of the Hippocampus." *Neuron* 75 (3): 410–17. <https://doi.org/10.1016/j.neuron.2012.07.015>.
- Peretz, Hagit, Adolfo E. Talpalar, Razi Vago, and Danny Baranes. 2007. "Superior Survival and Durability of Neurons and Astrocytes on 3-Dimensional Aragonite Biomatrices."

*Tissue Engineering* 13 (3): 461–72. <https://doi.org/10.1089/ten.2005.0522>.

Poli, Daniele, and Paolo Massobrio. 2018. “High-Frequency Electrical Stimulation Promotes Reshaping of the Functional Connections and Synaptic Plasticity in in Vitro Cortical Networks.” *Physical Biology* 15 (6). <https://doi.org/10.1088/1478-3975/aae43e>.

Poli, Daniele, Vito P. Pastore, and Paolo Massobrio. 2015. “Functional Connectivity in in Vitro Neuronal Assemblies.” *Frontiers in Neural Circuits* 9 (October): 1–14. <https://doi.org/10.3389/fncir.2015.00057>.

Poli, Daniele, Srikanth Thiagarajan, Thomas B. Demarse, Bruce C. Wheeler, and Gregory J. Brewer. 2017. “Sparse and Specific Coding during Information Transmission between Co-Cultured Dentate Gyrus and CA3 Hippocampal Networks.” *Frontiers in Neural Circuits* 11 (March): 1–14. <https://doi.org/10.3389/fncir.2017.00013>.

Poli, Daniele, Bruce C. Wheeler, Thomas B. Demarse, and Gregory J. Brewer. 2018. “Pattern Separation and Completion of Distinct Axonal Inputs Transmitted via Micro-Tunnels between Co-Cultured Hippocampal Dentate, CA3, CA1 and Entorhinal Cortex Networks.” *Journal of Neural Engineering* 15 (4). <https://doi.org/10.1088/1741-2552/aabc20>.

Quian Quiroga, R, and Z Nadasdy. 2004. “Communicated by Maneesh Sahani Unsupervised Spike Detection and Sorting with Wavelets and Superparamagnetic Clustering” 1687: 1661–87.

Quiroga, R Quian, Z Nadasdy, and Y Ben-Shaul. 2004. “Unsupervised Spike Detection and Sorting with Wavelets and Superparamagnetic Clustering.” *Neural Computation* 16 (8):

1661–87. <https://doi.org/10.1162/089976604774201631>.

Rajaraman, Swaminathan, Maxine A. McClain, Seong O. Choi, James D. Ross, Stephen P. DeWeerth, Michelle C. LaPlaca, and Mark G. Allen. 2007. “Three-Dimensional Metal Transfer Micromolded Microelectrode Arrays (MEAs) for in-Vitro Brain Slice Recordings.” *TRANSDUCERS and EUROSENSORS '07 - 4th International Conference on Solid-State Sensors, Actuators and Microsystems*, no. May 2014: 1251–54. <https://doi.org/10.1109/SENSOR.2007.4300364>.

Recording, Extracellular Single-unit. 2004. “2 Principles of Extracellular Single-Unit Recording.” *Microelectrode Recording in Movement Disorder Surgery* c: 8–13. <https://doi.org/10.1055/b-0034-56092>.

Rivnay, Jonathan, Huiliang Wang, Lief Fenno, Karl Deisseroth, and George G Malliaras. 2017. “Next-Generation Probes , Particles , and Proteins for Neural Interfacing.”

Roesler, R., and J. L. McGaugh. 2016. “Memory Consolidation.” *The Curated Reference Collection in Neuroscience and Biobehavioral Psychology*, 1–22. <https://doi.org/10.1016/B978-0-12-809324-5.21493-4>.

Rogers, J. A., Z. Bao, K. Baldwin, A. Dodabalapur, B. Crone, V. R. Raju, V. Kuck, et al. 2001. “Paper-like Electronic Displays: Large-Area Rubber-Stamped Plastic Sheets of Electronics and Microencapsulated Electrophoretic Inks.” *Proceedings of the National Academy of Sciences* 98 (9): 4835–40. <https://doi.org/10.1073/pnas.091588098>.

Rolls, Edmund T. 2010. “A Computational Theory of Episodic Memory Formation in the Hippocampus.” *Behavioural Brain Research* 215 (2): 180–96.

<https://doi.org/10.1016/j.bbr.2010.03.027>.

———. 2013. “A Quantitative Theory of the Functions of the Hippocampal CA3 Network in Memory.” *Frontiers in Cellular Neuroscience* 7 (JUNE): 1–24.

<https://doi.org/10.3389/fncel.2013.00098>.

Rounis, Elisabeth, and Ying Zu Huang. 2020. “Theta Burst Stimulation in Humans: A Need for Better Understanding Effects of Brain Stimulation in Health and Disease.”

*Experimental Brain Research* 238 (7–8): 1707–14. <https://doi.org/10.1007/s00221-020-05880-1>.

Roy, Dheeraj S., Takashi Kitamura, Teruhiro Okuyama, Sachie K. Ogawa, Chen Sun, Yuichi Obata, Atsushi Yoshiki, and Susumu Tonegawa. 2017. “Distinct Neural Circuits for the Formation and Retrieval of Episodic Memories.” *Cell* 170 (5): 1000–1012.e19.

<https://doi.org/10.1016/j.cell.2017.07.013>.

Rugg, M. D., L. J. Otten, and R. N. A. Henson. 2002. “The Neural Basis of Episodic Memory: Evidence from Functional Neuroimaging.” *Philosophical Transactions of the Royal Society B: Biological Sciences* 357 (1424): 1097–1110.

<https://doi.org/10.1098/rstb.2002.1102>.

Sasaki, Takuya, Rie Kimura, Masako Tsukamoto, Norio Matsuki, and Yuji Ikegaya. 2006. “Integrative Spike Dynamics of Rat CA1 Neurons: A Multineuronal Imaging Study.”

*Journal of Physiology* 574 (1): 195–208.

<https://doi.org/10.1113/jphysiol.2006.108480>.

Shahaf, G, and S Marom. 2001. “Learning in Networks of Cortical Neurons.” *The Journal of*

*Neuroscience : The Official Journal of the Society for Neuroscience* 21 (22): 8782–88.  
<https://doi.org/0270-6474/01/218782-0715.00/0>.

Sheridan, Graham K, Emad Moeendarbary, Mark Pickering, John J O'Connor, and Keith J Murphy. 2014. "Theta-Burst Stimulation of Hippocampal Slices Induces Network-Level Calcium Oscillations and Activates Analogous Gene Transcription to Spatial Learning." *PLOS ONE* 9 (6): e100546. <https://doi.org/10.1371/journal.pone.0100546>.

Shimono, Ken, Michel Baudry, Lam Ho, Makoto Taketani, and Gary Lynch. 2002. "Long-Term Recording of LTP in Cultured Hippocampal Slices." *Neural Plasticity* 9 (4): 249–54. <https://doi.org/10.1155/NP.2002.249>.

Shmoel, Nava, Noha Rabieh, Silviya M. Ojovan, Hadas Erez, Eilon Maydan, and Micha E. Spira. 2016. "Multisite Electrophysiological Recordings by Self-Assembled Loose-Patch-like Junctions between Cultured Hippocampal Neurons and Mushroom-Shaped Microelectrodes." *Scientific Reports* 6 (January): 1–11.  
<https://doi.org/10.1038/srep27110>.

Singh, Vandana, C K Suman, and Satyendra Kumar. 2006. "Indium Tin Oxide (ITO) Films on Flexible Substrates for Organic Light Emitting Diodes." *Asid*, 388–91.

Solomon, Ethan A., Michael R. Sperling, Ashwini D. Sharan, Paul A. Wanda, Deborah F. Levy, Anastasia Lyalenko, Isaac Pedisich, Daniel S. Rizzuto, and Michael J. Kahana. 2021. "Theta-Burst Stimulation Entrain Frequency-Specific Oscillatory Responses." *Brain Stimulation* 14 (5): 1271–84. <https://doi.org/10.1016/j.brs.2021.08.014>.

Sood, Disha, Karolina Chwalek, Emily Stuntz, Dimitra Pouli, Chuang Du, Min Tang-Schomer,

- Irene Georgakoudi, Lauren D. Black, and David L. Kaplan. 2016. "Fetal Brain Extracellular Matrix Boosts Neuronal Network Formation in 3D Bioengineered Model of Cortical Brain Tissue." *ACS Biomaterials Science and Engineering* 2 (1): 131–40. <https://doi.org/10.1021/acsbiomaterials.5b00446>.
- Sporns, Olaf. 2013. "Structure and Function of Complex Brain Networks." *Dialogues in Clinical Neuroscience* 15 (3): 247–62. <https://doi.org/10.1137/S003614450342480>.
- Su, Huan Chieh, Chia Min Lin, Shiang Jie Yen, Yung Chan Chen, Chang Hsiao Chen, Shih Rung Yeh, Weileun Fang, et al. 2010. "A Cone-Shaped 3D Carbon Nanotube Probe for Neural Recording." *Biosensors and Bioelectronics* 26 (1): 220–27. <https://doi.org/10.1016/j.bios.2010.06.015>.
- Tedesco, Maria Teresa, Donatella Di Lisa, Paolo Massobrio, Nicolò Colistra, Mattia Pesce, Tiziano Catelani, Elena Dellacasa, Roberto Raiteri, Sergio Martinoia, and Laura Pastorino. 2018a. "Soft Chitosan Microbeads Scaffold for 3D Functional Neuronal Networks." *Biomaterials* 156: 159–71. <https://doi.org/10.1016/j.biomaterials.2017.11.043>.
- . 2018b. "Soft Chitosan Microbeads Scaffold for 3D Functional Neuronal Networks." *Biomaterials* 156: 159–71. <https://doi.org/10.1016/j.biomaterials.2017.11.043>.
- Tien, Chuen Lin, and Tsai Wei Lin. 2021. "Out-of-Plane Thermal Expansion Coefficient and Biaxial Young's Modulus of Sputtered ITO Thin Films." *Coatings* 11 (2): 1–11. <https://doi.org/10.3390/coatings11020153>.
- Usui, Tatsuya, Masashi Sakurai, Hideyoshi Kawasaki, Takashi Ohama, Hideyuki Yamawaki,

and Koichi Sato. 2017. "Establishment of a Novel Three-Dimensional Primary Culture Model for Hippocampal Neurogenesis." *Physiological Reports* 5 (12).

<https://doi.org/10.14814/phy2.13318>.

Vakilna, Yash S., William C Tang, Bruce C. Wheeler, and Gregory J. Brewer. 2021. "The Flow of Axonal Information between Hippocampal Subregions. 1. Feedforward and Feedback Network Spatial Dynamics Underpinning Emergent Information Processing," April. <https://doi.org/10.5281/ZENODO.4679064>.

Wagenaar, Daniel A., Jerome Pine, and Steve M. Potter. 2006. "An Extremely Rich Repertoire of Bursting Patterns during the Development of Cortical Cultures." *BMC Neuroscience* 7: 1–18. <https://doi.org/10.1186/1471-2202-7-11>.

Wagenaar, Daniel A, Jerome Pine, and Steve M Potter. 2004. "Effective Parameters for Stimulation of Dissociated Cultures Using Multi-Electrode Arrays." *Journal of Neuroscience Methods* 138 (1): 27–37.

<https://doi.org/https://doi.org/10.1016/j.jneumeth.2004.03.005>.

Wang, Yingxue, Sandro Romani, Brian Lustig, Anthony Leonardo, and Eva Pastalkova. 2015. "Theta Sequences Are Essential for Internally Generated Hippocampal Firing Fields." *Nature Neuroscience* 18 (2): 282–88. <https://doi.org/10.1038/nn.3904>.

Wheeler, Bruce C., and Gregory J. Brewer. 2010. "Designing Neural Networks in Culture." *Proceedings of the IEEE* 98 (3): 398–406.

<https://doi.org/10.1109/JPROC.2009.2039029>.

Won, Sang Min, Enming Song, Jianing Zhao, Jinghua Li, Jonathan Rivnay, and John A. Rogers.

2018. "Recent Advances in Materials, Devices, and Systems for Neural Interfaces." *Advanced Materials* 30 (30): 1–19. <https://doi.org/10.1002/adma.201800534>.
- Xiang, Zhuolin, Jingquan Liu, and Chengkuo Lee. 2016. "A Flexible Three-Dimensional Electrode Mesh : An Enabling Technology for Wireless Brain – Computer Interface Prostheses." *Nature Publishing Group*, no. February. <https://doi.org/10.1038/micronano.2016.12>.
- Xie, Chong, Jia Liu, Tian Ming Fu, Xiaochuan Dai, Wei Zhou, and Charles M. Lieber. 2015. "Three-Dimensional Macroporous Nanoelectronic Networks as Minimally Invasive Brain Probes." *Nature Materials* 14 (12): 1286–92. <https://doi.org/10.1038/nmat4427>.
- Xie, Jiaheng, Patricia R. Jusuf, Patrick T. Goodbourn, and Bang V. Bui. 2019. "Electroretinogram Recording in Larval Zebrafish Using A Novel Cone-Shaped Sponge-Tip Electrode." *Journal of Visualized Experiments : JoVE*, no. 145: 1–7. <https://doi.org/10.3791/59487>.
- Yassa, Michael A, and Craig E L Stark. 2011. "Pattern Separation in the Hippocampus." *Trends in Neurosciences* 34 (10): 515–25. <https://doi.org/10.1016/j.tins.2011.06.006>.
- Zhao, Zongya, Ruxue Gong, Liang Zheng, and Jue Wang. 2016. "In Vivo Neural Recording and Electrochemical Performance of Microelectrode Arrays Modified by Rough-Surfaced Aupt Alloy Nanoparticles with Nanoporosity." *Sensors (Switzerland)* 16 (11): 1–19. <https://doi.org/10.3390/s16111851>.
- Zhu, Guoqi, Yan Liu, Yubin Wang, Xiaoning Bi, and Michel Baudry. 2015. "Different Patterns

of Electrical Activity Lead to Long-Term Potentiation by Activating Different Intracellular Pathways." *Journal of Neuroscience* 35 (2): 621–33.  
<https://doi.org/10.1523/JNEUROSCI.2193-14.2015>.